METAMORPHISM AND PROVENANCE OF THE HOLLY LAKE METAMORPHIC COMPLEX, HOTTAH TERRANE, NWT: A PETROGRAPHIC AND SHRIMP U-Pb DETRITAL ZIRCON STUDY

Lucy Newton

Submitted in Partial Fulfillment of the Requirements
for the Degree of Bachelor of Sciences, Honours
Department of Earth Sciences
Dalhousie University, Halifax, Nova Scotia
March 2011

Distribution License

DalSpace requires agreement to this non-exclusive distribution license before your item can appear on DalSpace.

NON-EXCLUSIVE DISTRIBUTION LICENSE

You (the author(s) or copyright owner) grant to Dalhousie University the non-exclusive right to reproduce and distribute your submission worldwide in any medium.

You agree that Dalhousie University may, without changing the content, reformat the submission for the purpose of preservation.

You also agree that Dalhousie University may keep more than one copy of this submission for purposes of security, back-up and preservation.

You agree that the submission is your original work, and that you have the right to grant the rights contained in this license. You also agree that your submission does not, to the best of your knowledge, infringe upon anyone's copyright.

If the submission contains material for which you do not hold copyright, you agree that you have obtained the unrestricted permission of the copyright owner to grant Dalhousie University the rights required by this license, and that such third-party owned material is clearly identified and acknowledged within the text or content of the submission.

If the submission is based upon work that has been sponsored or supported by an agency or organization other than Dalhousie University, you assert that you have fulfilled any right of review or other obligations required by such contract or agreement.

Dalhousie University will clearly identify your name(s) as the author(s) or owner(s) of the submission, and will not make any alteration to the content of the files that you have submitted.

If you have questions regarding this license please contact the repository manager at dalspace@dal.ca.

Grant the distribution license by signing and dating below.

_____ _____

Name of signatory Date

DALHOUSIE UNIVERSITY
Inspiring Minds

Department of Earth Sciences
Halifax, Nova Scotia
Canada B3H 4J1
(902) 494-2358
FAX (902) 494-6889

DATE: APRIL 25, 2011

AUTHOR: LUCY O. NEWTON

TITLE: METAMORPHISM AND PROVENANCE OF THE HOLLY LAKE METAMORPHIC COMPLEX, HOTTAH TERRANE, NWT: A PETROGRAPHIC AND SHRIMP U-PB DETRITAL ZIRCON STUDY

Degree: B.Sc. Honours Convocation: MAY Year: 2011

Permission is herewith granted to Dalhousie University to circulate and to have copied for non-commercial purposes, at its discretion, the above title upon the request of individuals or institutions.

Signature of Author

THE AUTHOR RESERVES OTHER PUBLICATION RIGHTS, AND NEITHER THE THESIS NOR EXTENSIVE EXTRACTS FROM IT MAY BE PRINTED OR OTHERWISE REPRODUCED WITHOUT THE AUTHOR'S WRITTEN PERMISSION.

THE AUTHOR ATTESTS THAT PERMISSION HAS BEEN OBTAINED FOR THE USE OF ANY COPYRIGHTED MATERIAL APPEARING IN THIS THESIS (OTHER THAN BRIEF EXCERPTS REQUIRING ONLY PROPER ACKNOWLEDGEMENT IN SCHOLARLY WRITING) AND THAT ALL SUCH USE IS CLEARLY ACKNOWLEDGED.

ABSTRACT

This thesis reports the results of 2010 fieldwork and U-Pb detrital zircon geochronology on semi-pelites and psammites of the Holly Lake metamorphic complex (HLMC). The oldest exposed unit of the Hottah terrane, the HLMC offers limited outcrops on the western margin of the Wopmay orogen along Leith Ridge, south of Great Bear Lake and northwest of Hottah Lake. The present study was undertaken in order to determine the metamorphic history, age and possible provenance sources for the HLMC; data that will aid in testing previously proposed tectonic interpretations of the Hottah terrane.

Outcrops within the Leith Ridge study area are composed of variably migmatitic, interlayered semi-pelitic and psammitic horizons (0.5-1 m). The rocks have undergone two distinct metamorphic events: a high temperature-low pressure event (> 700° C, < 6 kbar); and retrograde metamorphism. Peak mineral assemblages include K-feldspar + sillimanite + relict cordierite + leucosomes, representing upper amphibolite to lower granulite facie conditions.

U-Pb Sensitive High Resolution Ion Microprobe (SHRIMP) analysis was completed on 75 detrital zircons from a HLMC psammite sample. The data shows a polymodal age distribution with dominant modes at 2558, 2460 and 1970 Ma, with less significant ones at 2420 and 2026 Ma. The youngest group of five zircon analyses places the maximum deposition age at 1959 ± 9 Ma. This data reveals a mainly mid to early Paleoproterozoic and Neoarchean provenance for the HLMC.

Considering the age determinations, Neoarchean detrital zircons are interpreted as either derived from nonexposed Archean rocks in the Hottah terrane, adjacent terranes to the south or southwest, or the Slave craton to the east. Moreover, the age populations of the HLMC vary from crystallization ages of the Archean Slave craton. This is either further evidence that the Hottah terrane is allochthonous with respect to the Slave craton or that the Slave craton evolved through the Neoarchean and Paleoproterozoic and of this evolution are preserved within the Hottah terrane. Regardless, the wide range of detrital zircon ages is interpreted to reflect a complex Paleoproterozoic evolution in Hottah terrane.

Key Words: Holly Lake Metamorphic Complex, Leith Ridge, Hottah terrane, SHRIMP, U-Pb, Geochronology, Detrital Zircon, Provenance, Slave craton

Table of Contents

Table of Figures

Acknowledgements

I express my sincerest gratitude to a number of people who aided me in the development of this project and guided my understanding of the sciences involved. First and foremost, I would like to thank my external supervisor, Luke Ootes, who encouraged me to do this project and who guided me with patience, enthusiasm and constructive criticism. I am also indebted to Valerie Jackson for giving me the opportunity to work with her and her team during the summer field season and for introducing me to the beautiful Northwest Territories and its complex geological record. I would also like to thank Dr. Nicholas Culshaw, Dr. Becky Jamieson and Dr. Djordje Grujic of Dalhousie University for their scientific insight and thoughtful criticism with various aspects of this thesis. In addition to my supervisors, I thank the Northwest Territories Geoscience Office for providing helicopter transportation in the field, and air travel and accommodation during SHRIMP work. Additionally, GEM for funding my SHRIMP analysis, an essential element of the project. I am also grateful for the support of Bill Davis and his wonderful team at the SHRIMP lab in Ottawa who were so kind and helpful with the laboratory component of this research. Finally, I thank Pat Ryall for his helpful critiques, advice and support. Thank you all.

CHAPTER 1: INTRODUCTION

1.1 The Wopmay Orogen

From the early Archean to present day, the geological evolution of the northwestern Canadian Shield is one of recurring continental assembly and dispersal (Cook and Erdmer, 2005). It is the only region on Earth where nearly four billion years of lithospheric development can be studied consecutively from Archean shields to Proterozoic platforms. Tectonic accretion took place within the northwestern Canadian Shield during this extensive period of geologic history, as oceanic lithosphere was consumed and terranes amalgamated. It was during the early Proterozoic that terranes accreted onto Archean cratons, and orogenic zones developed, such as the Paleoproterozoic Wopmay orogen (Fig 1.1) (Hoffman, 1988; Cook et al., 1999; Hildebrand et al., 2010).

One of the first described Precambrian plate margins, the Wopmay orogen remains an outstanding example of orogenic scale tectonics (Hildebrand et al, 2010). Therefore, the northwestern Canadian Shield is important to understanding global structural events, tectonic environments, and continental assembly. Sedimentary basins preserve important information pertaining to the tectonic development of these orogenic belts (Ootes et al., 2009). However, Precambrian successions lack biostratigraphic markers making mapping and dividing Precambrian sedimentary successions difficult (Fedo et al., 2003; Ootes et al., 2009). U-Pb dating on detrital zircons is therefore currently being used as a tool for subdividing sedimentary successions in order to unravel provenance records, timing of deposition, consequently providing a tool for regional correlations (Ootes et al., 2009).

The Wopmay orogen is important for economic reasons as rich uranium and various base and precious metal deposits are found throughout it and diamondiferous kimberlites are located in Paleozoic cover to the northwest. Their provenance may be related to unexposed basement terranes of the Wopmay orogen.

The Wopmay orogen is situated on the western margin of the Slave craton and is comprised of a series of north-south trending tectonic elements. These include, from east to west, the Coronation margin, the Great Bear magmatic zone and the Hottah terrane (Hildebrand et al., 1987) (Fig.1.1). The (>1900 Ma) Hottah terrane is the oldest component of the Wopmay orogen, but its nature and origin remain enigmatic. Largely overlain by Phanerozoic cover with limited exposures, the Hottah terrane outcrops on the western margin of the orogen and is thought to extend as basement underneath much of the Great Bear magmatic zone (GBMZ). The oldest exposed supracrustal rocks of the Hottah terrane are referred to as the Holly Lake metamorphic complex (HLMC) and generally offer limited and cryptic surface exposures and remain poorly understood.

This thesis reports the results of 2010/2011 field-based research on supracrustal rocks of the HLMC. This includes the results of petrological investigations and SHRIMP (Sensitive High Resolution Ion Microprobe) U-Pb detrital zircon geochronology from Leith Ridge metasedimentary samples, located south of Great Bear Lake and northwest of Hottah Lake, Northwest Territories (NWT) (Fig. 1.2). The examination of supracrustal rocks of the Hottah terrane ties into a larger study underway by L. Ootes, W.J. Davis, and V.A. Jackson as part of the South Wopmay Bedrock mapping project conducted by the Northwest Territories

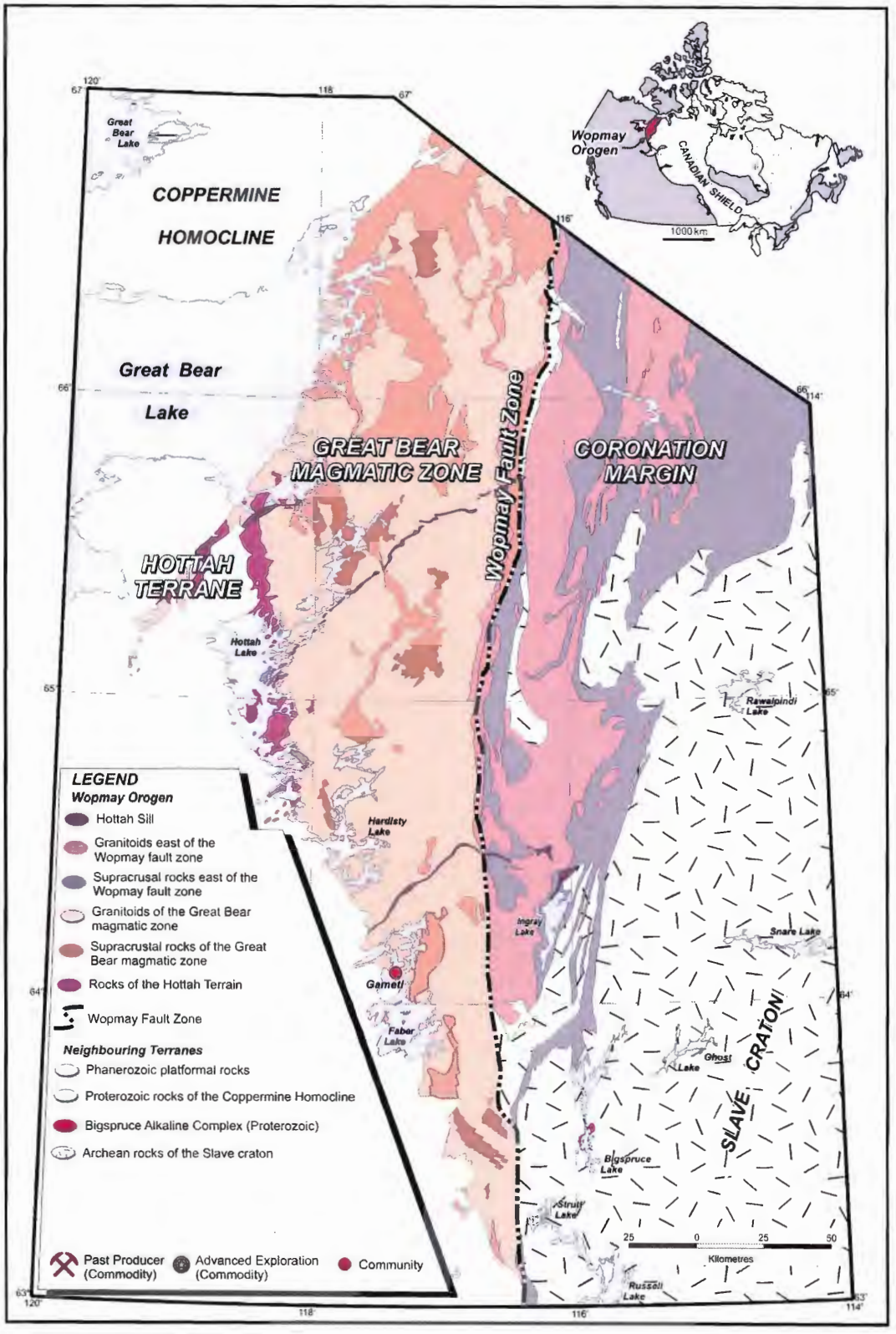

Figure 1.1: Regional map of the Wopmay orogen. Wopmay fault zone marks the boundary between Archean Slave craton basement to the east and the Proterozoic Hottah terrane to the west.

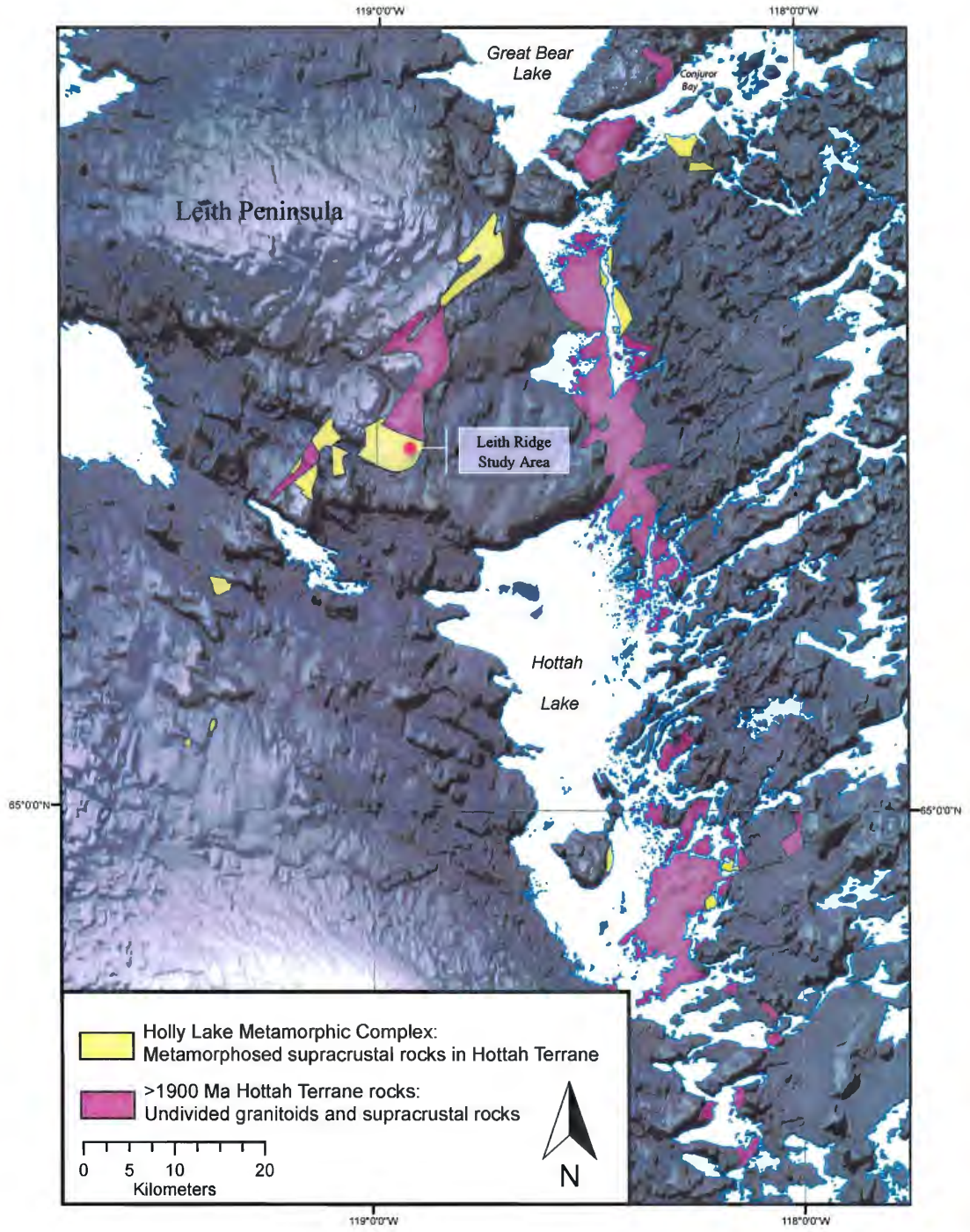

Figure 1.2: Outcrop extent of the Holly Lake metamorphic complex and rocks affiliated with the Hottah terrane in the Wopmay orogen. Base is shaded relief map. Leith Ridge study area located within red point.

Geoscience Office (NTGO) in partnership with the Geological Survey of Canada (GSC). Their South Wopmay bedrock-mapping project includes a re-investigation of bedrock assigned to the Hottah terrane in the vicinity of Hottah, Beaverlodge, and Rainy lakes, NWT.

This thesis is divided into three sections as follows:

(1) review of available data for the Hottah terrane in Wopmay orogen (Chapters 1 and 2);

(2) detailed petrography on metamorphic assemblages and their relationship to deformational fabrics from HLMC metasedimentary rocks retrieved along Leith Ridge and selected Cameco Corp. drill core samples (Chapter 3);

(3) SHRIMP II U-Pb detrital zircon geochronology of a metasedimentary sample from Leith Ridge and U-Pb zircon analyses of metamorphic rims on detrital zircons (Chapter 4); and

(4) Discussions and Conclusions (Chapter 5 and 6).

1.2 The Hottah Terrane

The Wopmay orogen was first mapped by Kidd (1936) and later by Lord (1942), finally being coined the Wopmay orogen by Fraser et al. in 1960. Since then it has been the focus of detailed exploration by geoscientists from around the world. Geologists including P.F. Hoffman, M.R. St-Onge, S.A. Bowring, J.P. Grotzinger, R.A. Hildebrand, A. Lalonde, S.S. Gandhi, V.A. Jackson, L. Ootes, L. Corriveau, H. Mumin, W. Bleeker and many others, have contributed insights into the geology and

tectonic processes within the orogen and its component tectonic domains. Despite detailed exploration and academic focus, the Hottah terrane remains a poorly understood tectonic element within the Wopmay orogen. To date, three techniques have been applied in order to assess the Hottah. These include the following methods:

(1) field-based research on limited bedrock exposures (Hildebrand et al., 1983, 1984, 2010; Hildebrand and Roots, 1985);

(2) isotopic analysis (Radiogenic Lead, Uranium-Lead and Neodynium) (Bowring, 1984; Housh et al., 1989; Bowring and Podosek, 1989); and

(3) widespread geophysical analysis (e.g. SNORCLE) (Cook and Erdmer, 2005; Fernández-Viegjo and Clowes, 2003; Aspler et al., 2003; Spratt et al., 2009).

1.2.1 Bedrock Exposures

In the northwestern Canadian Shield, many Proterozoic accreted terranes are buried beneath Phanerozoic cover. Fortunately, in the northern Hottah and Great Bear Lake area, the Hottah terrane does outcrop in limited surface exposures (Fig. 1.1, 1.2). Here, McGlynn (1976, 1979) discovered a suite of metamorphosed and deformed basement rocks unconformably underlying rocks of the Great Bear magmatic zone. However, it was not until Hildebrand and others (1981, 1982a,b, 1983, 1984, 1985) observed similar pre-Great Bear magmatic zone rocks in the Conjuror Bay area (Fig. 1.2) that they began referring to all deformed basement rocks as members of the Hottah terrane. Regional mapping projects, including the South Wopmay bedrock-mapping project (phase II), have recently remapped large portions of the southern

Hottah Lake area, providing confirmation of early observations by Hildebrand et al., (1983, 1984) and work is ongoing to provide value-added information, including geochemistry, and geochronology of key units.

Hottah terrane exposures occur along the southeast shores of Great Bear Lake, then trend north-south along the eastern shore of Hottah Lake. A second arm of this terrane trends northeast-southwest across Leith Peninsula (Fig. 1.2). The Hottah Lake exposures abut the Great Bear magmatic zone to the east, while inliers within Phanerozoic sediments occur along Leith Ridge.

1.2.2 Previous Isotopic Data

Isotopic analysis, including radiogenic Lead, Neodynium and Uranium-Lead, provided the first indirect evidence into the age and extent of the Hottah terrane underlying the Wopmay orogen west of the Wopmay fault zone and Phanerozoic cover further to the west (Fig 1.1). Bowring (1984) analyzed multigrain detrital zircon populations for U-Pb from a biotite schist sample taken from Hottah basement that yielded upper intercept dates of ca. 2.1 Ga (Fig. 1.3, S-83-H2). Analysis was completed on a sample of conglomerate that contained a sandy matrix with an upper intercept age of 2278 ± 10 Ma (Fig. 1.3, S-83-H1). Another metasedimentary sample was dated, that included 2.1 Ga detrital zircons. From these three ages obtained, Bowring was able to conclude that the age of the Hottah terrane source was ~ 2.1-2.3 Ga.

In addition to U-Pb isotopic age data, Housh et al., (1989) analyzed radiogenic Lead compositions from leached feldspars of plutons within three arcs preserved in

the Wopmay orogen, that include, the Great Bear magmatic zone, the Hepburn Intrusive Suite and the Hottah Arc (Housh et al., 1989). Results obtained were used to determine the age and characteristics of source regions for these arc magmas. Despite the broad geographical separation of the arcs, and differences in the episodes of arc magmatism and their bulk compositions, the isotopic results displayed a tightly clustered trend (Fig. 1.4b). Furthermore, Bowring and Podosek (1989) analyzed Neodynium isotopic concentrations from various magmatic suites within the Wopmay orogen. Results suggest that a 2.0-2.4 Ga crust is present beneath the Great Bear magmatic zone, whereas the Coronation margin to the east of Wopmay fault zone is underlain by > 2.5 Ga crust. Both Neodynium and Lead isotopic signatures indicate that magmas within the Wopmay orogen were sourced or interacted with an early Proterozoic Hottah basement that is no longer exposed (Bowring and Podosek, 1989; Housh et al., 1989) (Fig. 1.4).

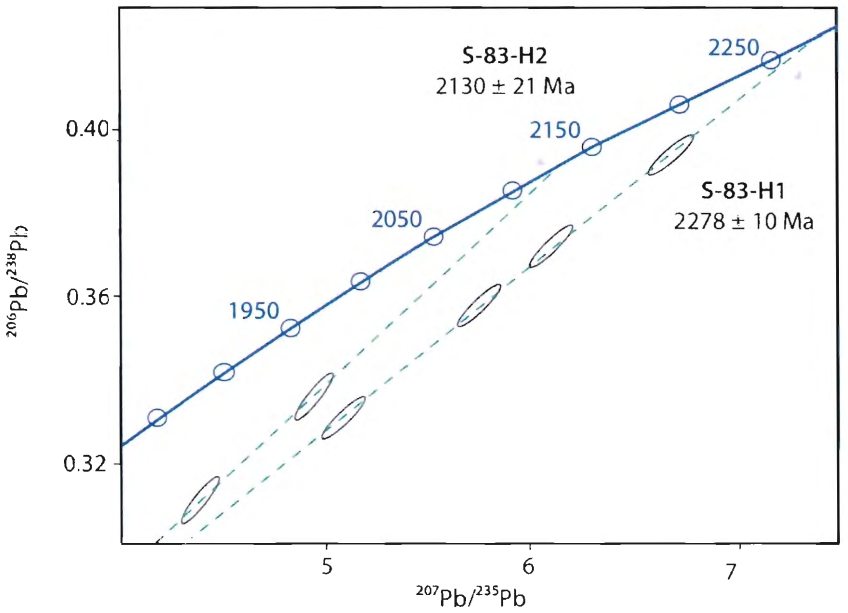

Figure 1.3: Concordia diagram showing multigrain TIMS data from detrital zircons of Leith Peninsula. Stretched pebble conglomerate and biotite schist with upper intercepts at 2130 ± 21 Ma and 2278 ± 10 Ma respectively. TIMS: Thermal Ionization Mass Spectrometry (Modified from Bowring 1984).

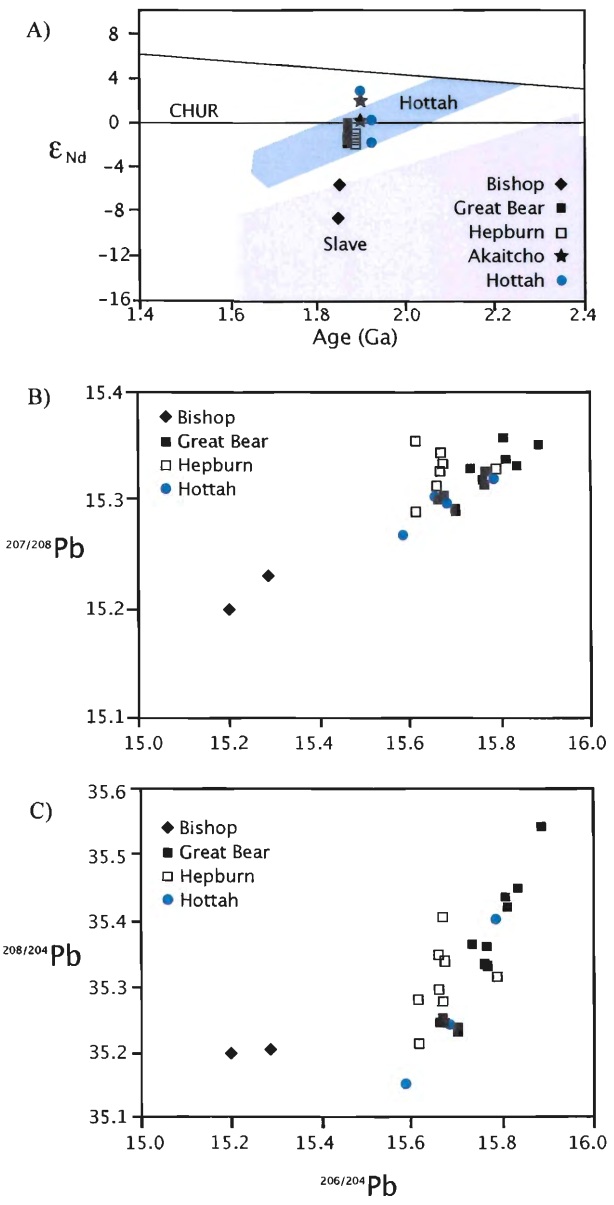

Figure 1.4: $^{206}Pb/^{204}Pb$-$^{207}Pb/^{204}Pb$ and $^{206}Pb/^{204}Pb$-$^{208}Pb/^{204}Pb$ and Neodynium plots of data from plutons within three magmatic arcs preserved within the Wopmay orogen (modified from Bowring et al., 1989; Bowring and Podosek 1989). (A) Relationship of age and initial Nd at that age for rocks of various magmatic suites of the Wopmay orogen. The Bishop suite of the Great Bear magmatic zone has distinctly lower Nd concentrations than the other plutons (Hepburn, Akaitcho and Hottah) as it interacted with rocks of the Slave craton to the east. (B) Radiogenic Lead from feldspars of different plutons of arcs preserved within the Wopmay orogen. Data is tightly clustered despite large geographical distances between the arcs, different episodes of magmatism and bulk composition variations. (Housh et al., 1989; Hildebrand et al., 2010).

1.2.3 Geophysical Surveys

Further advances in understanding the extent of the underlying Hottah terrane are derived from the completion of the Lithoprobe Slave – Northern Cordillera Lithospheric Evolution (SNORCLE) study that took place across northwestern North America (spanning from the Slave province to the western Cordillera). This Lithoprobe transect has been combined into an 1800 km cross-section of the lithosphere, the longest most "continuous" and detailed profiles of the continental lithosphere anywhere in the world (Cook and Erdmer, 2005) (Fig. 1.5). The transect comprised high-resolution geophysical data including, seismic reflection, refraction, electromagnetic and potential fields, backed up by bedrock studies. This lithospheric cross-section

provides evidence of a plate-tectonic style of arc-continent collision, terrane accretion and subduction during the Proterozoic that is similar to modern analogues (Cook et al., 1999). The continuous profile displays subsurface geometries from frozen subduction zones, magmatic arcs to accretionary boundaries (Fig. 1.5) (Cook and Erdmer, 2005). The study thus provides the first set of complete lithospheric profiles of the Hottah terrane buried beneath Phanerozoic cover, and extending as basement under the Great Bear magmatic zone (Fig. 1.5). Additional geophysical surveys include a magnetotelluric transect across the western Slave craton and Wopmay orogen (Spratt et al., 2009), aeromagnetic data compilation and interpretation (Aspler et al., 2003), and a teleseismic transect (D. Snyder, unpublished data). Both magnetotelluric and teleseismic transects are deep crustal studies, aimed to uncover the character of the mantle-crust transitions (Moho) in the northwest Canadian Shield.

The mysteries of the Hottah terrane are only just beginning to unravel despite previous isotopic analysis, bedrock geology and widespread geophysical surveys. With the advances in geochronological techniques, Hottah component ages are currently becoming more reliably constrained. In addition, with continued ground-based research projects and geophysical surveys, further information is being retrieved regarding the source, age and extent of the Hottah terrane and its implication within the greater Wopmay orogen.

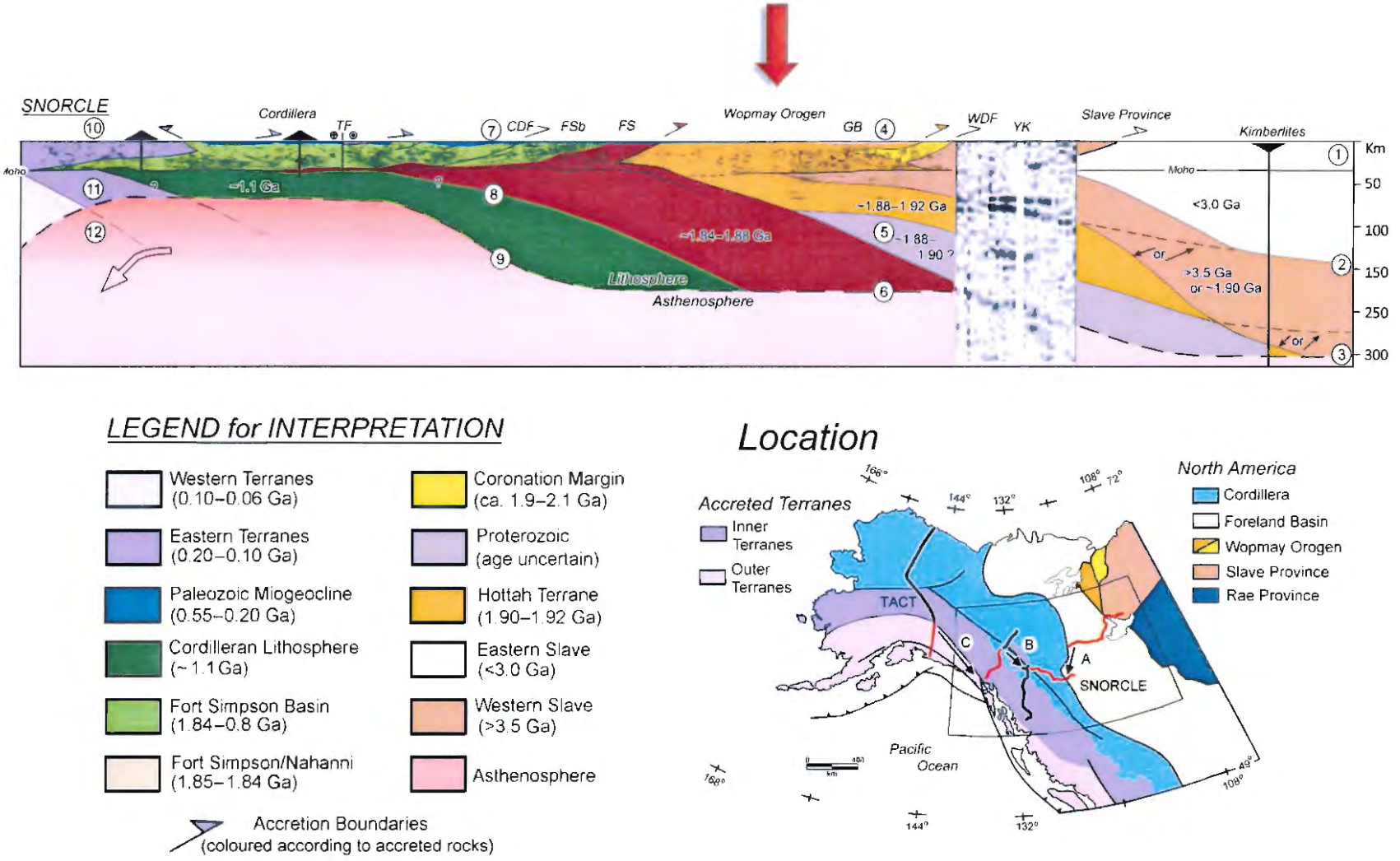

Figure 1.5: SNORCLE seismic map transect. The transect spans 1800 km from the Slave Province to the west coast Cordillera. Wopmay orogen represented in orange, see orange arrow (after Cook and Erdmer, 2005).

1.3 Objectives and Methods of Investigations

The purpose of this thesis is to further the understanding of the components of the Hottah terrane by studying supracrustal rocks of the HLMC. These metasedimentary rocks provide a unique opportunity to assess the Hottah terrane as detrital zircons within these rocks can provide a provenance record, while mineral assemblages and overprinting relationships provide clues into its metamorphic and depositional history. U-Pb detrital zircon geochronology was undertaken in order to constrain a maximum age of deposition, evaluate possible provenance sources, and thereby provide a better understanding of its tectonic history. This data can be used to test previous interpretations of the Hottah terrane, particularly its relationship with the Archean Slave craton. Petrographic analysis, detailed herein, on metamorphic assemblages and their relation to deformational fabrics in combination with the U-Pb data provides the first detailed metamorphic and provenance study of supracrustal rocks of the Hottah terrane.

CHAPTER 2: GEOLOGICAL SETTING

2.1 General Statement

This chapter reviews the tectonic components of the Wopmay orogen with emphasis on the Hottah terrane and its supracrustal rocks of the HLMC. Tectonic history of the Wopmay orogen during the Proterozoic are further discussed in order to fully understand provenance relationships pertaining to Chapter 4 (SHRIMP U-Pb detrital zircon geochronology).

2.2 The Wopmay Orogen at its Tectonic Domains

The Wopmay orogen is the northwestern margin of the Canadian Shield, situated between the Phanerozoic-covered Fort Simpson and Nahanni terranes to the west, and the Archean Slave craton to the east (Fig. 2.1). Thick Phanerozoic cover extends to the south of the Wopmay orogen, overlying major

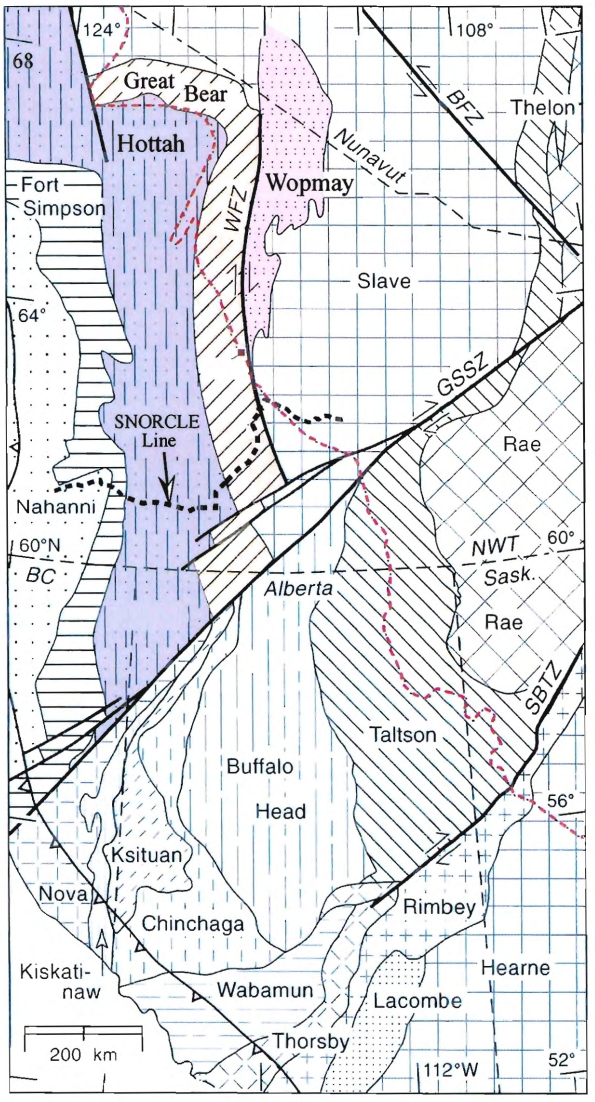

Figure 2.1: Tectonic elements of the Northwestern Canadian Shield (modified from Gandhi and van Breemen, 2005). Wopmay orogen in colour (Coronation margin in pink, Great Bear magmatic zone in orange and the Hottah terrane in purple) with SNORCLE transect represented by dashed line. The Phanerozoic sediment extent is shaded in blue with red dashed line indicating the limit of the Phanerozoic cover. Grey dashed lines indicate Provincial and Territorial borders.

terranes including the Buffalo Head and portions of the Taltson and Hearne terranes (Fig 2.1). The Great Slave Shear Zone (GSSZ) crosscuts the southern Wopmay orogen, displacing large crustal blocks to the southwest (Hoffman, 1988). Transecting the orogen from north to south is the Wopmay Fault Zone (WFZ) (Fig 2.1), that marks the boundary between Archean basement to the east and Proterozoic Hottah basement to the West (Bowring and Podosek, 1989; Housh et al., 1989).

As previously mentioned in Chapter 1, the Wopmay orogen is composed of three major tectonic elements (the Coronation margin, the Great Bear magmatic zone and the Hottah terrane) that run parallel to the trend of the orogenic belt itself (Hildebrand et al., 1987). However, with the recognition of new tectonic elements in recent years, Hildebrand et al. (2010) further divided the Wopmay orogen into five major tectonic components. These include from east to west, the Coronation margin, the Turmoil klippe, the Medial zone, the Great Bear magmatic zone, and the Hottah terrane (Fig. 2.2).

The **Coronation margin** consists of a sedimentary sequence represented by three distinct tectonic regimes including rift, passive margin and foredeep, collectively referred to as the Coronation Supergroup (Fig. 2.2). The rift-passive margin-foredeep sedimentary succession unconformably overlies Archean rocks of the Slave craton (Hildebrand et al., 2010). The **Great Bear magmatic zone** is a typical magmatic arc built on continental crust, situated on the western edge of the Coronation margin and Turmoil klippe. It is dominantly composed of calc-alkaline volcanic and plutonic rocks, found overlying the Hottah terrane. The **Medial zone** is situated on the eastern boundary of the Great Bear magmatic zone and includes rocks of all other zones that are tightly folded and cut by transcurrent faults (Hildebrand et al., 2010).

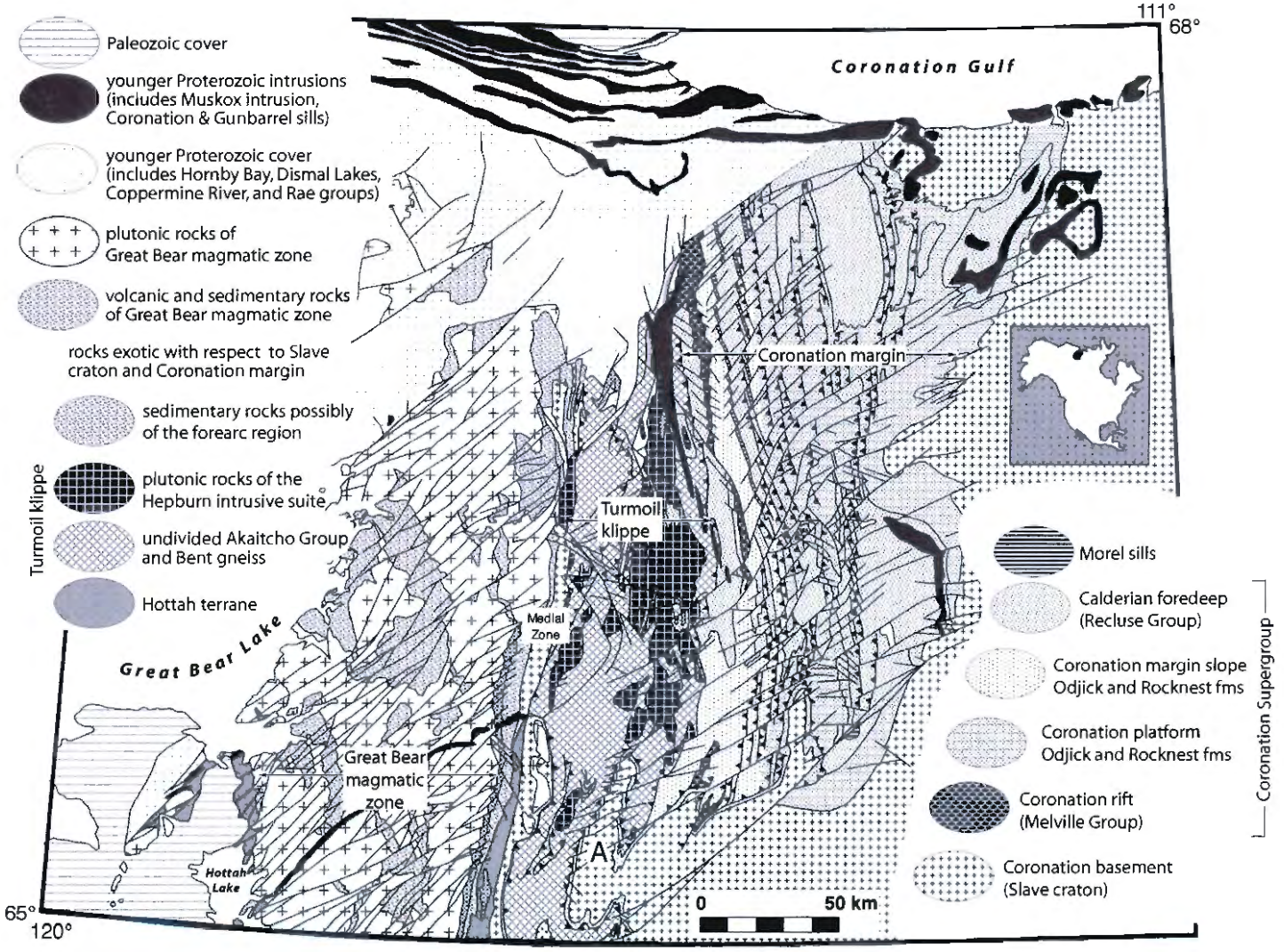

Figure 2.2: Geological map of the Wopmay orogen and its tectonic divisions. From East to West: (1) The Coronation Margin, (2) The Turmoil klippe, (3) The Medial Zone, (4) The Great Bear magmatic zone, (5) the Hottah Terrane. A- Acastas Gneiss (Hildebrand et al., 2010).

The **Hottah terrane** is the oldest tectonic element of the Wopmay orogen, exposed to the west of the Great Bear magmatic zone and to the east as an erosional remnant, referred to as the **Turmoil Klippe**. This erosional remnant is thrust upon the western boundary of the Coronation margin, some 55 km west of the Slave craton. It is composed of a crystalline basement unconformably overlain by metamorphosed sedimentary and volcanic rocks, intruded by the Hepburn intrusive suite (Fig 2.2) (Hildebrand et al., 2010).

To the west of the Great Bear magmatic zone, the Hottah terrane is composed of a crystalline basement and a volcanic and sedimentary cover sequence. Basement of the Hottah terrane, as previously mentioned, is referred to as the HLMC that has been intruded by ca. 1930 Ma plutons of the Hottah continental arc (Fig 2.3) (Ootes and Davis, unpublished data). This provides a minimum deposition age of ca. 1930 Ma for HLMC. Unconformably overlying the HLMC and the Hottah continental arc is the ca. 1900 Ma Bell Island Bay Group, represented by back-arc or rift basin volcanic deposits (e.g. subaerial basaltic and rhyolitic lavas and tuffs (Reichenbach, 1991)). The youngest unit within the Hottah terrane is the 1885-1875 Ma Treasure Lake Group, a platformal sedimentary sequence in the Hottah terrane only exposed south of 65° N (Gandhi and van Breemen, 2005; Bennett and Rivers, 2006). This Hottah terrane sequence is unconformably overlain and intruded by the ca. 1872 to 1855 Ma Great Bear magmatic zone (Fig. 2.3).

2.2.1 Holly Lake Metamorphic Complex

The HLMC is represented by metasedimentary and metavolcanic rocks, poorly exposed to the west of the Great Bear magmatic zone and largely overlain by thick Phanerozoic sediments. Due to limited outcrop exposures and minimal petrographic studies, the HLMC remains poorly understood. The complex is represented by orthogneiss and quartz-plagioclase-biotite ± muscovite ± sillimanite schist with minor garnet amphibolite, all intruded by deformed granitoids. These granitoids and the HLMC were deformed prior to the overlying deposition of the Bell island Bay group (Jackson and Ootes, in prep). Deformed pillow basalt and porphyritic andesite are also common near Hottah Lake, and are metamorphosed to amphibolite facies and subsequently regressed to greenschist facies. These are associated with psammites, pelitic schists, cordierite

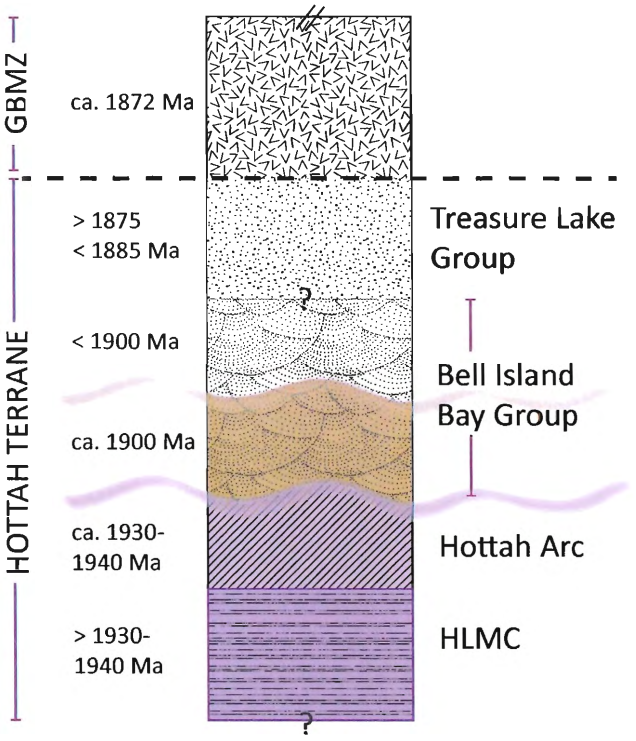

Figure 2.3: Stratigraphic and geochronological simplification of Hottah terrane and the Great bear magmatic zone (GBMZ). Wavy and dashed lines represent unconformity surfaces. (L. Ootes, 2010, unpublished data). Holly Lake metamorphic complex (HLMC): sedimentary and intermediate volcanic rocks. Hottah Arc: Calc-alkaline granitic plutons in the HLMC. Bell Island Bay Group: Continental arc environment deposits (lavas, tuffs, sandstones) unconformably overlain by back-arc basin environment deposits (basaltic flows, gabbro dykes, conglomerates, ext) (Gandhi and van Breemen, 2005; Bennett and Rivers, 2006).

paragneiss, volcaniclastic rocks, conglomerate and minor banded iron formation (Hildebrand et al. 2010).

Given that the majority of the HLMC is covered in thick Phanerozoic sequences, or where exposed is highly altered, studying this cryptic supracrustal group is challenging. The best preserved HLMC outcrop exposures are found within the Leith Peninsula along Leith Ridge (Fig 1.2). In addition, historical drilling for uranium in overlying strata pierced the Holly Lake metamorphic complex, providing examples of this unit in drill core.

Hildebrand et al. (1983, 1984) was the first to note that the oldest rocks along Leith Ridge were metasedimentary rocks of the HLMC. These metasedimentary rocks have been intruded by a series of deformed and undeformed igneous dykes that range in composition from gabbro to alkaline feldspar-granite. Moreover, larger deformed and undeformed plutons can be found in the area including syenogranites, muscovite-granites and porphyritic biotite granites (Hildebrand et al., 1983, 1984). Metasedimentary rocks of the HLMC along Leith Ridge are most commonly represented by strongly foliated sillimanite migmatites that trend roughly north to northwest.

On a smaller scale, pre-, syn-, and post-tectonic igneous dykes intrude the migmatites and include gabbros, diorites, granodiorites, pegmatites, aplites, among others. All units are cut by numerous faults that vary in orientation, although major faults generally trend to the northeast (Hildebrand et al., 1983, 1984).

2.3 Tectono-magmatic Development of the Wopmay Orogen

As previously stated, the Wopmay orogen is interpreted as a Paleoproterozoic collisional belt and post-collisional magmatic arc that formed as microcontinents and volcanic arcs accreted onto the western margin of the Slave craton between 1.97-1.84 Ga (Hildebrand et al., 2010). The Hottah terrane is suggested by Bowring and Groztinger (1992) and Hildebrand et al. (2010) to be an east-facing continental magmatic arc that accreted onto the western margin of the Slave craton at a ca. 1.88 Ga. This arc-continent collision was responsible for the main collisional phase of the orogen, referred to as the Calderian orogeny, a relatively short-lived collision. However, events that occurred prior to the Hottah-Slave collision significantly influenced the nature of the assembly (see Hildebrand et al., 2010).

The Coronation Supergroup was deposited as a continental passive margin depositional prism between 1.92-1.90 Ga, after lithospheric accretion ceased in the Slave Province (Hoffman and Bowring, 1984). A basin formed with the onset of rifting, which subsequently filled with sediments of the Coronation Supergroup. These sediments represent different stages of rifting, that include rift basin and crustal stretching, passive-margin subsidence, and the foundering of the shelf (Hoffman and Bowring, 1984). Oceanward of the Slave craton, westward-dipping oceanic lithosphere connected to the Slave craton subducted beneath the ca. 2.4-2.0 Ga Hottah plate to form the Hottah continental magmatic arc (Fig 2.4 A) (Bowring and Grotzinger, 1992; Hildebrand et al., 2010). Due to retreating subduction, volcanism within the Hottah arc migrated trenchward, changing in composition from an aphyric calc-alkaline to a bimodal tholeiitic suite. The change in magmatism was accompanied by subsidence, represented by high-

temperature low-pressure metamorphism within rocks of the upper plate that resulted from extension and asthenosphere upwelling due to rollback of the subduction hinge (Hildebrand et al., 2010). As the forearc region collided with the Slave craton, the stress regime shifted from extension to compression that generated hybrid magmas of the Hepburn intrusive suite (Fig. 2.4 B) (Hildebrand et al., 2010).

According to Hildebrand et al. (2010), with the onset of collision, convergence slowed down given the difficulty of subducting continental lithosphere of the Slave craton, and the Turmoil klippe resulted from the Hottah thrusting over the Slave (Fig 2.4 C). Within five million years, the subducting slab delaminated, triggering the intrusion of an extensive 200 km long series of mafic dyke swarms (Morel Sills) into the lower plate and trench sediments (Fig. 2.4 D). The Medial zone (Fig 2.2) likely defines the zone of detachment within the Wopmay orogen.

The Calderian orogeny was a short-lived collision, lasting less than 9 Mya. Within this short period, mafic magmas intruded the lower plate, the Turmoil Klippe was thrust upon the Slave margin, and rocks of the collision zone were quickly eroded. This short-lived collision is typical of some modern day, arc-continent collisional zones (Hildebrand et al., 2010).

After the main collisional event, an east-dipping subduction zone formed outboard of the accreted terrane, subsequently erupting volcanic rocks of the Great Bear magmatic arc between 1.88-1.84 Ga onto the eroded collisional zone (Bowring and Grotzinger, 1992; Hildebrand et al., 2010). This sequence represents the completion of the Calderian orogeny.

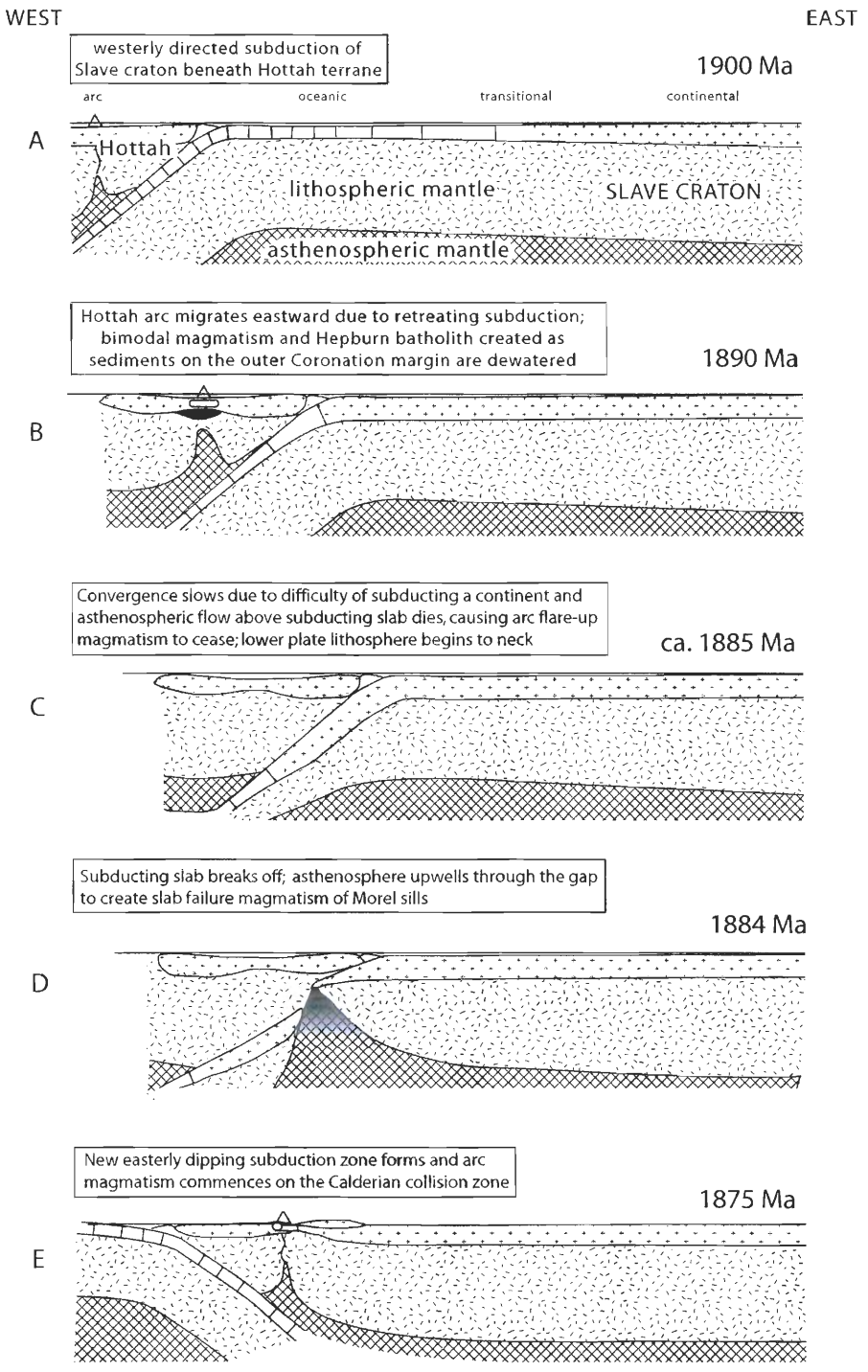

Figure 2. 4: Geological model for the tectonic evolution of the Wopmay Orogen. (After Hildebrand et al., 2010).

The tectonic model discussed above, propose a Wilson cycle model for the development of the Wopmay orogen that is highly dependant on the Hottah terrane, including the Turmoil klippe, being truly exotic with respect to the Slave craton (Hoffman, 1980). Given that almost all components of the Hottah terrane remain unknown, this theory is difficult to near impossible to test. It is worth noting that an alternative, although less publicized model exists. In the interpretation by Reichenbach (1991) the Hottah terrane is thought to have developed adjacent to the Slave Craton. Reichenbach argues that the geology, geochemistry and geochronology of the Bell Island Bay Group correlate with supracrustal rocks of the Turmoil Klippe (Akaitcho and Grant groups). These similarities suggest the supracrustal rocks of the Turmoil klippe and Bell Island Bay groups were deposited within the same marginal basin. In this model, the Turmoil klippe segment of Wopmay orogen is interpreted to be part of a back-arc sequence that formed autochthonous with respect to the Slave craton. In other words, although the Wopmay orogen is a true orogen, it remains possible that all of the preserved Hottah terrane developed adjacent to the Slave craton. Data in this study will aid in testing the two end-member hypotheses.

CHAPTER 3: PETROLOGY

3.1 General Statement

This chapter presents field-based and petrographic results from the Leith Ridge study area, located south of Great Bear Lake and ~ 13 km northwest of Hottah Lake, at 65°20'40"N, 118°56'15.80"W (Fig. 1.2). Reports and maps by Hildebrand et al. (1983, 1984) were used to target key outcrops within the study area.

Fieldwork was completed on August 6th 2010, accompanied by Luke Ootes from the Northwest Territories Geoscience Office, and Leanne Smar from the University of British Columbia. Helicopter transportation was an asset given the lengthy distance from field camp to study area, although accessing Leith Ridge remained a challenge given spotty outcrops and abundant deadfall produced by recent forest fires in the area. Three well-exposed outcrops were mapped within the study area (Fig. 3.1). In addition, prior to fieldwork, HLMC drill cores were retrieved from a drill box preserved by Cameco Corp. located on the south shore of Fenwick Lake, Leith Peninsula.

Fieldwork was completed in order to achieve the following objectives:

(1) to collect geochronology samples for SHRIMP U-Pb analysis;

(2) to identify principal lithologies in the Leith Ridge study area and their textural relationships; and

(3) to deduce potential depositional environments and specifics of metamorphism.

Petrography was completed on 23 thin-sections from outcrop and drill core in order to:

(1) document mineral assemblages and metamorphic grade of psammite and semi-pelite rocks in the Leith Ridge study area;

(2) determine the stages of deformation and mineral growth; and

(3) observe relationships between detrital zircon and monazite with metamorphic mineral assemblages.

3.2 Methods

Eleven oriented samples were collected during fieldwork. In addition to a geochronology and several 1960's era drill core samples that were carefully preserved by Cameco Corporation at Fenwick Lake. Core samples were retrieved from two separate boxes that were sampled from interval depths of 64.9-70.9 and 94.5-99.1 m respectively.

Field photos were taken and include a pen magnet for scale with magnetic pen tip oriented north. The rock samples were cut into manageable slabs (~ 15 cm), perpendicular and parallel to foliation, in Yellowknife at the Northwest Territories Geosicence office. From the 11 oriented samples, 23 representative thin sections (20 normal and 3 polished) were cut at the Dalhousie University thin-section preparation lab in Halifax. Petrography was completed in the Dalhousie University microscope lab using a Nikon 50*i* transmitted-light microscope and images captured with a Nikon eclipse camera (50*i* Pol, LV-UEP1).

3.3 Outcrops

As mentioned above, three outcrops were mapped within the Leith Ridge study area. Recent forest fires have burned off the moss and lichen covering, consequently, bare outcrops afford ideal conditions for geological mapping in the area (Fig 3.1 B). As a result, lithological variations, textural and crosscutting relationships were easily identified in the field.

All three outcrops display similar morphological, lithological and textural characteristics. Outcrops are low-lying and rounded (Fig. 3.1) and are intruded by numerous crosscutting igneous dykes of varying composition (Fig 3.2). The outcrops are composed of variably migmatitic, interlayered semi-pelitic and psammitic horizons that average 0.5 to 1.0 m thick. The semi-pelitic and psammitic layers are strongly foliated, defined by the alignment of biotite-rich layers that strike on average 315 degrees and dip 45 degrees to the northeast (Fig 3.3). Outcrop 1, the largest of the three outcrops (~ 40 x 25 m), is composed of strongly foliated semi-pelites with minor psammitic layers (Fig 3.1, 3.2). In comparison, outcrops 2 and 3 display far more prominent compositional layering defined by alternating psammite and semi-pelite layers (Fig 3.3). Incipient thin and discontinuous leucosome lenses (melt-in) are common (1-1.5 cm) throughout all three outcrops in both psammite and semi-pelite layers, forming lenticular pods aligned with the main foliation. Quartz veins (1-5 cm) are also common and generally are shallowly folded with axial planes parallel to the main foliation and limbs that cut the main foliation (Fig. 3.4 A). Quartz boudins are present near the contacts between semi-pelitic and psammitic inter-layers in outcrops 2 and 3 (Fig. 3.4 B).

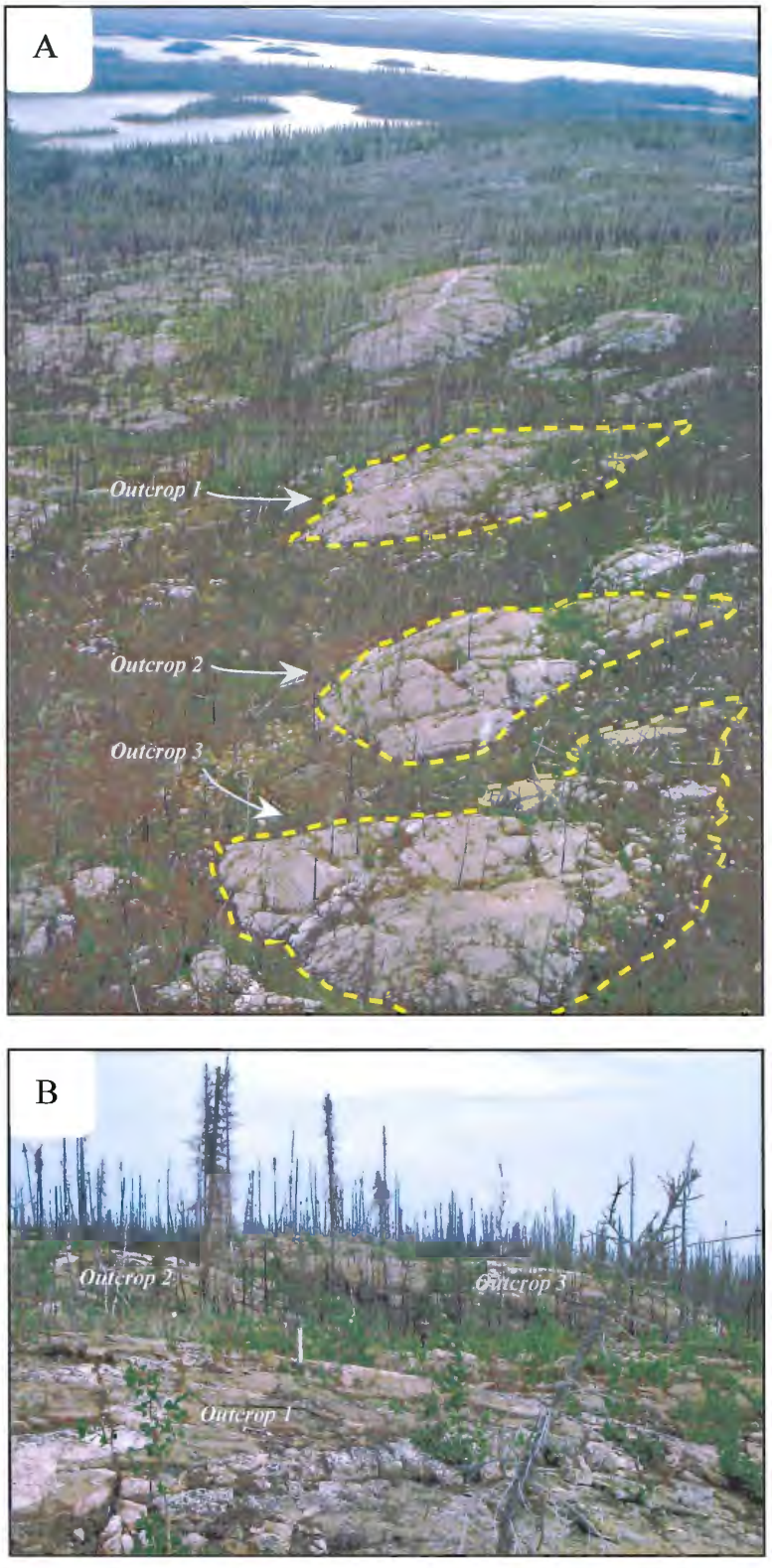

Figure 3.1: Leith Ridge study area outcrops. (A) Air photo of the three mapped outcrops, oriented to the south-west. (B) Ground photo displaying rounded outcrop morphologies, burnt standing trees and new growth after the recent forest fire in the area.

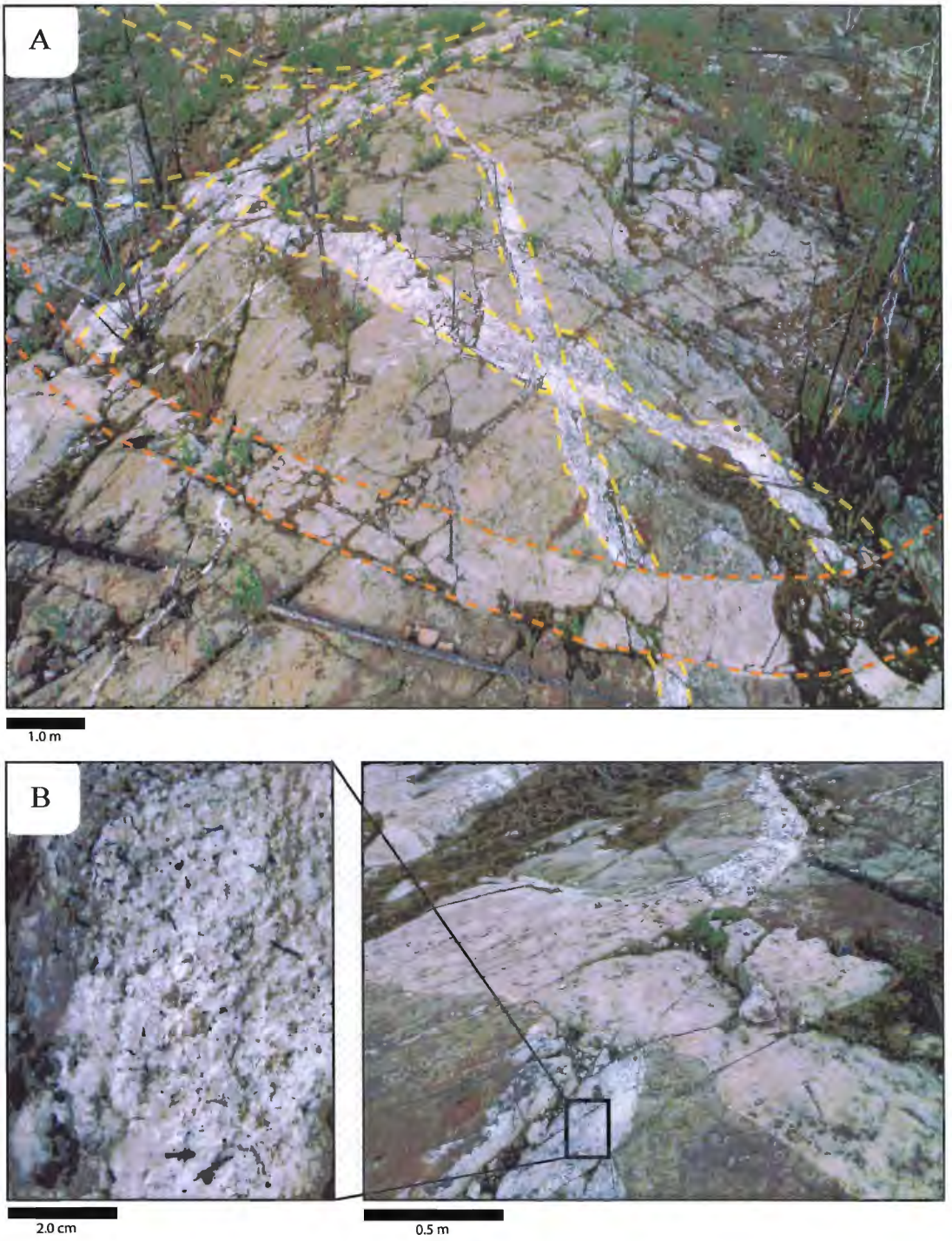

Figure 3.2: Igneous dyke intrusions within outcrop 1. (A) Air photo of igneous dyke intrusion crosscutting relationships. Yellow dashed lines represent early tourmaline-bearing pegmatite dyke (I_1) and yellow dashed line represents late amphibole-bearing granodiorite dyke (I_2). (B) Ground photo of cross cutting relationships between pegmatite and granodiorite dykes. On the left is a zoomed image of the pegmatite dyke with abundant tourmaline, quartz and feldspar.

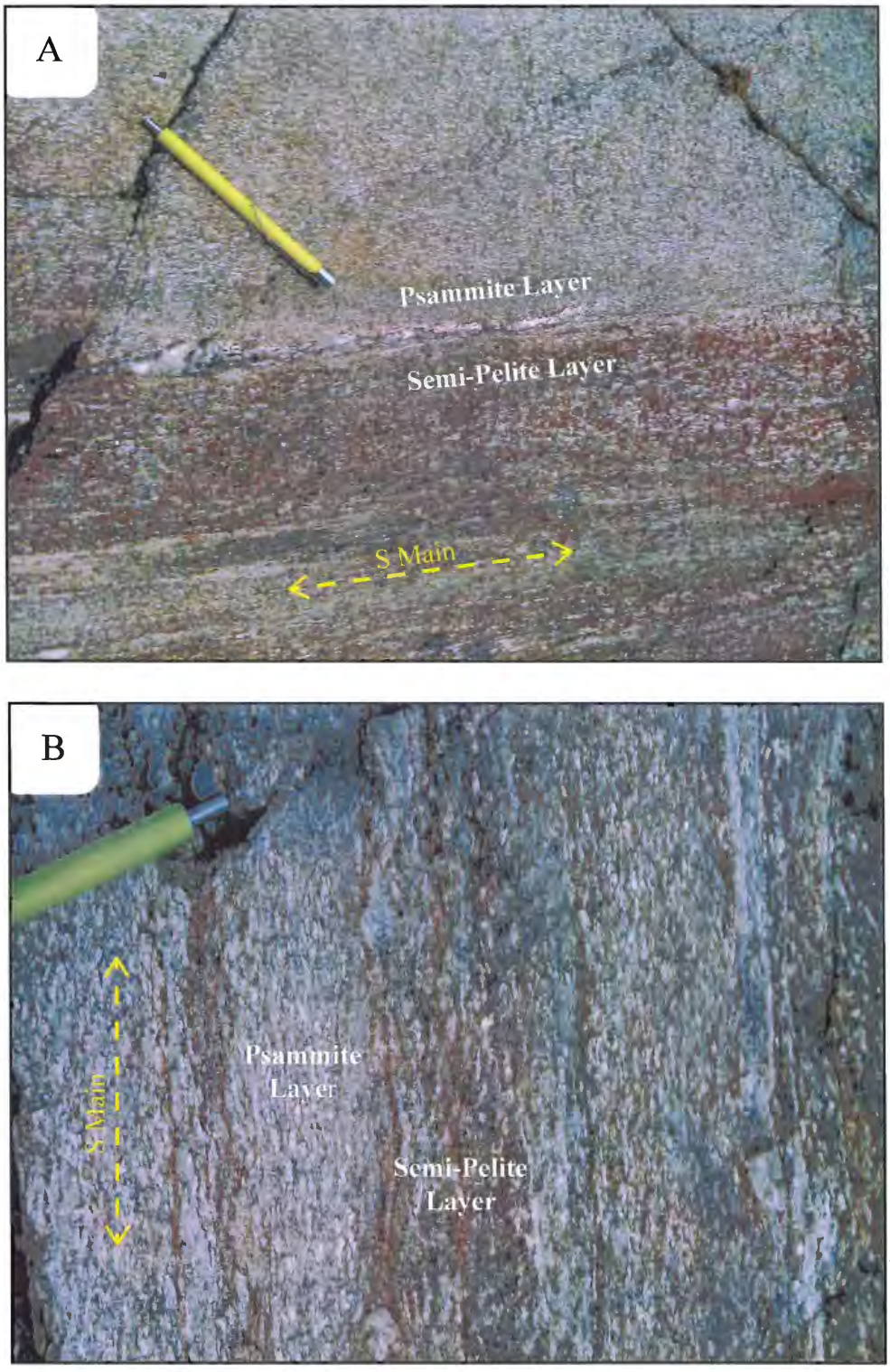

Figure 3.3: Outcrop textural relationships between semi-pelitic and psammite inter-layers. (A) Semi-pelitic and psammitic compositional layering, foliation defined by the alignment of biotite (S-main, striking northwest, dipping to the southeast). (B) A psammite rich horizon with foliation (S-main) defined by the alignment of biotite verses thicker quartzo-feldspathic assemblages. Pen magnet for scale, tip oriented north.

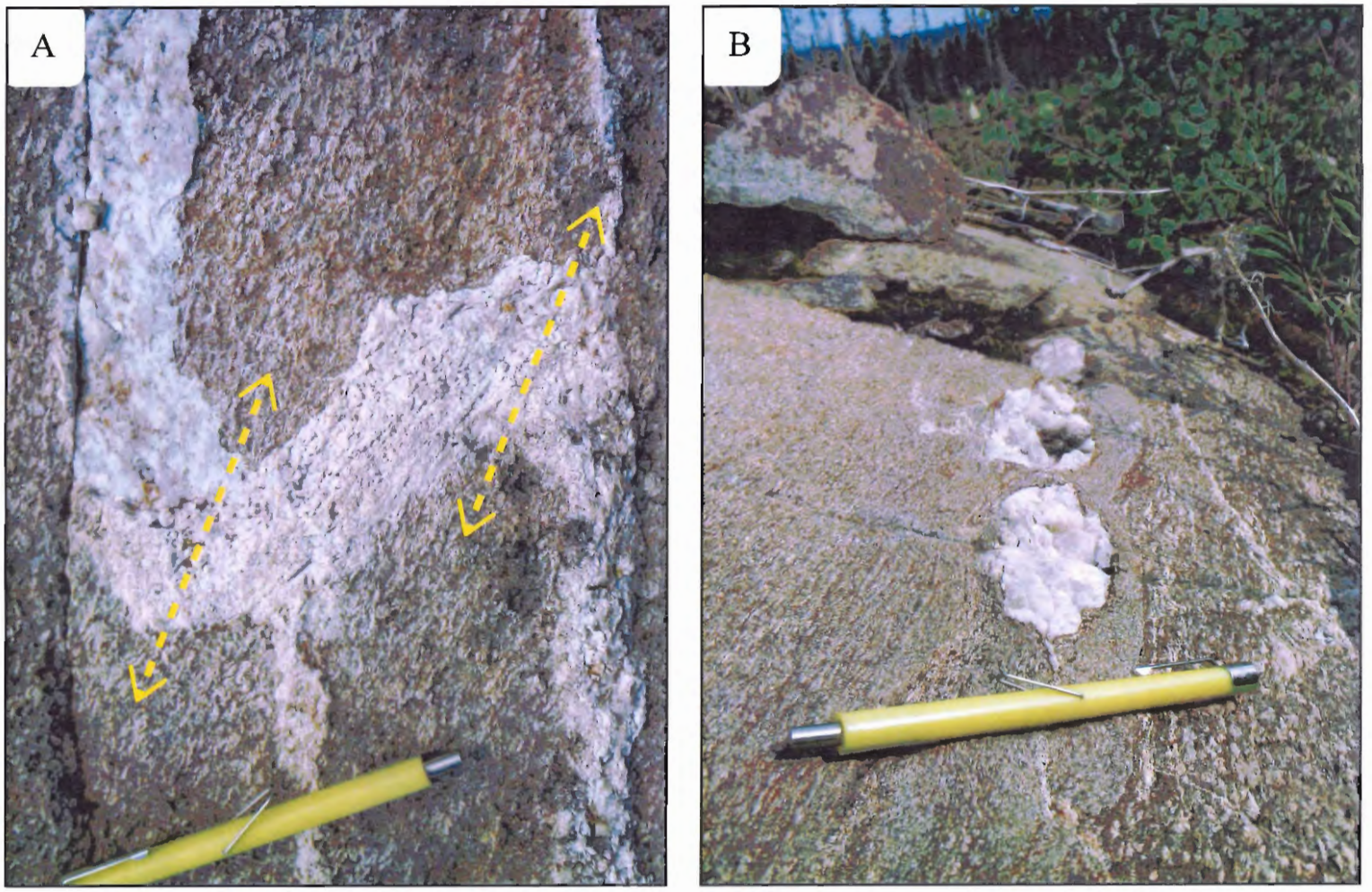

Figure 3.4: Quartz folds and boudins. (A) Shallowly plunging folded quartz vein with axial trace parallel to the main foliation (defined by the yellow arrows). (B) Quartz boudins near contact between psammitic and semi-pelitic inter-layers. Pen magnet for scale, tip oriented north.

Igneous dykes intrude all three outcrops and extend the full length of Leith Ridge. Intrusions within the study area include a suite of tourmaline-bearing pegmatites (0.5 m) that are cut by a series of deformed granodiorite dykes (1-1.5m). Both series of igneous dykes crosscut the main foliation. The pegmatite dykes are off-white with a speckled appearance due to abundant elongated tourmaline crystals (1-1.5 cm) (Fig. 3.2 B). Displaying no preferred trend, the pegmatite dykes crosscut the outcrops in a wide array of orientations (Fig 3.2). Hand samples of the fine-grained granodiorite are aphanitic with weathered surfaces that appear light-brown and fresh surfaces slate-grey. The granitic dykes are curvy-linear with an average nearly north-south strike.

3.4 Petrography

Pelites are distinguished from other common rocks types by high Al_2O_3, K_2O, SiO_2 and low CaO (Winter, 2010). Moreover, pelite compositions range from high Al to low Al types and grade through semi-pelites to lithic sandstones (Winter, 2010). Based on petrographic analysis it is the former lithology that dominates within the Leith Ridge study area, given moderate amounts of Al, high K_2O, SiO_2 and low CaO.

Semi-pelitic samples are medium-grained with inequigranular grain sizes ranging from 0.5 to 1.5 mm with smaller clastic grains < 0.01- 0.1 mm (e.g. detrital zircon). Semi-pelites consist mainly of biotite, quartz, potassium-feldspar and plagioclase (0.5-1.5 mm), with lesser amounts of muscovite, microcline, tourmaline, sillimanite and detrital grains. Gneissic, or migmatitic foliation is defined by alternating biotite-rich and quartzo-

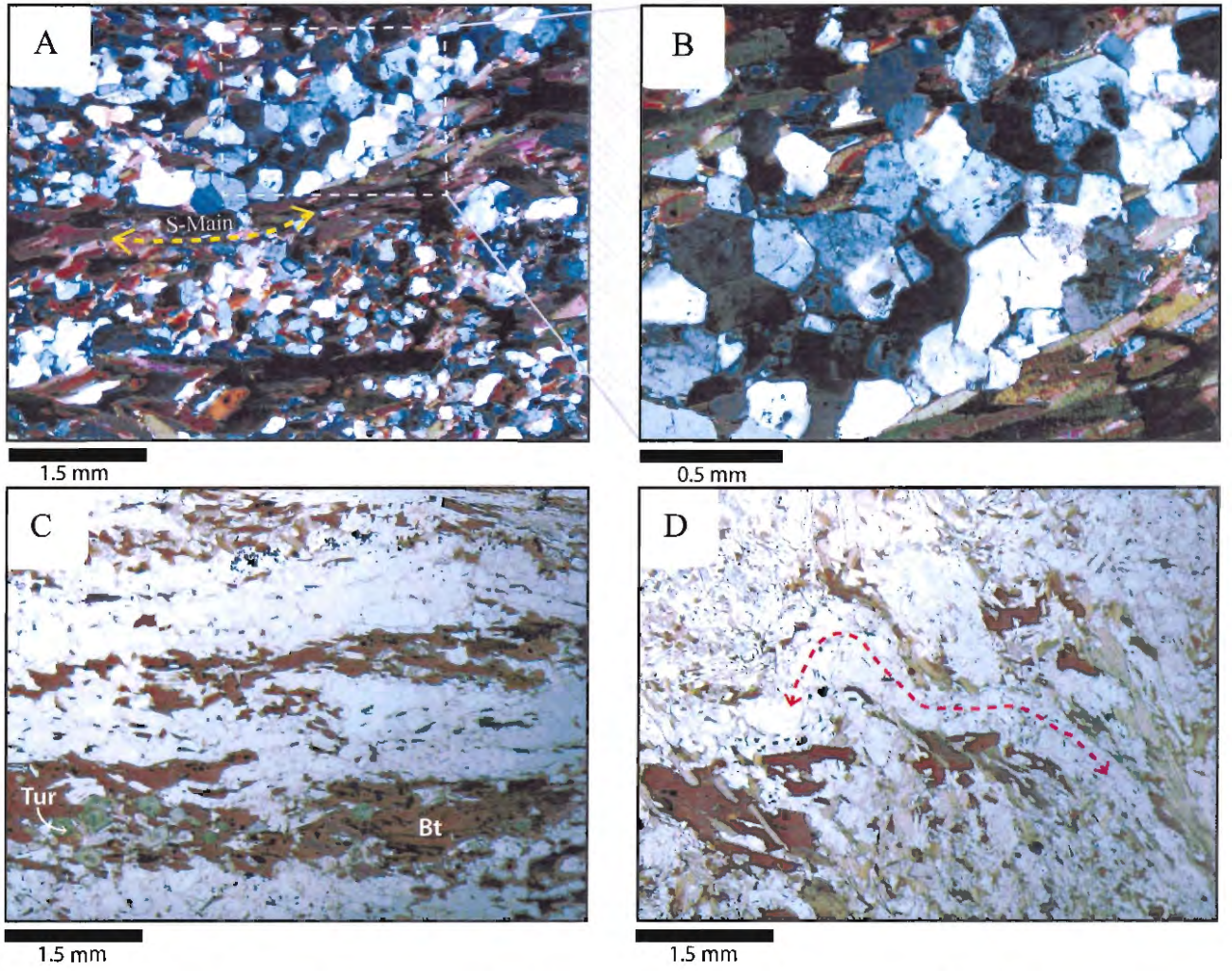

Figure 3. 5: Representative textures and mineral assemblages in semi-pelitic samples. (A), (C) Gneissosity defined by the alternation of platy biotite-rich layers and quartz-feldspar layers (*Sample 10Ln4002B-F, XPL*). (B) Enlarged image of (A), Microlithons of quartzo-feldspathic minerals displaying polymineralic granoblastic polygonal texture (*Sample 10Ln4002B-F, XPL*). (C) Tourmaline clustering in biotite-rich layers. Pleochroic halos spotted throughout given the abundance of radioactive mineral inclusions (*Sample 10Ln5005-Af, PPL*) (D) Quartzo-feldspathic rich layers shallowly folded, axial trace parallel to the main foliation (*Sample 10ln4002-A1, PPL*).

feldspathic layers, striking to the northwest and dipping to the southeast (315/45) (Fig. 3.5 A, B, C). Biotite grains (> 1.5-0.4 mm) contain abundant radioactive mineral inclusions that cause spotted pleochroic halos throughout that are likely zircon or monazite (Fig. 3.6 B). Some of the larger biotite grains display evidence of kink banding (Fig 3.8 A).

Microlithons of quartz, potassium-feldspar with local plagioclase and microcline display polymineralic granoblastic polygonal textures wedged between biotite foliation (Fig. 3.5 A, B). These quartzo-feldspathic domains are locally folded, with biotite aligned along the axial trace (Fig. 3.5 D), as also observed in the field (Fig 3.4 A). Clusters of idioblastic to subidioblastic tourmaline porphyroblasts are common within biotite-rich compositional layers. These crystals display distinct growth zoning (Fig. 3.6) and inclusion trails (Fig. 3.7). Tourmaline inclusions include quartz, sillimanite and iron-oxides and potentially fluid, that preserve an original fine-grained fabric (S_i) that runs nearly perpendicular to the main foliation (S_{main}) (Fig. 3.7). Generally, the quartz and iron-oxide inclusions form an inner-core aligned along a common orientation, with silli-

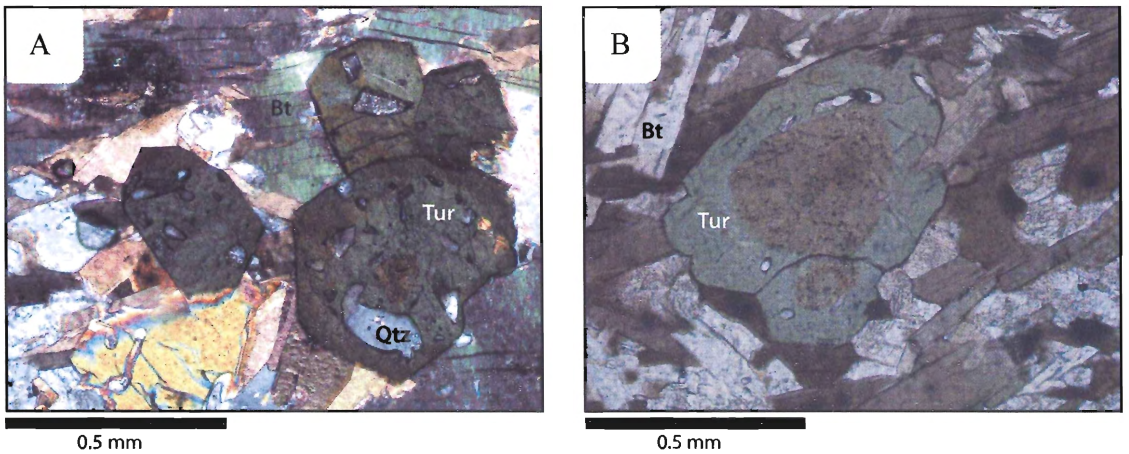

Figure 3. 6: Tourmaline porphyroblasts with quartz inclusions and distinct growth zoning. (A) A Nicely zoned tourmaline with small rounded quartz inclusions and abundant biotite with pleochroic halos (*Sample 10Ln4005-Ap, XPL*). (B) Idioblastic tourmaline porphyroblasts with distinct growth zoning (PPL).

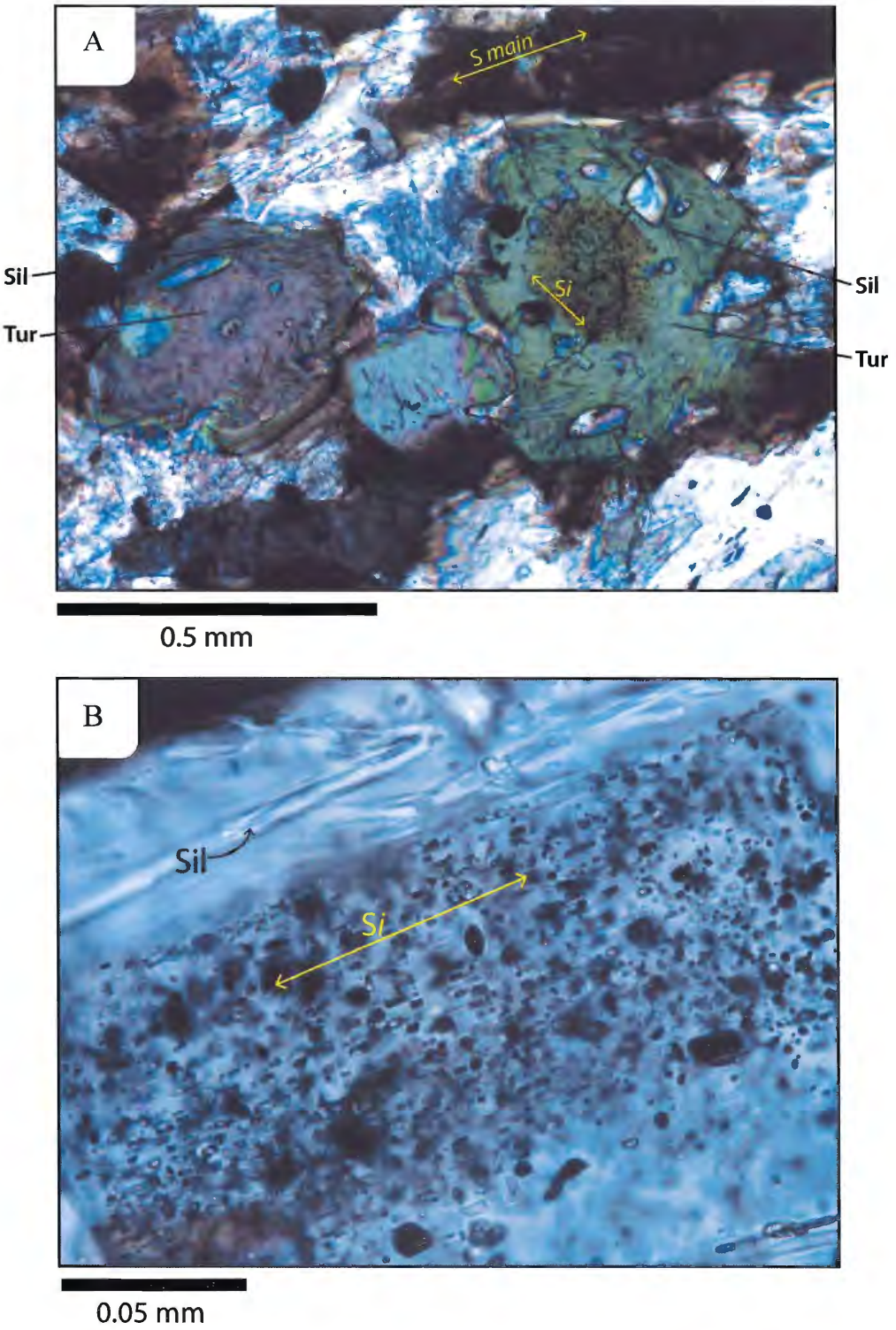

Figure 3. 7: Tourmaline with quartz + iron-oxide + sillimanite + fluid? inclusion trails. (A) Inner core inclusions rich in iron-oxides and quartz, striking nearly perpendicular to the main foliation (S_i= internal foliation). Sillimanite forming an outer-rim around tourmaline inner-core. (B) A zoomed image of the inclusion trails within tourmaline porphyroblasts, note the elongation of quartz inclusions and the abundance of iron-oxides forming an internal fabric (S_i).

imanite concentrated along the outer-core (Fig 3.7 B). In other cases, tourmaline grains lack the inner quartz and iron-oxide-rich core, and contain abundant randomly oriented sillimanite.

Muscovite is rare, and is intergrown with biotite and other minerals (Fig. 3.8 B), suggesting a retrograde origin. Moreover, muscovite is commonly found forming a mimetic texture, as fibrous aggregates replace previously existing rounded crystal shapes, possibly representing cordierite pseudomorphs (Fig 3.8 C, D).

Accessory minerals include monazite, zircon, apatite, iron-oxides and chlorite. Monazite is present throughout the samples, and displays distinct pleochroic halos where found as inclusions in biotite. It generally forms equant grains that range in size from 0.01 to 0.05 mm (Fig. 3.9 D). Zircons typically form irregular fractured grains with minor inclusions (0.05-2 mm), although prismatic zircons are also present (Fig 3.9 B, C) (for further zircon descriptions see Chapter 4). Apatite forms tabular, prismatic, fine-grained crystals dispersed evenly throughout the pelitic samples (< 0.05 mm). Iron-oxide minerals form irregular grain boundaries and are generally more common as inclusions within tourmaline porphyroblasts than in the matrix, and in many cases, are found only as inclusions.

Psammitic samples have more quartz and feldspar and less biotite when compared to semi-pelitic samples, and lack tourmaline porphyroblasts, cordierite pseudomorphs and apatite. Gneissic or migmatitic banding is lacking in psammitic samples, which instead display a schistosity defined by the alignment of platy biotite. Seritization is evident throughout both psammitic and pelitic lithologies, mainly affecting grain boundaries and calcium-rich plagioclase inner-cores.

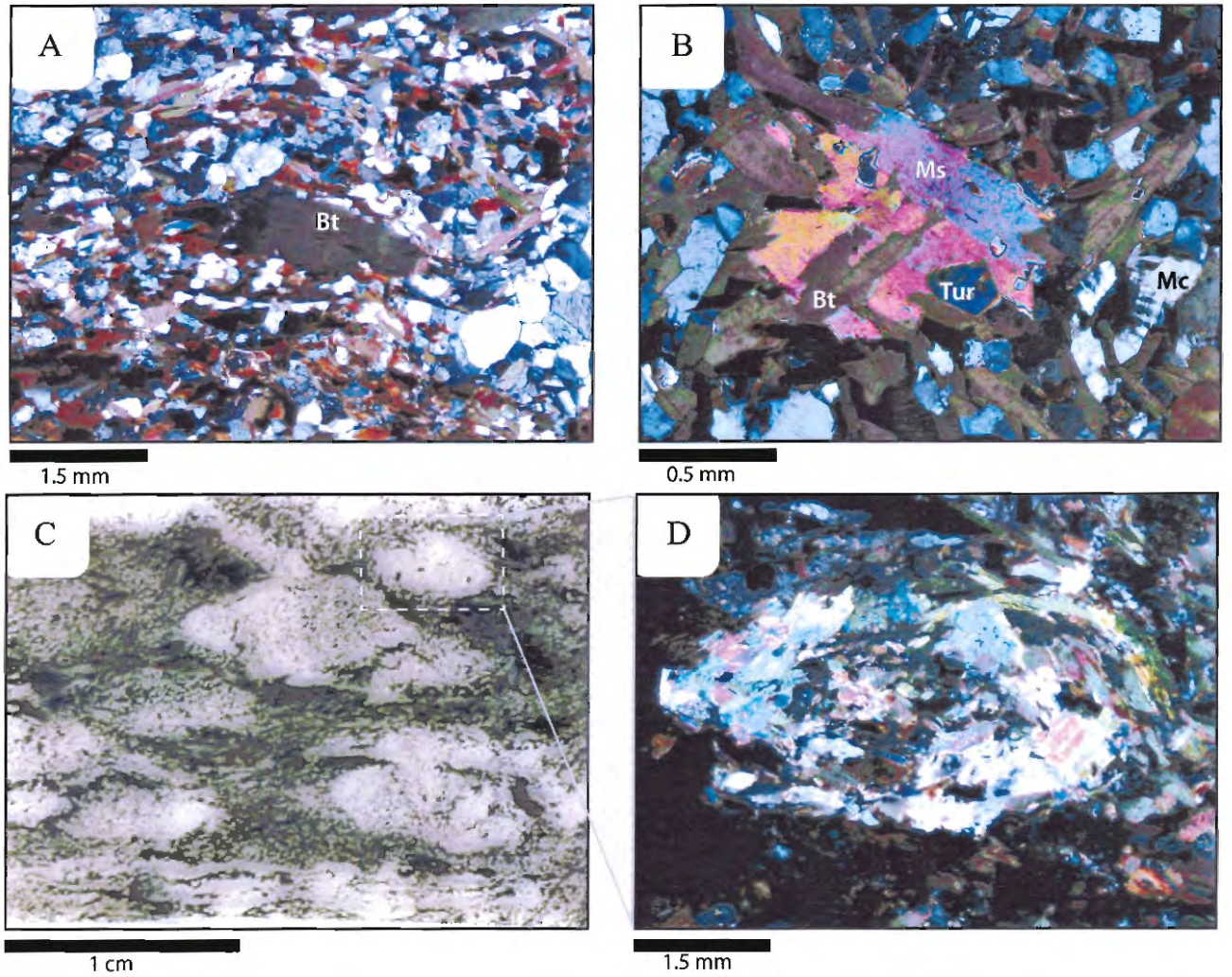

Figure 3. 8: Representative textures and mineral assemblages in semi-pelitic samples. (A) Course grained biotite with kink banding (*Sample 10Ln4002-Bf, XPL*). (B) Late muscovite overgrowing biotite and tourmaline. (C) A scanned image of a sample littered with potential cordierite pseudomorphs. (D) Potential cordierite pseudomorph, completely replaced by fibrous muscovite aggregates (*Sample 10Ln4005-A*).

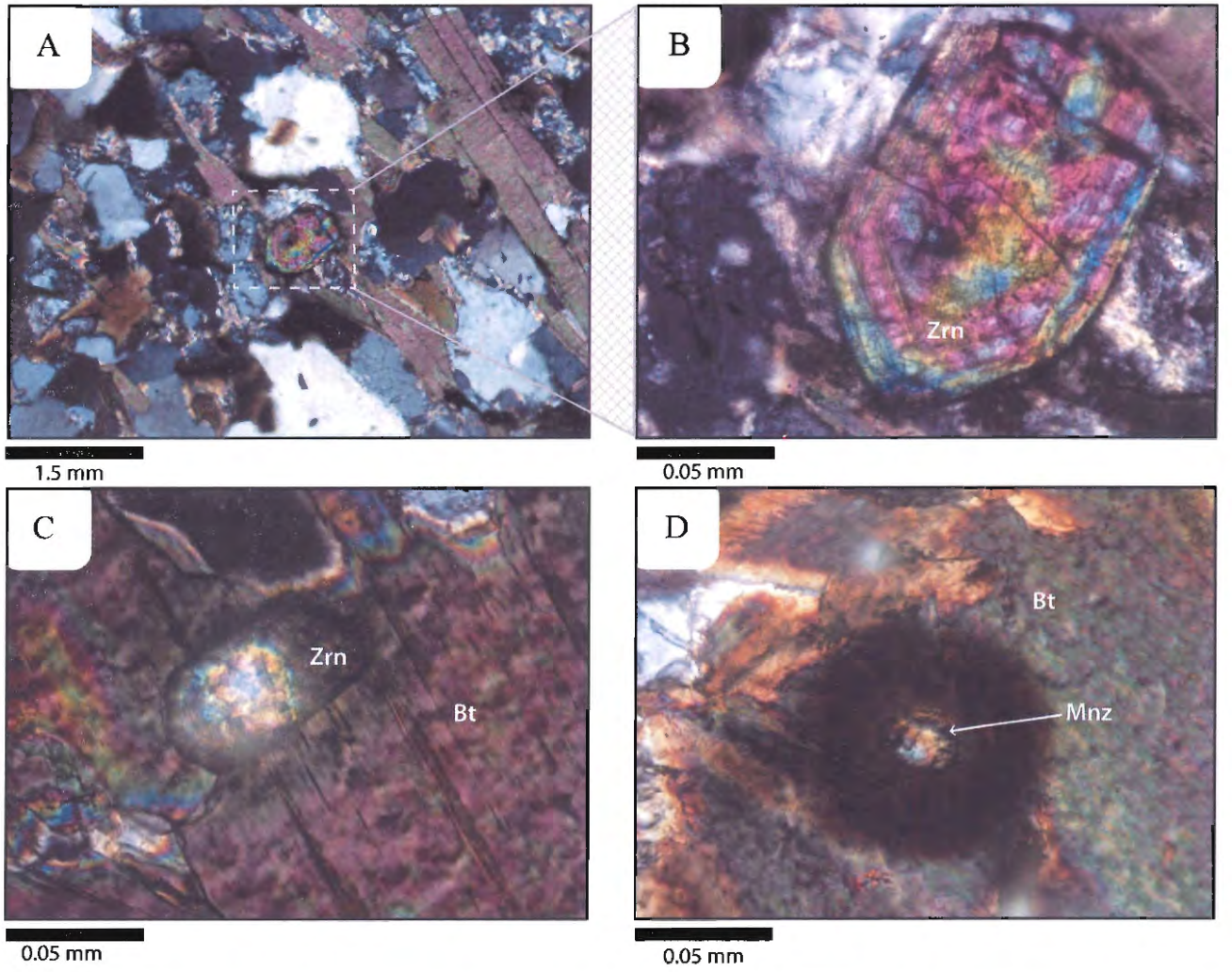

Figure 3. 9: Representative accessory mineral assemblages in pelitic and psammitic samples. (A) and (B): Unusually large detrital zircon grain with distinct oscillatory zoning. (C): A common euhedral zircon found as an inclusion within biotite, with corresponding faint pleochroic halo (*Sample 10Ln4005-Af, XPL*). (D) Equant monazite grain found as inclusion within biotite with corresponding perfectly round pleochroic halo (*Sample 10Ln4005-Af, XPL*).

3.4.1 Igneous Intrusions

The late granodiorite dykes that cross-cut the metasedimentary rocks and pegmatites are composed of plagioclase, quartz, potassium-feldspar, biotite and amphibole (Fig. 3.10). Quartz grains are generally fine-grained, although coarser (> 1.5 mm) grains are randomly dispersed throughout the sample (Fig. 3.10 A). Euhedral to subhedral amphibole phenocrysts are also present, ranging from fine (< 0.1mm) to coarse grained (> 1mm) (Fig 3.10 C).

A weak foliation is defined by aligned biotite (Fig 3.10 A), although this deformation was not identified in the field. Plagioclase commonly displays serrated grain boundaries (Fig. 3.10 D) and calcium-rich cores and grain boundaries are commonly sericitised (Fig. 3.10 B, D).

3.4.2 Drill Core Samples

HLMC core samples display distinct variations from the mineralogical and textural relationships observed in outcrop samples. In particular core samples are almost completely hematized, as evident from the rich rusty colouration (Fig. 3.11). As a result, many important mineralogical and textural relationships have been obliterated and petrographic results are limited. Irregular patchy leucosomes (~ 5 cm) dispersed throughout the core samples are similar, although larger, to those observed in the Leith Ridge outcrops. Furthermore, foliation is defined by the alignment of phyllosilicates (Fig 3.12 A, B).

The cores are mainly composed of quartz, potassium-feldspar, muscovite and graphite. Quartz and potassium-feldspar are recrystalized with irregular annealed textures

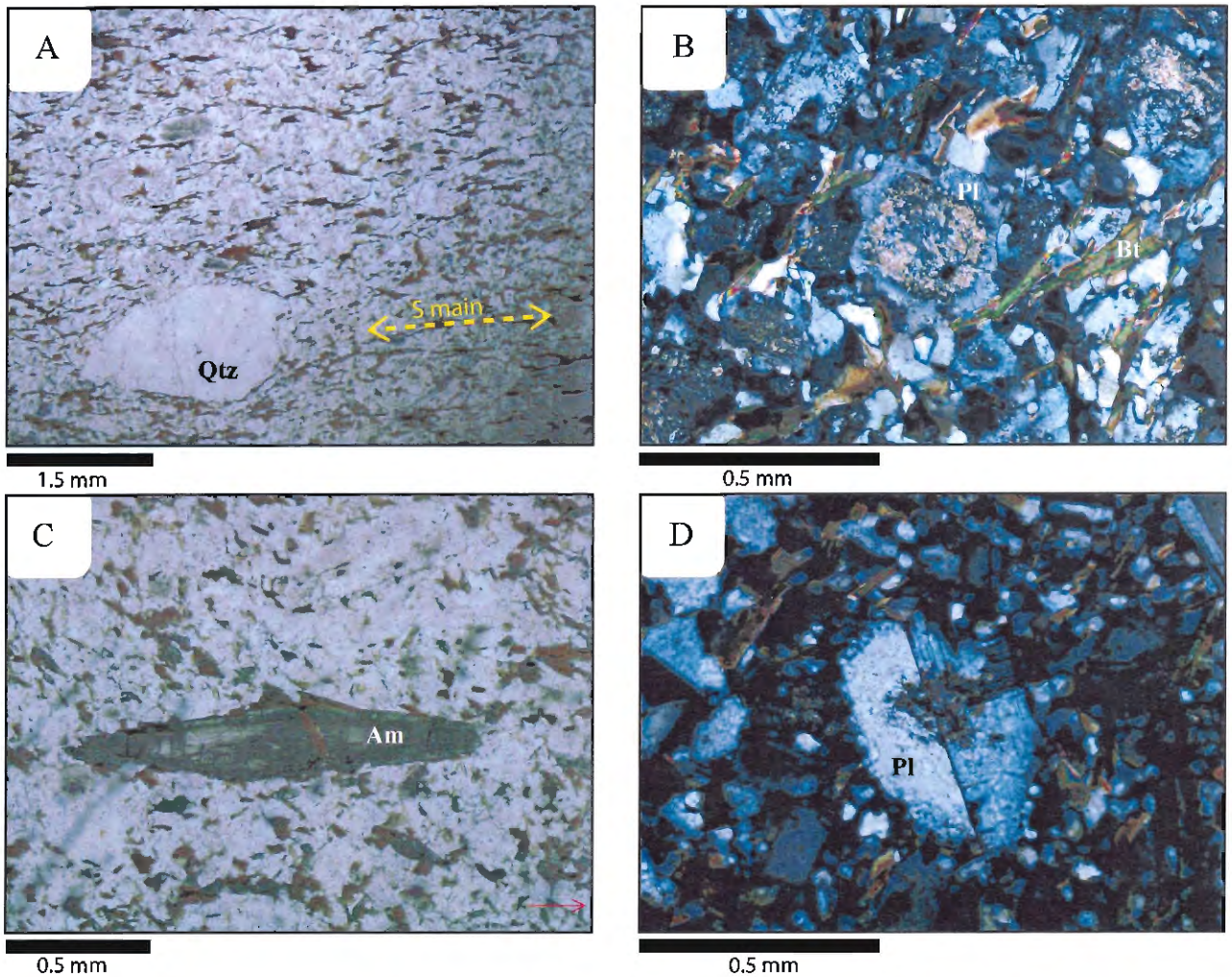

Figure 3. 10: Representative textures and mineral assemblages within granodiorite dyke (*Sample 10Ln4002-C*). (A) Foliation defined by alignment of biotite (S-main), note the coarse grained clastic quartz grain (*PPL*). (B) and (D) Plagioclase with inner calcium-rich core breaking down into sericite (*XPL*). (C) Coarse grained amphibole, with finer grains littered throughout the sample

and sutured grain boundaries (Fig 3.12 D). Muscovite displays kink banding and more commonly forms aligned fibrous aggregates, neither of which were observed in outcrop samples discussed above (Fig. 3.12 A, B). Graphite forms fine-grained fibrous aggregates displaying radial textures. In general, hematite has replaced most of the minerals, infilling mineral cleavages and obliterating textural relationships.

Figure 3. 11: HLMC core samples retrieved from Cameco core box on Fenwick Lake, Leith Peninsula. Cores are highly hematized, evident by the rusty coloration. Melt pods abundant with foliation defined the alignment of phyllosilicates.

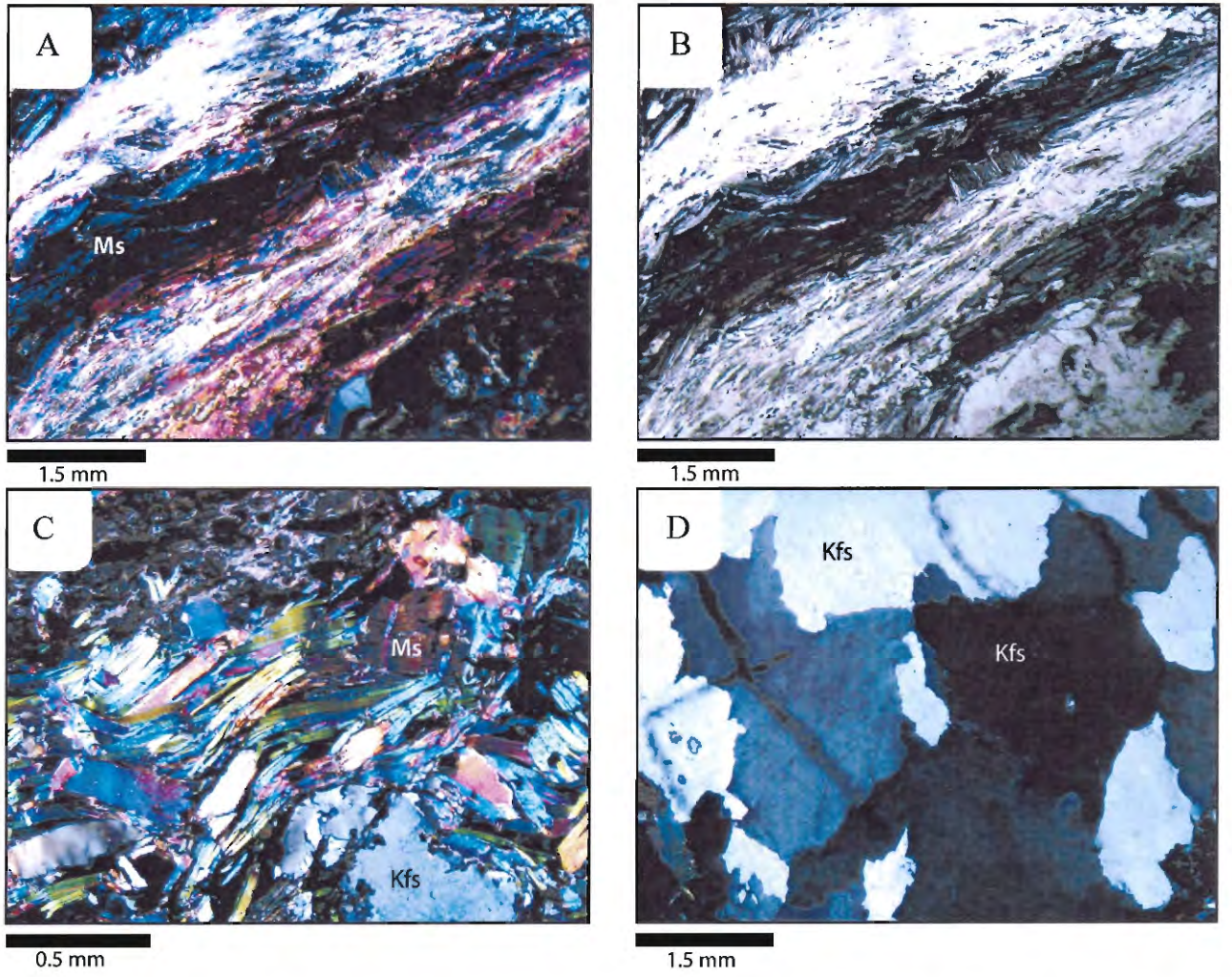

Figure 3. 12: Representative textures and mineral assemblages in core samples. (A) and (B): Fibrous muscovite that has been almost completely replaced by hematite, defining the main foliation (*A=XPL, B=PPL*). (C): Kink banding within muscovite (*XPL*). (D): Recrystalized feldspar with irregular grain boundaries. (*XPL*).

CHAPTER 4: SHRIMP U-Pb DETRITAL ZIRCON GEOCHRONOLOGY

4.1 Sample Location and Description

Detrital zircons were retrieved from a ~ 2.5 kg psammite sample collected from outcrop 2. The outcrop at the sample site is composed 0.5 to 2 m thick semi-pelitic and psammitic inter-layers. Psammitic layers are pale-grey in colour, mainly uniform and massive (1.5 to 2.0 m thick) with foliation defined by the alignment of biotite. All sedimentary features are completely transposed into the main metamorphic fabric that strikes to the northwest and dips to the southeast. The sample is composed of quartz, feldspars (plagioclase and K-feldspars), biotite and accessory minerals including zircon, monazite and minor amounts of iron-oxides. Zircons range from 15 to 40 grains per slide.

4.2 Analytical Methodology

U-Pb analyses were performed on the SHRIMP II at the J.C. Roddick Ion Microprobe SHRIMP Laboratory located at the Geological Survey of Canada (GSC), Ottawa, Ontario. Specific analytical procedures using the SHRIMP II are outlined in Stern (1996, 1997) and Stern and Amelin (2003).

Zircons were extracted from the rock sample by standard crushing, heavy liquid, and magnetic separation techniques in Ottawa. 127 zircon grains were selected at random from the least-magnetic fractions with grain sizes ranging from 65 to 200 μm with an average size of ~ 100 μm. Grains were mounted on a 2.5 cm epoxy disk and polished to half-grain thicknesses. With a scanning electron microscope (SEM) (Cambridge S-360 model with an Oxford Link Analytical eXL-II), back-scattered electron (BSE) and cathodoluminescence (CL) images were taken and used to locate and guide individual

analysis, targeting zircon cores while avoiding fractures and inclusions (See Appendix A for BSE images). Lighter areas of a zircon in the BSE image are indicative of higher than average atomic weight, in zircons in general that indicates higher U and/or Hf concentrations relative to Pb. This imaging technique is particularly useful for revealing internal structures otherwise not detected by transmitted light microscopy (Guan et al., 2002). Internal structures in zircons were also used to help interpret mineral genesis (e.g. magmatic vs. metamorphic) and multiple growth history (Guan et al., 2002); this information was used for interpretation of the geochronology data herein. Metamorphic textures include single or multiple overgrowths, "soccer ball" or resorbed textures and distinctive cathodoluminescence zoning whereas oscillatory zoning is the most indicative texture of igneous zircons (Corfu et al., 2003). Ratios between Th and U are also commonly used to distinguish metamorphic and igneous zircons. Igneous derived zircons typically have high Th/U ratios (0.2-1.5) (Hartmann and Santos, 2004) and zircons grown during metamorphism have low Th/U ratios (0.001-0.1, and high U (ppm) concentrations) (Rubatto, 2002; Hartmann and Santos, 2004). Moreover, zircons enrichment of HREE with respect to LREE can also indicate that they grew during metamorphism (Rubatto, 2002).

Included on the epoxy disk was GSC zircon standard 6266 ($^{206}Pb/^{238}U$ age = 559 Ma) and standard 1242 (2681 Ma), that were used to calibrate U-Pb ratios according to the methods described in Stern and Amelin (2003) (See appendix C for standard isotopic data). A measured uncertainty of 1% in the calibration was propagated to the unknowns.

A total of 88 spots were analyzed on 75 grains out of the 127 mounted zircon grains. Generally, one spot was analyzed per zircon grain however, several grains were

analyzed numerous times and metamorphic overgrowths targeted (grains analyzed numerous times include grain no. 7, 50, 47, 51, 63, 78, 85 and 102). The full analyses took two full days and one overnight run.

Primary beam currents were on average ~ 5 nA. These generated elliptical pits with a diameter of 25 μm. Individual analysis took 15 minutes per spot, creating pits < 1 μm deep. Measured isotopic ratios for common lead were corrected for by estimates of monitored ^{204}Pb. Ages and corrected ratios presented in Table 1 are 1σ errors at 68% confidence level (unless otherwise noted). Different operation conditions were applied for core and for the metamorphic overgrowths. For metamorphic overgrowths the beam currents were reduced to ~ 0.5 nA, and the beam diameter was significantly reduced in order to target thin single rims.

SHRIMP U-Pb data reduction was completed at the GSC laboratory using SQUID 2.5 (Ludwig, 2009). The processed data were applied to calculate raw isotope ratios, radiogenic Pb isotope ratios and ages for the U-Th-Pb system. After the data were processed, it was placed in a "dead" Excel workbook for graphical manipulations. Concordia and frequency-probability plots were completed with Isoplot 3.7 (Ludwig, 2008) and Age-Display macro (Sircombe, 2003). Herein, age discussions and graphical representations are based on $^{207}Pb/^{206}Pb$ apparent ages rather than $^{206}Pb/^{238}U$ ages (Table 1, bolded), given that ages within this study are > 1.0 Ga. Discordance of each analysis is based on $^{207}Pb/^{235}Pb$ and $^{206}Pb/^{238}Pb$ correlation. The discordance between $^{206}Pb/^{238}U$ and $^{207}Pb/^{235}U$ ages greater than 500 Ma may be the result of lead loss during later metamorphism. For this reason, $^{207}Pb/^{206}Pb$ ages are considered more reliable for analysis greater than 500 Ma (e.g., Martin et al., 2005).

Zircon analysis with less than 95% and over 105% concordance are excluded in further discussions, interpretations and graphical representations except where otherwise noted (64 out of 75 analysis remain with concordance between 95-105%). Refer to Appendix C for a complete list of U-Pb analytical results.

4.3 Analytical Results

4.3.1 Detrital Zircon Core Ages

The zircon U-Pb isotopic results are listed in Table 1, and graphically represented on a concordia diagram and a frequency-probability histogram (Fig 4.1). The data have an age range from ca. 2640 to 1950 Ma. The concordance-filtered graph displays a polymodal age distribution, with two predominant age peaks and several smaller ones. The largest peak is at ca. 1970 Ma, followed by another older peak at ca. 2460 Ma. Smaller, yet significant peaks are located at ca. 2558 and ca. 2420 Ma. Other individual ages include 2164 ± 7, 2184 ± 9, 2288 ± 6, 2308 ± 17, 2336 ± 18 and 2640 ± 13 Ma. The youngest and oldest zircon grains are 1951 ± 11 Ma and 2640 ± 13 Ma, respectively (Fig 4.1). The age of the 5^{th} youngest detrital zircons grain is 1959 ± 9 (95% confidence) interpreted as the maximum deposition age of the HLMC. In addition, the age distribution indicates that 83% (53 out of 64) of the zircons are derived from a middle to early Paleoproterozoic source, with a remaining 17 % (11 out of 64) derived from a Neoarchean Source.

Table 1: U-Pb SHRIMP isotopic data for detrital zircon grains from a psammite sample of the Holly Lake Metamorphic complex, Leith Ridge, NWT.

Spot No.	U (ppm)	Th (ppm)	Th/U	Pb* (ppm)	$^{204}Pb/^{206}Pb$	err (%)	com^{206}Pb (%)	$^{208}Pb^*/^{206}Pb^*$	err (%)	$^{207*}Pb/^{235}U$	err (%)	$^{206}Pb/^{238}U$	err (%)	$^{206*}Pb/^{238}U$	err (%)	$^{208}Pb/^{232}Th$	err (%)	Apparent Ages (Ma) 204 corr $^{206}Pb/^{238}U$	1σ	207 Corr $^{206}Pb/^{238}U$	1σ	208 Corr $^{206}Pb/^{238}U$	1σ	204 Corr $^{207}Pb/^{206}Pb$	1σ	204 Corr $^{208}Pb/^{232}Th$	1σ	Conc. (%)
10319-102.2	279	23	0.08	77	3.5E-3	19	6.09	0.029	8.6	4.7	9.6	0.34	2.0	0.32	2.4	0.640	10.2	1798	37	1806	37	1795	15	**1742**	**170**	2125	1799	103.7
10319-85.2	754	195	0.27	199	1.0E-3	5	1.79	0.094	1.6	4.8	1.4	0.31	1.2	0.31	1.2	0.153	2.0	1727	18	1711	20	1715	5	**1851**	**14**	2079	60	92.4
10319-63.1	131	59	0.47	41	1.6E-4	22	0.27	0.130	3.0	6.0	1.4	0.37	1.2	0.37	1.2	0.106	3.3	2022	21	2040	26	2026	8	**1924**	**13**	1961	64	106.0
10319-63.1.2	138	63	0.47	43	1.1E-4	69	0.19	0.132	3.3	6.0	1.8	0.37	1.4	0.37	1.4	0.105	3.6	2016	24	2032	29	2019	8	**1929**	**19**	1967	79	105.3
10319-50.1	410	160	0.40	179	3.7E-4	16	0.64	0.130	2.2	8.3	1.9	0.51	1.7	0.51	1.7	0.181	2.8	2646	36	2951	74	2625	12	**1930**	**15**	3064	93	145.3
10319-78.2	195	68	0.36	60	1.4E-4	24	0.25	0.096	2.9	5.9	1.4	0.36	1.2	0.36	1.2	0.101	3.3	1988	20	1998	24	1994	7	**1932**	**11**	1854	62	103.3
10319-63.1.3	134	62	0.47	43	2.3E-4	32	0.40	0.137	3.3	6.1	1.6	0.37	1.2	0.37	1.2	0.114	3.5	2044	20	2065	25	2043	8	**1933**	**19**	2063	80	106.7
10319-50.2	358	303	0.87	102	1.5E-3	5	2.54	0.269	1.2	5.4	1.6	0.33	1.0	0.34	1.0	0.123	1.6	1845	17	1831	19	1831	8	**1936**	**21**	1960	36	94.6
10319-85.2.2	704	285	0.42	184	1.4E-3	11	2.40	0.146	3.2	5.0	2.3	0.31	1.1	0.30	1.2	0.145	3.4	1715	18	1685	19	1696	7	**1939**	**36**	2051	103	87.0
10319-47.1	764	148	0.20	246	8.3E-4	13	1.44	0.054	4.0	6.1	1.8	0.38	1.1	0.37	1.2	0.158	4.2	2049	20	2069	24	2052	8	**1944**	**25**	1930	157	106.3
10319-50.1.2	268	155	0.60	86	3.9E-4	13	0.67	0.172	1.9	6.1	1.3	0.37	1.1	0.38	1.0	0.117	2.2	2044	18	2062	22	2042	8	**1945**	**13**	2070	49	105.9
10319-47.1	263	82	0.32	79	2.7E-4	16	0.47	0.091	2.4	5.8	1.2	0.35	1.0	0.35	1.0	0.109	2.6	1934	18	1932	20	1936	7	**1951**	**11**	1896	57	99.0
10319-36.1	499	220	0.46	149	3.4E-6	203	0.01	0.133	1.5	5.8	1.1	0.35	1.0	0.35	1.0	0.102	1.9	1929	17	1925	20	1927	6	**1952**	**6**	1963	35	98.6
10319-29.1	204	140	0.71	64	1.0E-4	28	0.17	0.210	2.0	6.0	1.2	0.37	1.1	0.37	1.1	0.111	2.3	2011	18	2022	22	2004	8	**1954**	**10**	2084	46	103.4
10319-78.3	738	397	0.55	212	1.5E-4	13	0.27	0.160	1.3	5.5	1.1	0.33	1.0	0.34	1.0	0.100	1.7	1861	16	1847	19	1861	6	**1957**	**6**	1868	31	94.4
10319-50.3	297	158	0.55	93	1.8E-4	44	0.30	0.153	2.4	6.1	1.4	0.37	1.0	0.37	1.0	0.106	2.7	2009	18	2018	21	2013	8	**1959**	**17**	1956	61	103.0
10319-78.1	719	380	0.55	202	6.8E-4	6	1.17	0.167	1.1	5.4	1.3	0.33	1.1	0.33	1.1	0.115	1.6	1822	18	1801	20	1814	6	**1960**	**9**	1922	33	91.9
10319-21.1	290	129	0.46	86	4.4E-5	60	0.08	0.132	1.9	5.8	1.2	0.35	1.1	0.35	1.1	0.101	2.2	1921	19	1913	22	1921	7	**1966**	**8**	1917	43	97.3
10319-118.1	229	229	1.03	71	4.4E-5	37	0.08	0.304	1.6	6.0	1.1	0.36	1.0	0.36	1.0	0.108	1.9	1998	18	2004	21	1990	9	**1967**	**8**	2058	37	101.9
10319-69.1	507	442	0.90	156	3.5E-5	39	0.06	0.261	1.1	6.0	1.3	0.36	1.2	0.36	1.2	0.104	1.6	1971	21	1971	24	1967	8	**1968**	**6**	1997	31	100.1
10319-25.1	198	58	0.30	61	1E-32	100	0.00	0.088	3.1	6.0	1.3	0.36	1.2	0.36	1.2	0.104	3.3	1973	20	1974	24	1972	7	**1969**	**9**	2000	63	100.2
10319-68.1	169	49	0.30	52	1.0E-4	27	0.18	0.088	3.1	6.0	1.2	0.36	1.1	0.36	1.1	0.112	3.4	1989	19	1993	22	1987	7	**1969**	**10**	2054	69	101.2
10319-53.1	425	206	0.50	120	5.9E-4	7	1.03	0.149	1.4	5.5	1.2	0.33	1.0	0.33	1.0	0.113	1.8	1833	16	1812	19	1829	6	**1970**	**10**	1892	39	92.0
10319-76.1	364	111	0.32	110	1.4E-4	19	0.24	0.090	2.1	5.9	1.1	0.35	1.0	0.35	1.0	0.106	2.4	1939	17	1934	20	1939	6	**1971**	**8**	1933	49	98.1
10319-59.1	383	164	0.44	121	2.5E-5	103	0.04	0.130	1.7	6.1	1.1	0.37	1.0	0.37	1.0	0.109	2.0	2021	18	2029	22	2017	7	**1973**	**8**	2084	42	102.8
10319-17.1	171	28	0.17	52	7.8E-5	34	0.14	0.044	4.3	5.9	1.2	0.35	1.1	0.35	1.1	0.100	4.5	1955	18	1951	21	1958	6	**1974**	**10**	1807	87	98.9
10319-23.1	152	78	0.53	46	1.4E-4	26	0.24	0.157	2.4	5.9	1.3	0.35	1.1	0.35	1.1	0.108	2.7	1954	18	1950	22	1950	7	**1976**	**12**	2007	54	98.7
10319-52.1	263	188	0.74	76	8.5E-4	9	1.48	0.217	1.6	5.6	1.5	0.34	1.2	0.34	1.2	0.113	2.1	1868	19	1851	21	1865	8	**1977**	**17**	1902	44	93.6
10319-51.1	235	40	0.18	75	2.2E-4	18	0.39	0.048	3.5	6.2	1.2	0.37	1.1	0.37	1.1	0.119	3.7	2042	18	2054	22	2044	7	**1978**	**11**	1946	90	103.8
10319-1.1	67	58	0.90	21	1.2E-4	24	0.20	0.266	3.0	6.1	1.5	0.36	1.2	0.36	1.2	0.108	3.2	1977	20	1974	24	1969	10	**1994**	**15**	2042	63	99.0
10319-74.1	334	228	0.71	105	2.6E-5	110	0.05	0.207	1.5	6.2	1.2	0.37	1.1	0.37	1.1	0.108	1.8	2007	18	2009	22	2002	8	**1995**	**8**	2063	38	100.7
10319-20.1	156	60	0.40	48	7.1E-5	37	0.12	0.114	2.8	6.1	1.2	0.36	1.1	0.36	1.1	0.106	3.0	1991	18	1990	22	1991	7	**1996**	**10**	1993	60	99.7
10319-54.1	153	205	1.39	44	2.1E-4	22	0.37	0.412	1.7	5.7	1.4	0.33	1.2	0.34	1.2	0.101	2.1	1860	19	1839	22	1849	10	**1997**	**13**	1917	38	92.1
10319-10.1	202	74	0.38	64	2.4E-4	18	0.41	0.100	2.7	6.2	1.3	0.37	1.1	0.37	1.1	0.106	3.0	2015	19	2017	23	2022	7	**2002**	**12**	1875	61	100.8
10319-51.2	64	21	0.34	19	2.6E-4	29	0.45	0.101	4.6	6.0	1.8	0.35	1.4	0.35	1.4	0.113	4.8	1937	24	1925	28	1934	8	**2007**	**20**	1992	105	96.0
10319-40.1	127	39	0.32	40	5.5E-5	37	0.10	0.097	3.4	6.2	1.3	0.37	1.1	0.37	1.1	0.112	3.6	2010	19	2010	23	2006	7	**2007**	**11**	2112	74	100.2
10319-70.1	456	318	0.72	134	6.8E-4	7	1.17	0.213	1.2	5.9	1.2	0.34	1.0	0.35	1.0	0.113	1.6	1898	17	1877	19	1893	7	**2022**	**10**	1951	33	92.9
10319-121.1	158	51	0.34	50	5.3E-5	25	0.09	0.103	3.1	6.4	1.3	0.37	1.2	0.37	1.2	0.116	3.3	2026	21	2027	24	2020	7	**2026**	**10**	2172	69	100.0
10319-85.1	414	162	0.40	129	1.0E-5	175	0.02	0.120	1.7	6.3	1.1	0.36	1.0	0.36	1.0	0.108	2.0	2000	18	1995	21	1997	7	**2028**	**6**	2069	41	98.4
10319-37.1	119	67	0.58	39	1.7E-4	30	0.29	0.167	2.6	6.6	1.5	0.38	1.3	0.38	1.3	0.114	2.9	2079	22	2088	27	2076	9	**2033**	**14**	2112	62	102.6
10319-79.1	459	315	0.71	139	2.0E-4	13	0.35	0.210	1.2	6.1	1.2	0.35	1.0	0.35	1.0	0.108	1.6	1945	17	1930	20	1939	7	**2034**	**11**	2006	32	95.0
10319-26.1	39	24	0.63	13	2.3E-4	142	0.39	0.167	4.7	6.6	3.8	0.38	1.4	0.38	1.3	0.107	4.9	2078	24	2082	27	2087	11	**2054**	**62**	1955	161	101.4
10319-27.1	158	72	0.47	51	1.3E-4	25	0.22	0.137	2.5	6.6	1.3	0.38	1.2	0.38	1.2	0.112	2.8	2055	21	2055	25	2054	8	**2056**	**10**	2078	57	100.0
10319-39.1	140	139	1.03	47	6.1E-5	38	0.11	0.292	2.9	6.9	1.5	0.39	1.4	0.39	1.4	0.112	3.2	2116	25	2124	30	2115	12	**2082**	**10**	2123	66	101.9

Table 1: *Continued from previous page.*

Spot No.	U (ppm)	Th (ppm)	Th/U	Pb* (ppm)	$^{204}Pb/^{206}Pb$	err (%)	com ^{206}Pb (%)	$^{208}Pb^*/^{206}Pb^*$	err (%)	$^{207*}Pb/^{235}U$	err (%)	$^{206*}Pb/^{238}U$	err (%)	$^{206*}Pb/^{238}U$	err (%)	$^{208}Pb/^{232}Th$	err (%)	Apparent Ages (Ma) 204 Corr $^{206}Pb/^{238}U$	1σ	207 Corr $^{206}Pb/^{238}U$	1σ	208 Corr $^{206}Pb/^{238}U$	1σ	204 Corr $^{207}Pb/^{206}Pb$	1σ	204 Corr $^{208}Pb/^{232}Th$	1σ	Conc. (%)
10319-48.1	163	11	0.07	48	9.6E-4	21	1.66	0.026	10.3	6.1	3.1	0.35	1.7	0.34	1.8	0.297	10.8	1891	29	1859	32	1887	8	**2084**	**44**	2366	683	89.3
10319-24.1	1380	26	0.02	369	2.6E-4	7	0.45	0.007	2.7	5.5	1.1	0.31	1.0	0.31	1.0	0.262	2.9	1746	16	1697	17	1745	5	**2086**	**4**	2032	195	81.398
10319-67.1	73	31	0.43	24	1.3E-4	64	0.22	0.131	3.9	6.8	1.6	0.38	1.2	0.38	1.2	0.119	4.1	2080	21	2077	26	2074	9	**2094**	**20**	2195	98	99.205
10319-75.1	321	91	0.29	109	2.3E-5	83	0.04	0.085	3.7	7.3	1.1	0.39	1.0	0.39	1.0	0.116	3.9	2145	19	2140	23	2143	8	**2164**	**7**	2204	83	98.9
10319-18.1	132	83	0.65	45	4.5E-5	40	0.08	0.197	2.3	7.6	1.6	0.40	1.6	0.40	1.6	0.122	2.8	2174	29	2171	35	2163	10	**2186**	**9**	2306	61	99.4
10319-87.1	70	32	0.48	26	1.7E-4	25	0.30	0.137	3.7	8.4	2.1	0.43	1.9	0.44	1.9	0.131	4.2	2326	38	2355	50	2323	11	**2226**	**14**	2383	98	105.4
10319-7.2	978	12	0.01	320	7.3E-4	13	1.26	0.010	5.8	7.4	1.6	0.39	1.2	0.38	1.2	1.097	6.1	2078	22	2043	25	2073	7	**2241**	**18**	5227	1611	91.51
10319-7.1	230	58	0.26	84	2.7E-5	30	0.05	0.072	2.7	8.5	1.1	0.42	1.0	0.42	1.0	0.120	2.9	2282	20	2280	26	2283	9	**2288**	**6**	2259	63	99.7
10319-89.1	123	84	0.71	46	6.9E-4	14	1.19	0.203	2.1	8.9	1.5	0.44	1.1	0.44	1.1	0.142	2.4	2344	22	2355	28	2339	11	**2308**	**17**	2397	68	101.88
10319-14.1	107	94	0.90	38	1.8E-4	26	0.31	0.262	2.2	8.3	1.4	0.41	1.2	0.41	1.2	0.121	2.5	2212	22	2184	27	2206	11	**2321**	**12**	2263	55	94.4
10319-73.1	67	39	0.60	25	6.5E-5	146	0.11	0.182	3.2	8.8	1.6	0.43	1.2	0.43	1.2	0.131	3.5	2303	24	2293	31	2291	11	**2336**	**18**	2452	92	98.3
10319-91.1	324	127	0.40	124	2.0E-5	213	0.03	0.114	1.8	9.3	1.2	0.45	1.1	0.45	1.1	0.127	2.1	2375	22	2377	28	2374	10	**2367**	**8**	2394	57	100.4
10319-8.1	125	40	0.33	49	1.9E-5	216	0.03	0.098	3.1	9.6	1.6	0.45	1.4	0.45	1.4	0.136	3.4	2413	29	2420	39	2407	10	**2389**	**10**	2558	90	101.2
10319-95.1	128	52	0.42	49	3.7E-4	18	0.65	0.118	2.7	9.5	1.4	0.45	1.1	0.45	1.1	0.140	2.9	2386	23	2383	30	2385	10	**2394**	**13**	2391	82	99.6
10319-13.1	227	54	0.25	79	1.5E-4	20	0.26	0.075	2.7	8.7	1.3	0.41	1.3	0.41	1.3	0.131	3.0	2194	23	2141	28	2190	8	**2400**	**8**	2330	73	89.9
10319-19.1	266	136	0.53	107	9.2E-5	24	0.16	0.148	1.8	10.1	1.1	0.47	1.1	0.47	1.1	0.134	2.1	2470	22	2488	30	2469	11	**2418**	**7**	2488	51	102.6
10319-116.1	421	207	0.51	165	4.0E-5	44	0.07	0.147	1.7	9.9	1.1	0.46	1.0	0.46	1.0	0.134	2.0	2426	21	2427	28	2420	10	**2421**	**5**	2512	48	100.2
10319-34.1	128	96	0.78	50	5.4E-5	21	0.09	0.231	3.0	9.8	1.2	0.45	1.1	0.45	1.1	0.135	3.2	2410	22	2406	29	2397	13	**2421**	**8**	2540	77	99.4
10319-5.1	83	106	1.32	30	1.8E-4	37	0.31	0.370	2.0	9.1	1.4	0.42	1.1	0.42	1.1	0.119	2.3	2252	22	2203	27	2255	13	**2429**	**13**	2238	51	91.4
10319-94.1	90	64	0.73	36	6.8E-5	73	0.12	0.221	2.4	10.1	1.6	0.46	1.4	0.46	1.4	0.141	2.8	2452	29	2457	39	2435	12	**2441**	**11**	2639	72	100.6
10319-2.1	118	99	0.87	46	6.0E-5	39	0.10	0.244	2.1	9.8	1.2	0.45	1.1	0.45	1.1	0.128	2.4	2393	22	2378	29	2392	12	**2442**	**9**	2406	55	97.6
10319-113.1	107	102	0.98	42	1.9E-4	61	0.33	0.292	2.0	10.0	1.8	0.46	1.4	0.46	1.4	0.139	2.4	2428	29	2422	38	2409	13	**2443**	**17**	2569	69	99.2
10319-110.1	219	181	0.85	88	7.6E-5	64	0.13	0.239	1.6	10.3	1.2	0.47	1.0	0.47	1.0	0.133	1.9	2484	22	2499	30	2482	12	**2443**	**9**	2502	48	102.0
10319-46.1	61	40	0.68	23	1.4E-4	39	0.25	0.192	3.0	9.8	1.5	0.44	1.3	0.45	1.3	0.129	3.3	2371	25	2345	32	2369	12	**2453**	**13**	2392	79	96.0
10319-57.1	44	34	0.80	18	1.7E-4	45	0.30	0.223	3.5	10.5	2.2	0.48	1.6	0.48	1.6	0.137	3.9	2516	34	2540	49	2515	15	**2454**	**25**	2524	98	103.0
10319-82.1	500	257	0.53	196	1.4E-5	24	0.02	0.147	1.3	10.1	1.1	0.46	1.0	0.46	1.0	0.127	1.6	2423	21	2412	28	2424	10	**2455**	**4**	2411	37	98.43
10319-22.1	103	56	0.56	40	4.0E-5	21	0.07	0.155	2.8	10.0	1.2	0.46	1.1	0.46	1.1	0.128	3.1	2417	22	2404	30	2418	11	**2456**	**9**	2416	70	98.131
10319-11.1	391	286	0.76	158	6.8E-5	21	0.12	0.213	1.2	10.4	1.1	0.47	1.0	0.47	1.0	0.134	1.6	2485	21	2493	29	2482	11	**2463**	**5**	2513	38	101.1
10319-114.1	202	137	0.70	83	1.4E-4	21	0.25	0.211	1.8	10.6	1.1	0.48	1.0	0.48	1.0	0.148	2.2	2511	22	2530	31	2493	12	**2464**	**7**	2719	57	102.3
10319-119.1	309	200	0.67	126	2.0E-4	19	0.35	0.191	1.5	10.5	1.1	0.47	1.0	0.47	1.0	0.140	1.8	2498	21	2510	30	2493	11	**2466**	**7**	2558	48	101.6
10319-111.1	173	127	0.76	69	8.5E-5	50	0.15	0.219	1.9	10.3	1.4	0.46	1.3	0.46	1.3	0.136	2.3	2457	26	2451	35	2449	12	**2472**	**9**	2542	58	99.2
10319-71.1	108	84	0.81	44	7.9E-5	58	0.14	0.239	2.2	10.5	1.3	0.47	1.1	0.47	1.1	0.141	2.5	2490	24	2496	33	2475	13	**2474**	**11**	2638	65	100.8
10319-9.1	291	130	0.46	118	1.2E-4	19	0.21	0.132	1.7	10.6	1.1	0.47	1.0	0.47	1.0	0.139	2.0	2489	21	2491	30	2485	11	**2484**	**6**	2555	50	100.2
10319-33.1	158	62	0.40	65	5.6E-5	122	0.10	0.113	2.6	10.9	1.5	0.48	1.3	0.48	1.3	0.138	3.0	2534	27	2548	38	2533	11	**2500**	**11**	2560	89	101.7
10319-49.1	129	131	1.05	52	8.6E-4	10	1.50	0.315	1.6	10.7	1.7	0.47	1.3	0.48	1.3	0.156	2.1	2488	28	2483	38	2462	14	**2501**	**17**	2675	58	99.4
10319-43.1	110	46	0.43	44	6.1E-5	25	0.11	0.124	2.9	10.6	1.2	0.47	1.1	0.47	1.1	0.136	3.2	2475	23	2463	31	2472	11	**2507**	**9**	2534	76	98.5
10319-84.1	465	282	0.63	191	8.0E-5	21	0.14	0.183	1.1	11.2	1.1	0.48	1.0	0.48	1.0	0.142	1.5	2516	21	2500	29	2506	11	**2555**	**4**	2645	39	98.1
10319-6.1	60	30	0.51	26	1.8E-4	42	0.31	0.140	3.6	11.6	1.5	0.49	1.2	0.49	1.2	0.142	3.9	2585	25	2598	37	2586	13	**2556**	**14**	2575	106	101.4
10319-112.1	103	50	0.51	43	3.1E-4	19	0.54	0.142	2.8	11.4	1.2	0.49	1.1	0.49	1.1	0.148	3.0	2553	23	2551	32	2551	12	**2559**	**11**	2586	81	99.7
10319-98.1	186	117	0.65	77	4.9E-5	91	0.09	0.191	1.8	11.3	1.2	0.48	1.1	0.48	1.1	0.143	2.2	2536	24	2525	33	2524	12	**2562**	**8**	2682	59	98.7
10319-81.1	135	60	0.46	55	7.1E-5	30	0.12	0.135	2.6	11.1	1.2	0.47	1.1	0.47	1.1	0.142	2.8	2486	22	2455	30	2477	11	**2565**	**8**	2634	71	96.3
10319-30.1	133	55	0.42	53	2.1E-5	316	0.04	0.119	2.6	11.0	1.3	0.47	1.1	0.47	1.1	0.132	2.9	2465	23	2427	30	2463	11	**2567**	**11**	2498	84	95.2
10319-61.1	77	49	0.66	32	3.2E-4	22	0.55	0.179	2.8	11.5	1.6	0.49	1.4	0.49	1.4	0.141	3.1	2555	29	2547	41	2559	13	**2574**	**13**	2511	81	99.1
10319-103.1	84	57	0.70	36	4.2E-4	19	0.72	0.187	2.5	12.3	1.8	0.50	1.6	0.50	1.6	0.143	3.0	2602	34	2585	49	2610	13	**2640**	**13**	2512	81	98.2

Note: Rows highlighted in grey indicate U-Pb data with concordance less than 95% or over 105% (not included in concordia or probability-frequency plots (Fig. 4.5)). Rows shaded in blue refer to metamorphic isotopic data. Refer to Appendix A for a complete list of isotopic analysis. Spot No. identifies grain number on mount; number after decimal indicates spot number.
Pb*: Radiogenic Pb. Com ^{206}Pb: mole fraction of total ^{206}Pb that is due to common Pb, calculated using the ^{204}Pb-method. Concordance: 100 x ($^{206}Pb/^{238}U$ age)/($^{207}Pb/^{206}Pb$ ages).

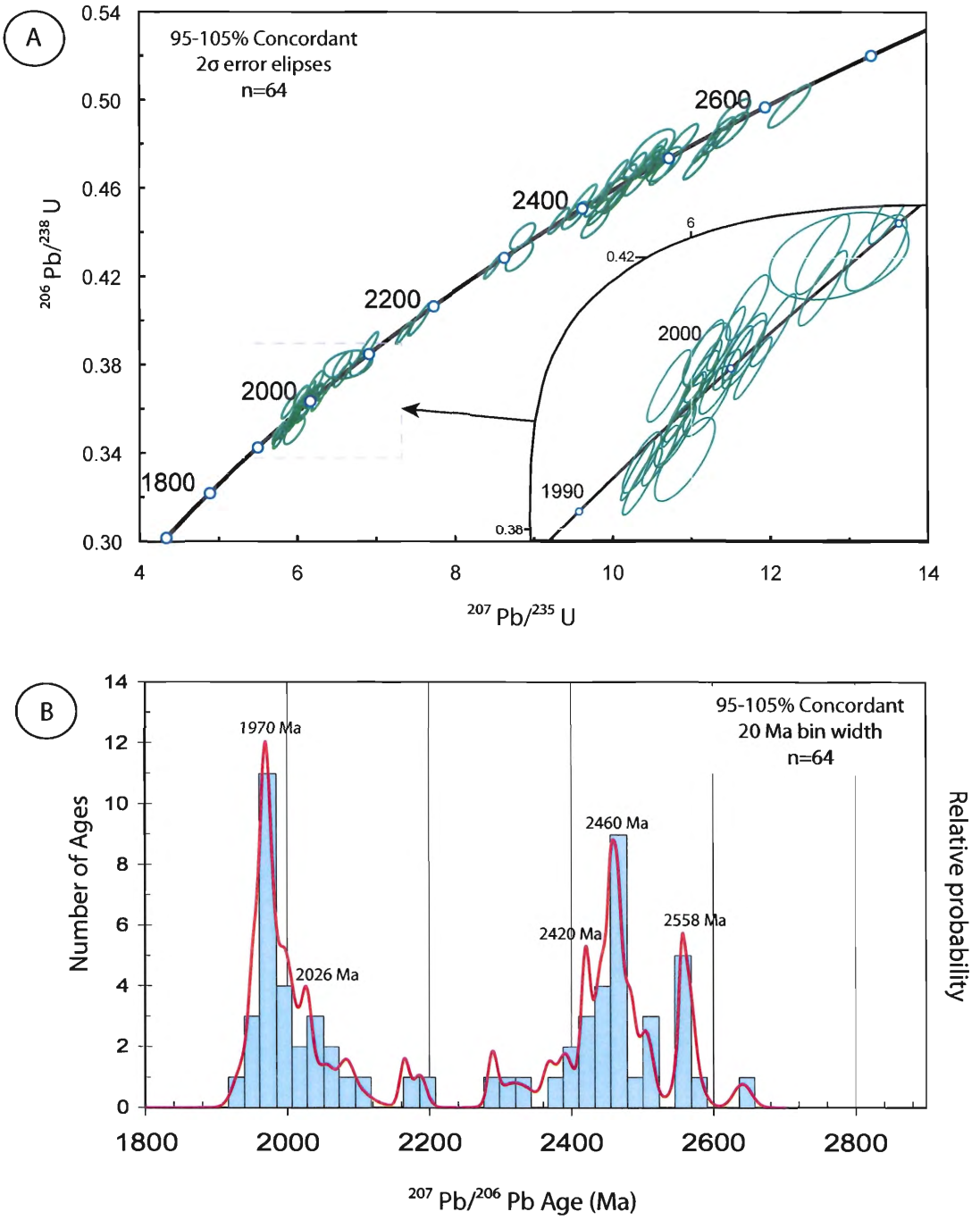

Figure 4. 1: SHRIMP U-Pb detrital zircon geochronology isotopic data. (A) Concordia diagram. (B) Frequency-probability graph at 95-105% concordance, density distribution in red, frequency histogram in behind with bin widths of 20 Ma.

4.3.2 Zircon Morphologies

There is a wide array of preserved zircon morphologies. Zircon sizes along the longest axis range from 60-270 μm with an average size of ~ 100 μm. Morphologies vary from well rounded to elongated prismatic zircons (Fig. 4.2). A large proportion of the zircon population is equant in shape with jagged irregular grain boundaries, many of which represent fragments of previously existing larger zircon grains (Fig. 4.2 B). Most zircons are highly fractured with radial, concentric or random fractured patterns (Fig. 4.3). Thin oscillatory-zoning, typical of igneous derived zircons can also be observed in many of the zircon grains (Fig. 4.4).

Transmitted light images are particularly useful for observing zircon morphologies and color variations. The majority of zircons are completely transparent, while others have a "dirtier", much less transparent quality (Fig. 4.2 C). There appears to be no correlation between Th/U ratios with colour or age (Th/U values range from 0.02 to 1.32)

4.3.3 Metamorphic Zircon and Metamorphic overgrowths

Single-rim overgrowths (5-15 μm) are common within the zircon population with fractures that penetrate perpendicular to the grain boundaries (Fig 4.5). Six of these metamorphic rims were targeted during analysis in order to obtain a consistent metamorphic age and to further constrain a minimum age of deposition for the HLMC (refer to Table 1. for metamorphic overgrowths isotopic results, in blue). Overgrowth rims targeted within this study generally yielded Th/U ratios > 0.1, with corresponding ages of 1932 ± 11, 1939 ± 36 and 1944 ± 25 Ma (Fig. 4.6). However, several rims

targeted had Th/U < 0.1. The later include ages of 1742 ± 170 Ma (10319-102.2, Th/U = 0.08), 2084 ± 44 Ma (10319-48.1, Th/U=0.07), and 2241 ± 18 Ma (10319-7.2, Th/U=0.01).

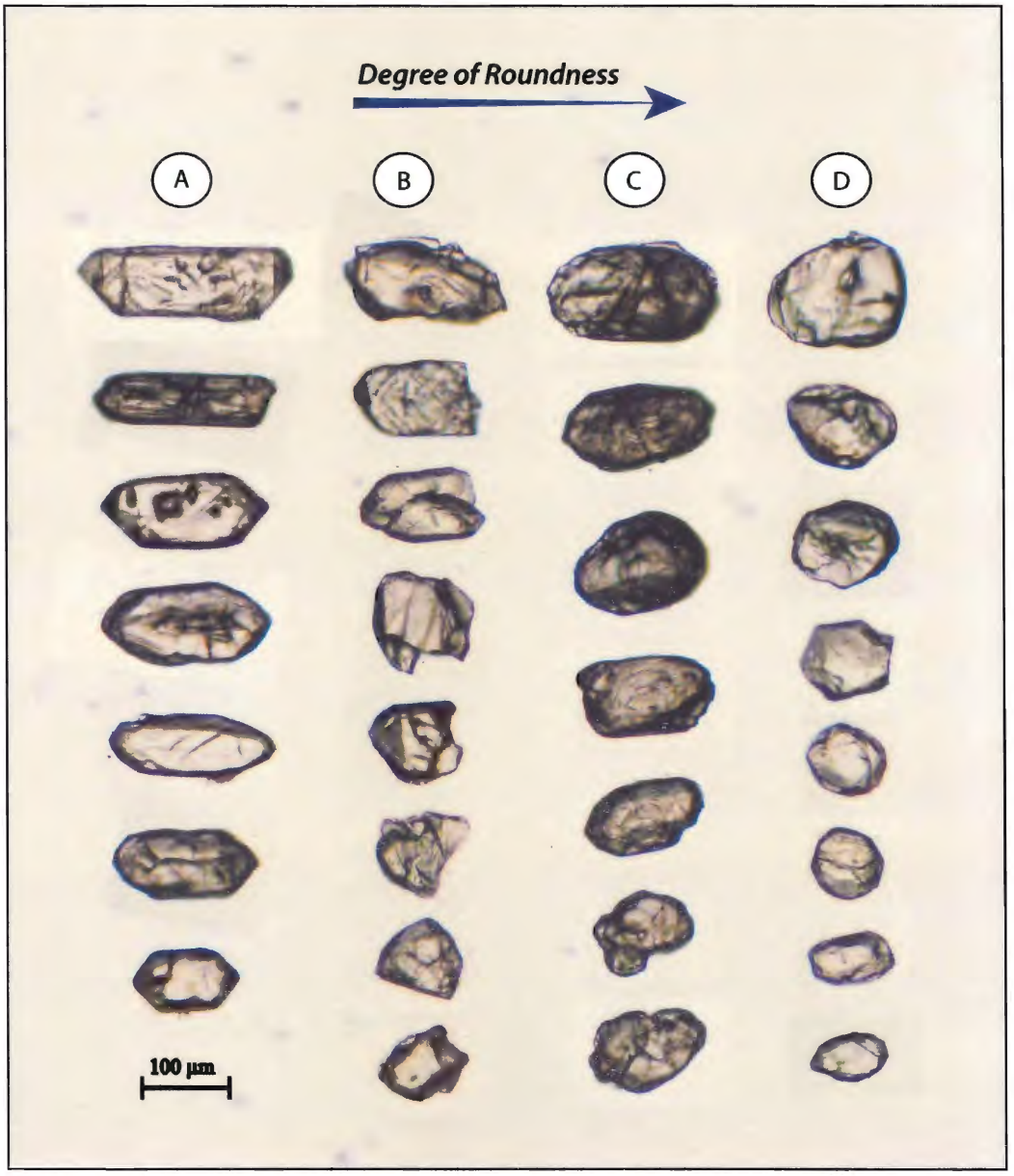

Figure 4. 2: Optical images of representative zircon morphologies. Arrow indicates the increasing degree of roundness. (A) Elongated prismatic zircons. (B) Equant zircon grains with irregular grain boundaries, representing zircon fragments. (C) Zircons rounded to oval shapes with distinct color variations. (D) Equant well rounded zircon grains.

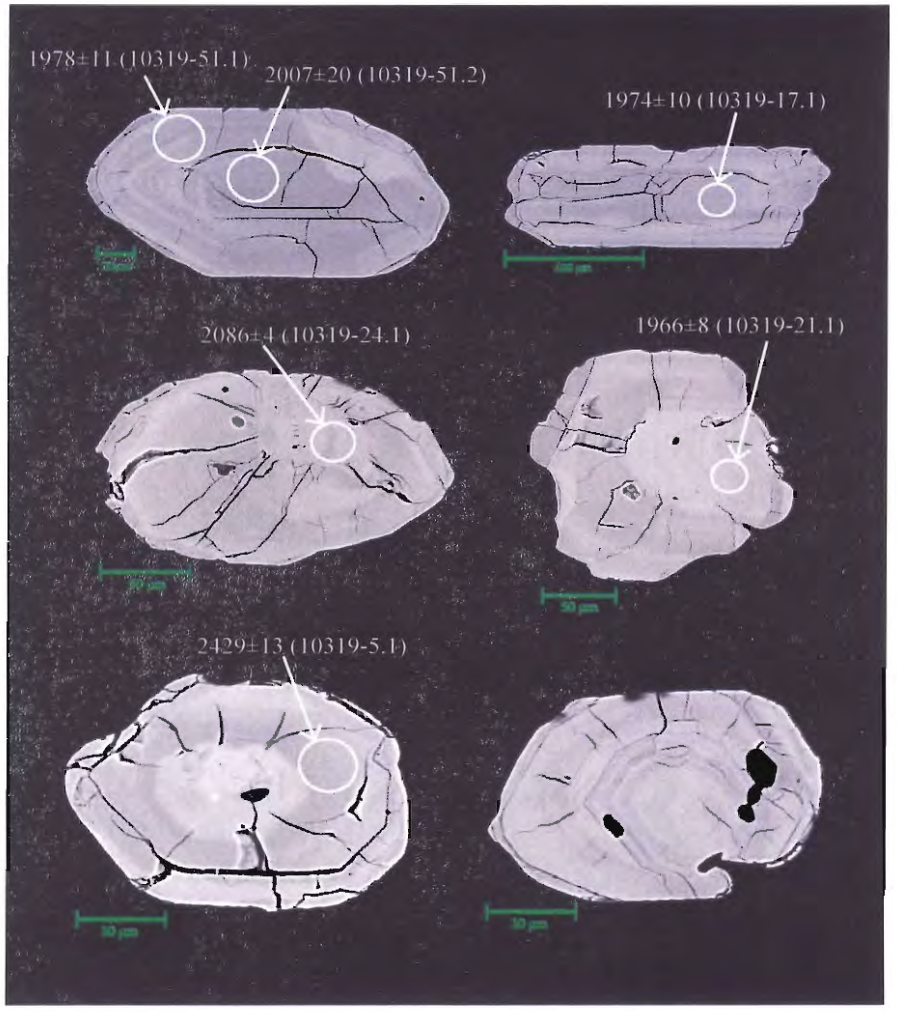

Figure 4. 3: Back-Scattered Electron (BSE) images of fracture patterns within detrital zircon with corresponding isotopic age data. Row 1: Concentric fractured patterns. Rows 2 and 3: Radial and concentric fracture patterns.

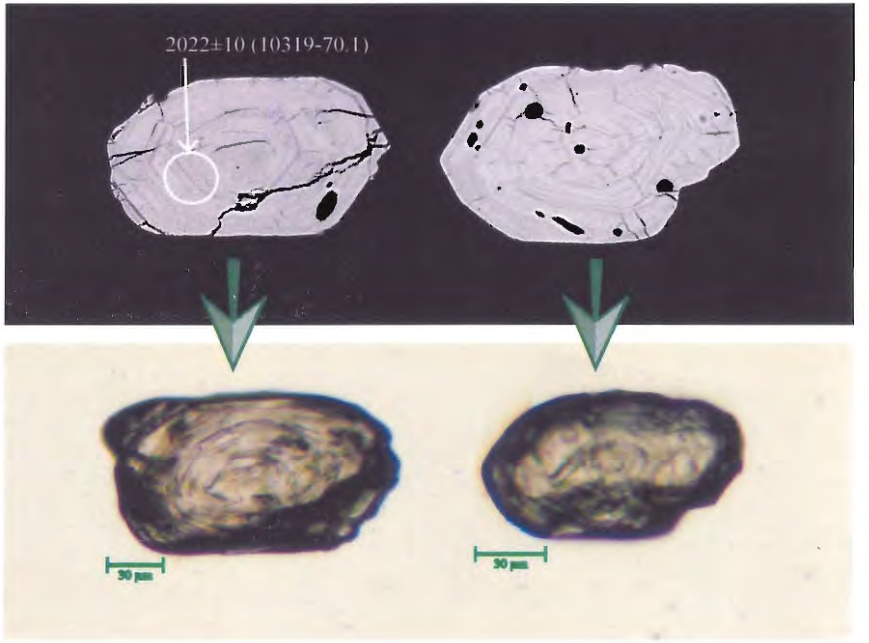

Figure 4. 4: BSE and optical images of thin undulatory zoning within two detrital zircon grains with corresponding isotopic age data. No age data for the zircon on the right. Zircons interpreted as magmatically derived.

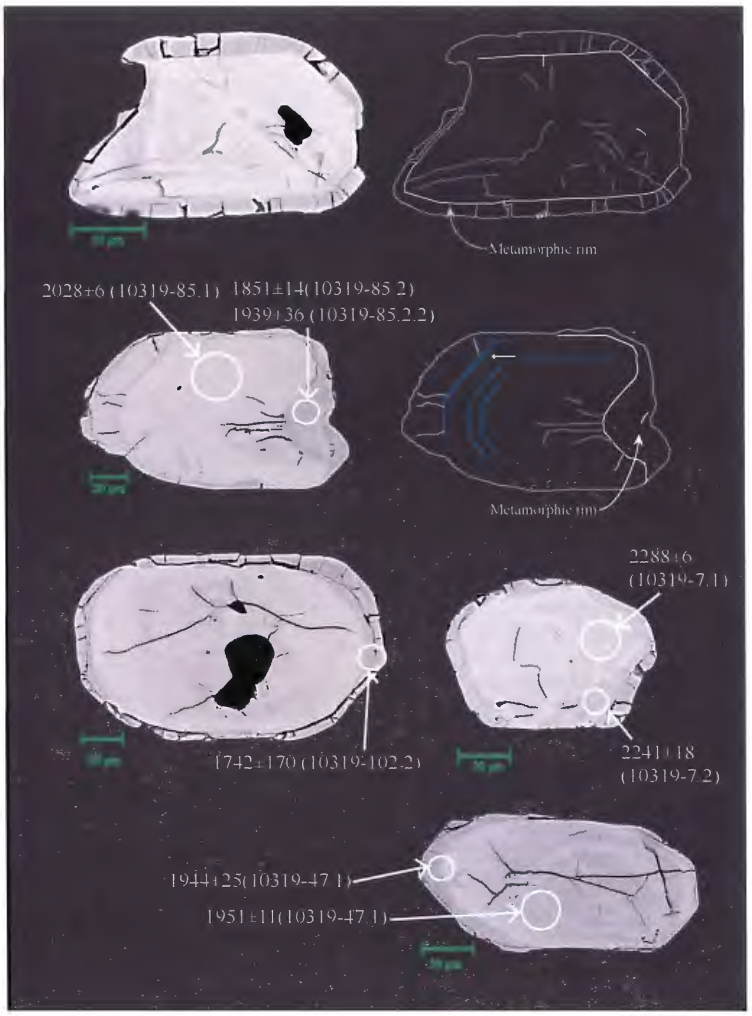

Figure 4.4: BSE images of overgrowth metamorphic rims and corresponding age data. Note size differences between core and rim spots. All rim age data presented here is discordant.

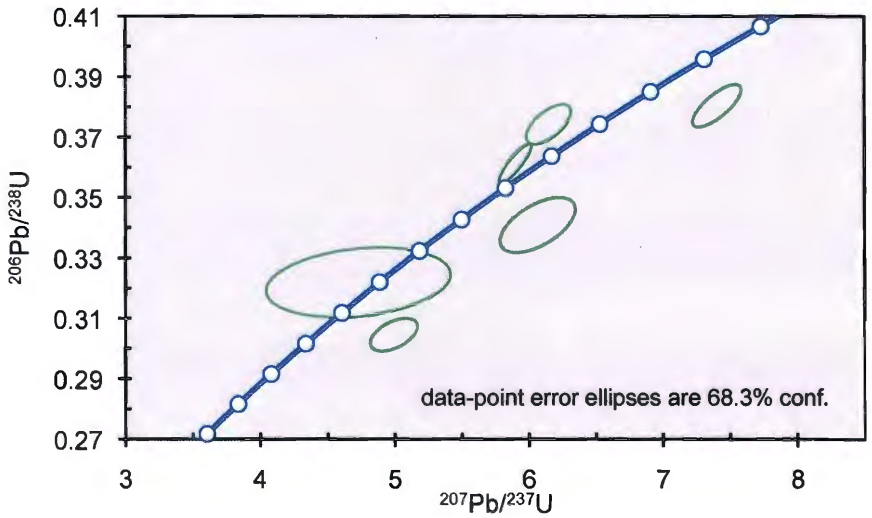

Figure 4. 3: Metamorphic rim concordia diagram, generally displaying discordant age results.

CHAPTER 5: DISCUSSION

5.1 General statement

In order to better understand the tectonic evolution of the Hottah terrane, this study has presented field data, petrography and U-Pb geochronology to build on the previous work by Hildebrand et al. (1983, 1984) and Bowring (1984). SHRIMP U-Pb detrital zircon geochronology has provided a valuable fingerprint for supracrustal ages of the Hottah terrane. This geochronological data set allows potential sources to be identified and a maximum deposition age to be constrained for the HLMC.

Peak mineral assemblages of the metasedimentary rocks from the HLMC unfortunately do not provide sufficient information for thermobarometric analysis. However, some conclusions can be drawn from the mineral assemblages and their corresponding textural relationships. This chapter discusses the major petrological and geochronological results and compares them to previous work (Hildebrand et al. 1983, 1984; Bowring, 1984).

5.2 Petrology

Outcrops within the study area provide some of the best exposures of the HLMC within the Hottah terrane. Cameco drill-cores provide subsurface samples of the supracrustal complex; however, extensive alteration limits their usefulness for petrographic analysis.

Within the Leith Ridge study area, all primary sedimentary structures have been obliterated. Any previously existing way-up indicators, ripple marks, or bedding have

been completely transposed into the main metamorphic fabric. Therefore, the only constraint on a depositional environment is that it is some kind of clastic sedimentary basin with a significant proportion of fine to medium grained detritus. The inter-layered psammites and semi-pelites may represent a greywacke-siltstone protolith, deposited in a sub-marine environment. Generally, true pelites (high Al geochemical content) accumulate in the distal portions of a wedge of sediment off the continental shelf/slope of both active and passive margins. Pelites tend to grade to greywacke towards their continental source (Winter, 2010).

The compositionally layered psammites and semi-pelites within the three outcrops are intimately intruded by a series of igneous dykes that provide a clear sequence of metamorphism-deformation-time events within the study area. The igneous dykes display clear crosscutting relationships within the study area, however they have been reported to display more complex age relationships regionally given multiple intrusive events and superimposed shearing and boudinage (Hildebrand et al., 1984).

The metasedimentary rocks within the study area were deposited after 1959 ± 9 Ma, constrained by age of the 5th youngest detrital zircon age. Sometime after diagenesis, the sedimentary package was metamorphosed and foliated along a common northwestern orientation (D_1). Considering that the HLMC was intruded by Hottah continental arc plutons at ca. 1930 Ma, this could also be the timing of metamorphism. Two zircon metamorphic rim ages of ca. 1930 and 1940 Ma may corroborate this (Fig 4.6; Table 1). Incipient melt pods indicate these metasedimentary rocks were partially migmatised and underwent high-grade metamorphism. Following deformation the psammites and semi-pelites were intruded by a series of granitic dykes. The first intrusions were tourmaline

bearing pegmatite dykes (I_1), concentrated in boron-rich fluids that subsequently infiltrated the metasedimentary rocks. The early pegmatite dykes were later cut by a series of amphibole-bearing fine-grained granodiorite dykes (I_2).

From the petrographic analysis, it appears that metasedimentary rocks within Leith Ridge have undergone at least two distinct metamorphic events, including high temperature-low pressure and retrograde metamorphism. Tourmaline porphyroblasts preserve mineral assemblages and inclusion trails representing an earlier stage of foliation development. Inclusion trails of fine-grained elongated quartz and iron-oxides generally strike to the northeast - southwest, nearly perpendicular to the main metamorphic foliation defined by the alignment of biotite. In addition, sillimanite can be found as inclusions within tourmaline porphyroblasts, in randomly oriented or concentric patterns (Fig. 3.7). The origin of the tourmaline is unknown and beyond the scope of this study, however several conditions could have contributed to its growth. Commonly, rocks enriched in Fe-Mg that are deposited in submarine environments are also frequently enriched in boron and later develop tourmaline during metamorphism. Tourmaline may also have been introduced by the boron-rich fluids associated with the pegmatite dyke intrusions. Alternatively, some of the larger crystal cores may have originated as detritus, increasing in size with metamorphism. Sillimanite is only found as inclusions within the tourmaline porphyroblasts, indicating that the sillimanite grown during peak P/T events in the main mineral assemblage was obliterated during retrograde metamorphism. Tourmaline therefore plays an important role in constraining the sequence of metamorphic mineral growth within the study area as it preserves sillimanite, a key index mineral.

Muscovite is present in minor amounts and overgrows all other mineral assemblages and metamorphic fabrics. This relationship indicates that the muscovite in these rocks grew during retrograde metamorphism and not during peak pressure-temperature conditions. Furthermore, fibrous elliptical aggregates of muscovite are common and resemble strongly retrogressed cordierite porphyroblasts (Fig. 3.8, C, D). Hildebrand et al. (1984) also noted outcrops with abundant cordierite and cordierite pseudomorphs within HLMC metasedimentary rocks, and it is possible that these muscovite aggregates represent cordierite pseudomorphs. The absence of muscovite and the presence of K-feldspar + sillimanite during peak P/T is consistent with upper amphibolite facies conditions, above the muscovite + quartz stability field and within the sillimanite isograd (Fig. 5.1). These rocks were partially migmatised, evident by the incipient leucosomes lenses and melt textures, indicating that these rocks underwent peak P/T conditions above the granite-wet solidus (Fig 5.1).

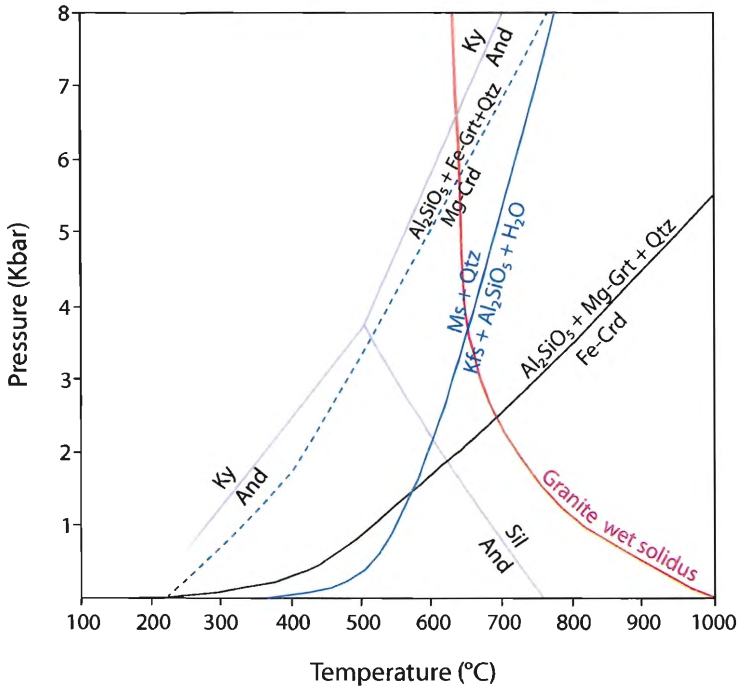

Figure 5. 1: Pressure-Temperature diagram of stability zones reached during peak metamorphic conditions within metasedimentary rocks of the Holly Lake metamorphic complex (modified from Berman 2007, calculated using win TWQ). Holly Lake metamorphic complex stability zone located within the shaded P/T space (> 700 °C, < 6 Kbar).

General field observations within the study area closely match those made by Hildebrand et al. (1983, 1984). However, Hildebrand et al. (1984) noted some distinct mineralogical and textural variations including tiny garnets concentrated in melt pods, sillimanite "knots", and numerous pre-, syn-, and post-tectonic igneous bodies. The mineral assemblages observed by Hildebrand et al. (1984) (feldspar + garnet + sillimanite + leucosome), together with the peak mineral assemblages observed within the study area (sillimanite + relict cordierite + potassium-feldspar + leucosome) indicate that these rocks reached upper amphibole to lower granulite facies conditions, with high temperature (> 700 °C) and low-pressure (< 6 Kbar) (Fig. 5.1).

Inclusion trails observed in tourmaline porphyroblasts suggest that the original sedimentary rocks were very fine grained, with a concentration of iron-rich minerals, with a relict fabric striking along a northeast - southwest orientation. This fabric may represent an early metamorphic fabric or relict sedimentary bedding (S_i).

5.3 SHRIMP Data

SHRIMP U-Pb detrital zircon data has been obtained from a psammite sample from Leith Ridge. Other sample-site locations within sediments of the HLMC have been targeting for U-Pb detrital zircon geochronology in the past, however, the sites were too altered for analysis (L. Ootes, personal communication, 2010). Leith Ridge, therefore is a key site for detrital zircon geochronology within the Hottah terrane. Consequently, this dataset has provided a unique reference pertaining to the age and provenance of the Hottah terrane supracrustal sequence.

5.3.1 Age Constraints on the Holly Lake metamorphic complex

Utilizing U-Pb detrital zircon data to determine the maximum age of deposition for Precambrian successions is a robust estimate in the absence of biostratigraphic markers (Fedo et al., 2003). Generally, only a maximum age of deposition is revealed based on the principle that the age of deposition must be younger than the age of the youngest detrital zircon (given there is no disturbance to the U-Pb isotopic system). However, in some cases a minimum age of deposition can be determined when detrital zircon geochronology is linked with geochronology of younger magmatic or metamorphic events (Fedo et al., 2003).

The youngest single detrital zircon core within sediments of the HLMC is dated at 1951 ± 11 Ma, constraining the maximum age of deposition for the HLMC. The maximum age of deposition has been constrained by the 5^{th} youngest grains with an age of 1959 ± 9, an age contained within the probability of the dominant 1970 Ma age peak (Fig. 4.1). It is therefore clear that the crystallization of a large portion of the detrital zircons only slightly predates sedimentation.

Metamorphic rims were targeted in order to constrain a metamorphic age, and thereby constraining a minimum age of deposition for the HLMC. Unfortunately, zircon overgrowths by and large generated discordant age data and yielded Th/U ratios greater than normal amounts (> 0.1) (Fig 4.6). Taking into account discordant data, there was a broad age range from 1741 ± 170 to 2241 ± 18 Ma. Rims with Th/U < 0.1 include ages of 1742 ± 170 Ma, 2084 ± 44 Ma and 2241 ± 18 Ma and were interpreted as metamorphic. Metamorphic age data that remains within 6 percent discordancy includes ages of 1742 ± 170 Ma, 1932 ± 11 Ma and 1944 ± 25 Ma (Fig. 4.6). The youngest metamorphic age,

dated at ca. 1742 Ma, may be related to volcano-plutonism of the Great Bear magmatic zone or younger, unidentified events (e.g. collision of the Fort Simpson and Nahanni terranes to the west). Alternatively, this young metamorphic age (ca. 1742) may correspond to the intrusion of the south-east striking Cleaver dykes at 1740 Ma (Hildebrand, 1982b). Some of the older ages may, however, give an indication of an even older metamorphic event in the Hottah terrane. But, given the inconsistency of the metamorphic zircon rim data, further analysis is needed (e.g. dating of monazite grains in foliation planes) in order to more thoroughly constrain the of age of metamorphism and thus the minimum age of deposition for the HLMC. For now, the minimum age of deposition for the HLMC is constrained by the intrusion of plutons of the Hottah continental arc at a ca. 1930 Ma (L. Ootes and W.J. Davis have precisely dated a plutonic phase of the Hottah arc at 1930 ± 1 Ma (L. Ootes, personal communication, 2011)).

This dataset has provided new insights into the age of the HLMC. Previous reported multigrain detrital zircon ages, indicating components older than ca. 2200 Ma, are confirmed by more precise SHRIMP data indicating multiple ages older than this.

5.3.2 Provenance of the Holly Lake metamorphic complex

This is the first study to provide a provenance record of the Hottah terrane. However, sedimentary features within the metasediments of Leith Ridge, including way-up indicators (e.g. ripple marks or cross-stratification), have been completely transposed and overprinted by late deformation and metamorphic events. Therefore, younging directions or direction of sediment transport cannot be determined. Furthermore, observing the maturity of these metasedimentary rocks is impossible given the degree of

recrystalization and alteration. Consequently, distances from source rocks cannot be estimated based on relict sedimentary features.

The frequency-probability histogram (Fig. 4.1) clearly demonstrates that there are two major sources for the HLMC, with lesser addition of detritus from numerous other age sources. The two largest peaks are represented by zircons derived from a middle Paleoproterozoic and early Paleoproterozoic source, with a smaller Neoarchean source contributor. As previously stated, significant peak ages are ca. 1970 (n=11), 2460 (n=9) and 2558 Ma (n=5), with smaller ones at 2026 (n=3), and 2420 (n=3) Ma. The magnitude of the peaks may provide some clues into the distance from source to catchment basin. A large peak may represent a close proximity from source rock to catchment basin. Alternatively, a large peak may also represent a far more extensive source located at a further distance from source rock to catchment basin. Moreover, there appears to be a minor correlation between the degree of roundness with age. Many of the detrital zircons in the 1970 Ma peak have elongated prismatic crystal habits (Fig. 4.2 A), whereas many of the older grains are more rounded to oval in shape (Fig 4.2 D).

Several relationships may indicate that the middle Paleoproterozoic and early Paleoproterozoic detrital zircon peak populations were derived from a local source. These include the tendency for young grains to be elongated with euhedral crystal habits, that the crystallization of a large portion of the detrital zircons only slightly predates sedimentation and the large size of the 1970 Ma peak. Furthermore, given that the Neoarchean peak (2558 Ma) is far smaller than the Paleoproterozoic peaks, and that many of the older grains are more rounded, may indicate a larger distance from source rock to depositional basin or that Archean grains were recycled. However, a much larger

dataset is needed in order to target specific end member-morphologies to confirm the relationship.

From this detrital zircon dataset, it is clear that the metasedimentary rocks originated from a complex crustal block, as evident by the polymineralic age distribution, with a middle to early Paleoproterozoic to Neoarchean provenance. Gandhi and van Breemen (2005) interpreted the Archean detrital zircon grains in the Treasure Lake Group platformal cover sequence of the Hottah terrane as either recycled grains from the Hottah terrane, or derived directly from some Archean rocks in the Hottah terrane or adjacent terranes to the south or southwest (Gandhi and van Breemen, 2005). Therefore, the eleven (out of 64) Archean detrital zircons discovered within this study provide further evidence to those obtained in the much younger Treasure Lake Group by Gandhi and van Breemen (2005) and Bennett and Rivers (2006) that some enigmatic late Archean source may be preserved within the Hottah terrane, either from the Slave craton or a currently unexposed basement. This finding is significant to current diamond exploration within the overlying Phanerozoic cover to the west. Diamondiferous kimberlites have been found North of Great Bear Lake in regions where the crust and mantle composition and age remain unknown, but are thought to be underlain by Hottah lithosphere. Given that it is well known that the development of diamondiferous kimberlites depends on both Archean mantle and crust it is of great interest to determine the source and target crustal rocks for these diamond-bearing pipes. Determining whether or not the Hottah terrane has an Archean component that facilitates these deposits is a key question moving forward with diamond exploration. The dataset provided here, in concurrence with Archean zircons in younger sedimentary horizons of the Hottah Terrane

(Gandhi and van Breemen, 2005; Bennett and Rivers, 2006; L. Ootes, W.J. Davis, and V.A. Jackson, unpublished data) provide an indication that a Archean Hottah component may exist beneath Phanerozoic cover to the North, South and West.

As previously stated in chapter 2 there are two proposed tectonic models for the development of the Wopmay orogen in which the development of the orogen is dependent on the Hottah terrane (including the Turmoil klippe) being either allochthonous (Bowring and Grotzinger, 1992; Hildebrand et al., 2010) or autochthonous (Reichenbach, 1991) with respect to the Archean Slave craton. In order to test these theories, a compilation of crystallization ages of the Slave craton are compared with the HLMC age signature obtained in this study. As evident by Figure 5.2 there is a large

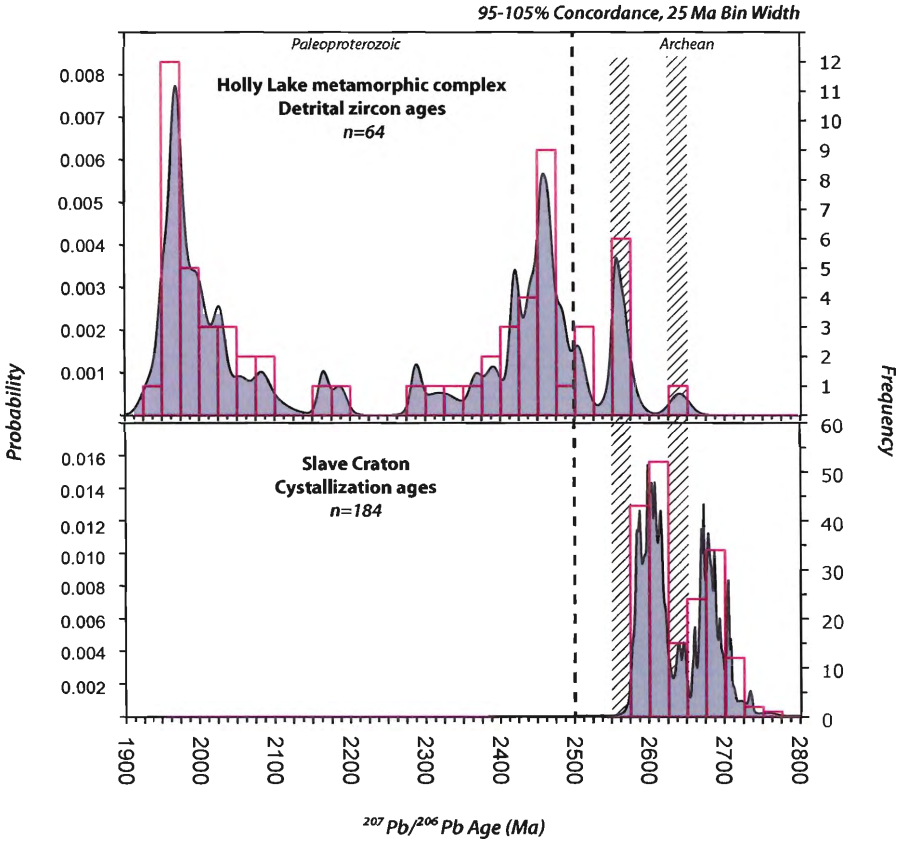

Figure 5. 2: Isotopic age comparison between detrital zircons of Holly Lake metamorphic complex and a compilation of crystallization ages of the Slave craton. Vertical dashed line represents the boundary between the Paleoproterozoic and the Archean (2.5 Ga). Hatched thick vertical lines highlight the main Archean age peaks of the Holly Lake Metamorphic Complex in order to compare them with peaks of the of the Slave craton.

variation between the two plots, however, some similarities exist between Neoarchean age data. The distinct differences in the age spectrums between the HLMC and the Slave craton is similar to the current accepted model presented by Hildebrand et al. (2010). The model states that the Hottah terrane is allochthonous with respect to the Archean Slave craton (Hildebrand et al., 2010), and therefore, age signatures should vary between the Slave craton and the HLMC. In this context, a different Archean cratonic fragment is preserved or was a source to the Hottah itself.

If the Hottah terrane is exotic with respect to the Slave craton determining its

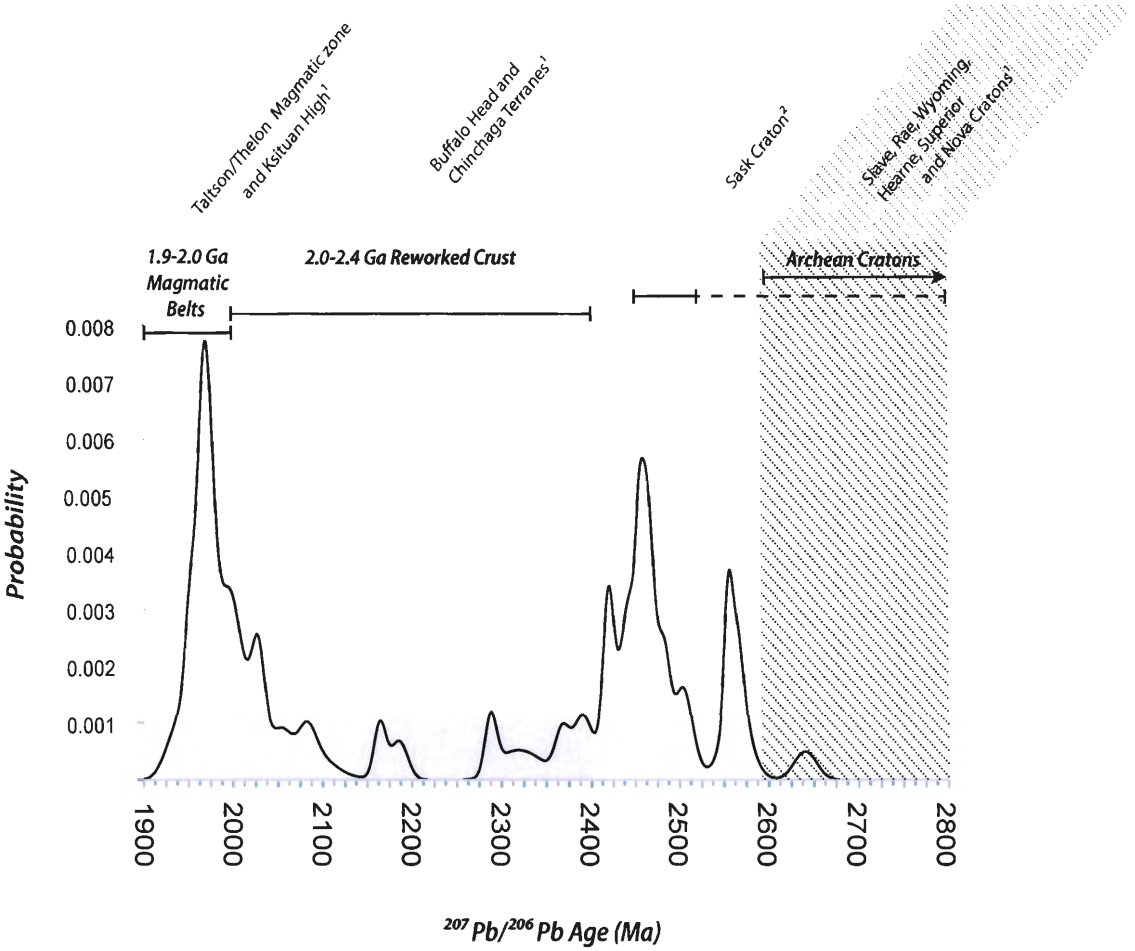

Figure 5. 3: U-Pb Normalized age probability graph for the Holly Lake Metamorphic Complex. The colored bands represent ages that correspond with known igneous crystallization ages of potential source rocks in the Northwestern Canadian Shield. 1- Chacko et al., 2000, 2-Bickford et al, 2005. See figure 2.1 for terrane locations south of the Wopmay orogen.

provenance is beyond the scope of this study. However, some age similarities can be observed between detrital zircon age signatures of the HLMC with crystallization ages of terranes situated south of the Wopmay orogen. Similar ages to those in the 1970 Ma peak have been reported in the Taltson magmatic zone and the Ksituan High situated to the south of the Wopmay orogen (Fig. 5.3) (Chacko et al., 2000; see Fig. 2.1). While igneous crystallization ages in the Sask craton also match those in the 2460 Ma peak (Bickford et al, 2005) (Fig 5.3). The smaller, less significant peaks between 2.0-2.4 Ga could have been sourced from a wide array of terranes including the Buffalo head or Chinchaga terranes currently buried beneath think Phanerozoic cover (Chacko et al., 2000, Fig 1.) (Fig 5.3). While some of the oldest Neoarchean ages observed in this study could have potentially originated from a handful of Archean cratons within the Northwestern Canadian Shield or represent an Archean Hottah component currently not exposed.

To test the alternative, less publicized, model for the development of the Wopmay orogen by Reichenbach (1991), an age comparison must be made between units within the Hottah terrane, including the Turmoil Klippe, and the Slave craton. Figure 5.3 is a compilation of detrital zircon data from metasedimentary units of the Hottah terrane (HLMC and Treasure Lake Group), the Turmoil klippe (Akaitcho Group), and platformal strata adjacent to the Slave craton (Snare Group) (Jackson et al., 2010). The platformal Snare Group is derived from the Slave craton (representing all major tectonic assemblages of the Slave craton) whereas the Akaitcho Group has Archean and Paleoproterozoic source detritus (the later corresponding to known Hottah ages) (Jackson et al., 2010). Similarities exist between all units within the compilation, most notably between the Treasure Lake Group and the HLMC, and between the Neoarchean modal

peaks (highlighted in orange) (Fig 5.3). This data compilation by Jackson et al. in addition to HLMC data obtained in this study may pose a challenge to the current accepted model for the development of the Wopmay orogen by Hildebrand and others (1990, 2010). This alternative option suggests that the western Slave craton evolved through the late Neoarchean but these rocks are not preserved on the craton *senso stricto,* but are within Wopmay orogen. This could have evolved into the Paleoproterozoic and these older grains could reflect such a source terrane.

The source of the Hottah terrane is still unknown and further work is needed in order to fully understand its interaction with the Slave craton. However, the age signature obtained in this study fills in a large gap in the understanding of the Hottah terrane in Wopmay orogen.

Figure 5. 4: Detrital zircon frequency-probability compilation including plots of the Snare Group, Akaitcho Group, Treasure Lake Group and the Holly Lake Metamorphic Complex (Modified from Jackson et al., 2010). The Snare Group composite plot includes quartz arenite, feldspathic arenite and one sample of quartz pebble conglomerate. The Akaitcho Group composite plot includes a quartz arenite and a gneissic felsic volcaniclastic as well as a sillimanite-bearing semi-pelite. The Treasure Lake Group composite plot includes a polydeformed arkosic siltstone (previously reported in Gandhi and van Breemen, 2005). The Holly Lake Metamorphic complex includes a sample of sillimanite-bearing semi-pelite. Note: Dark grey curves include data that is 5% discordant (maximum) and light grey includes up to 10% discordant age data.

Stratigraphic implication of the Hottah terrane shown below (modified from (Ootes, unpublished data) corresponding to frequency-probability plots to the right.

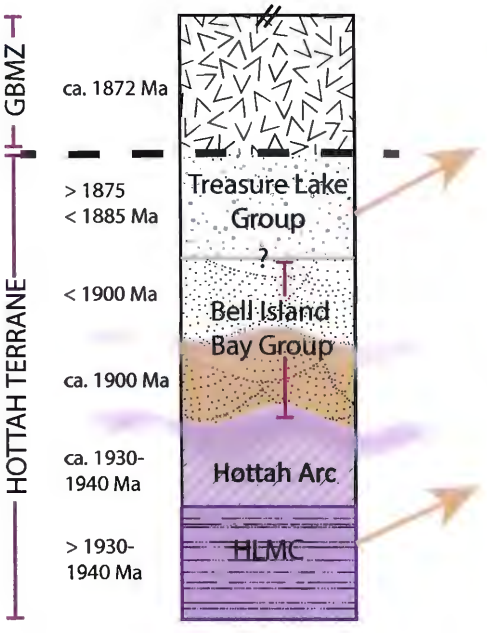

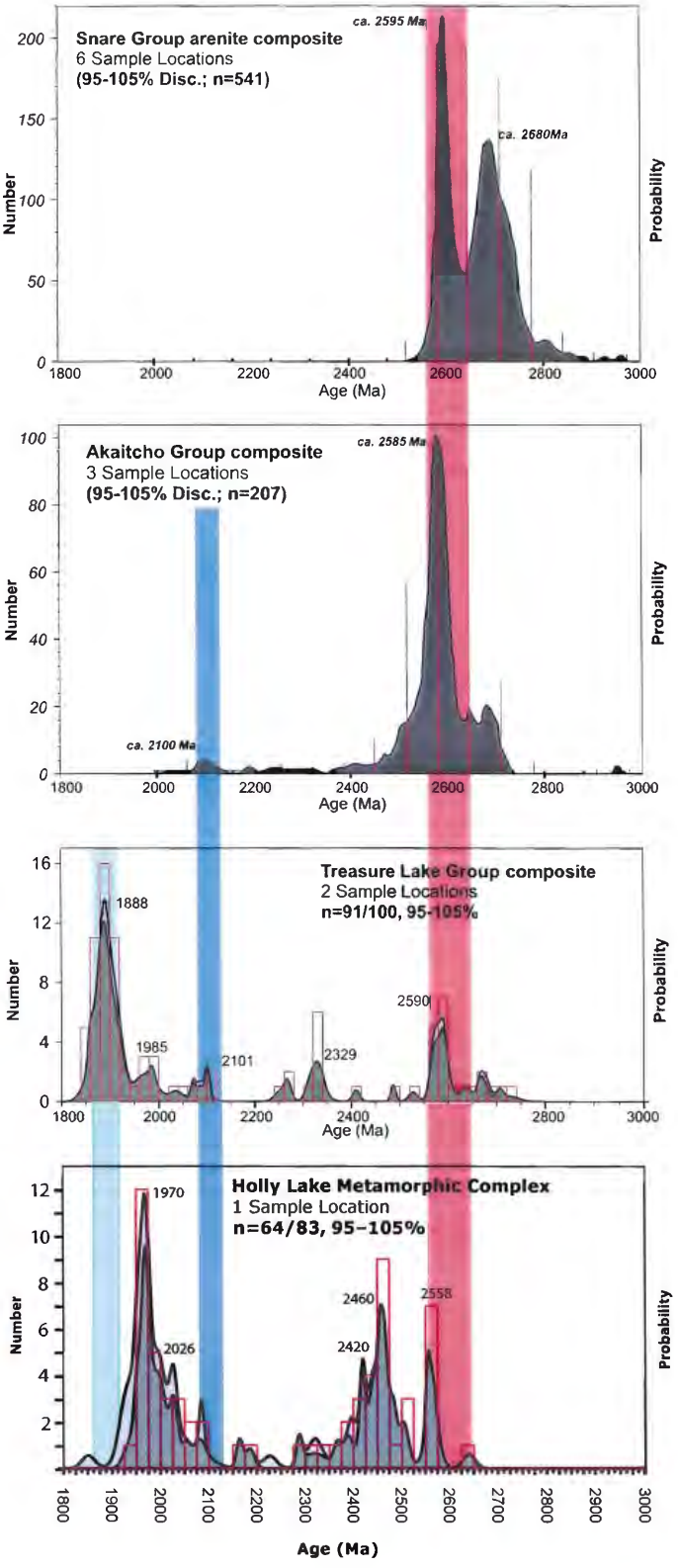

CHAPTER 6: CONCLUSIONS

1) Semi-pelites and psammites within the Leith Ridge study area have undergone two distinct metamorphic events from high temperature – low pressure to retrograde metamorphism. Peak mineral assemblages include sillimanite + potassium-feldspar + relict cordierite + leucosomes (melt). This peak mineral assemblage is qualitatively interpreted to represent the upper amphibolite to lower granulite facies, with temperatures > 700° C and pressures < 6 Kbar.
2) SHRIMP U-Pb detrital zircon isotopic data reveals a polymodal age distribution for the HLMC. This age distribution indicates a complex crustal source, with a mid-Paleoproterozoic and early Paleoproterozoic to Neoarchean provenance. Major peaks include ages of ca. 1970, 2460 and 2558 Ma, with lesser significant modes at ca. 2420 and 2026 Ma. The wide range of detrital zircon ages in the HLMC is interpreted to represent a complex Paleoproterozoic evolution for the Hottah terrane.
3) The maximum age of deposition falls within the 1970 Ma main peak, represented by a weighted mean age of 1959 ± 9 Ma. This indicates the crystallization of a large portion of the detrital zircons only slightly predates sedimentation. Metamorphic overgrowths were targeted in order to obtain a metamorphic age, and thereby constrain a minimum age of deposition for he Holly Lake metamorphic complex. Results possibly indicate that metamorphism was synchronous with ca. 1930 Ma plutonism of the Hottah continental arc.
4) Eleven Archean detrital zircons are present out of the 64 grains analyzed (< 5% discordance) analyzed within this study. These Archean detrital zircons may have

originated from an enigmatic Archean craton or an Archean Hottah terrane component that is currently unexposed to the north. This discovery is important to current diamond exploration as it further indicates a possible Archean component to the Hottah terrane.

5) The age populations of the HLMC appear to significantly vary from that of the Archean Slave craton. This either provides further evidence that the Hottah terrane is allochthonous with respect to the Slave craton, or possibly the Slave craton evolved through the late Noeoarchean and was totally reworked on its western margin.

REFERENCES

Aspler, L.B., Pilkington, M., and Miles, W.F., 2003. Interpretations of Precambrian basement based on recent aeromagnetic data, Mackenzie Valley, Northwest Territories: in current research, Part C2: Geological Survey of Canada, Paper 2003-C2.

Bennett, V., and Rivers, T., 2006. U-Pb ages of detrital primary crystallization and inheritance for magmatic rocks of the southern Wopmay orogen, Northwest Territories: Northwest Territories Geoscience Office, NWT Open Report 2006-006, p. 64.

Berman, R.G., 2007. winTWQ, version 2.3: A software package for performing internally-consistent thermobarometric calculations: Geological Survey of Canada, Open File 5462.

Bickford, M.E., Mock, T.D., Steinhard W.E., Collerson, K.D., and Lewry, J.F., 2005. Origin of the Archean Sask craton and its extent within the Trans-Hudson orogen: evidence from Pb and Nd isotopic compositions of basement rocks and post-orogenic intrusions: Canadian Journal of Earth Sciences, **42**: p. 659-684.

Bowring, S.A., 1984. U-Pb Zircon Geochronology of Early Proterozoic Wopmay Orogen, N.W.T., Canada: An Example of Rapid Crustal Evolution: Unpublished Ph.D. thesis, University of Kansas, Lawrence, Kansas, p. 148.

Bowring, S.A., and Grotzinger, J.P., 1992. Implications of new chronostratigraphy for tectonic evolution of Wopmay orogen, northwest Canadian Shield: American Journal of Science, **292**: p. 1-20.

Bowring, S.A., and Podosek, F.A., 1989. Nd isotopic evidence from Wopmay orogen for 2.0–2.4 Ga crust in western North America: Earth and Planetary Science Letters, **94**: p. 217–230.

Bowring, S.A., King, J.E., Housh, T.B., Isachsen, C.E., and Podosek, F.A., 1989, Neodymium and lead isotope evidence for enriched early Archean crust in North America: Nature, **340**, p. 222–225.

Canadian Geochronology KnowledgeBase [online], 2011. Geoscience Data Repository, Geological Survey of Canada, Earth Sciences Sector, Natural Resources Canada of Government. Accessed March 10, 2011, available from <http://gdr.nrcan.gc.ca/geochron/index_e.php>

Chacko, T., De., S.K., Creaser, R.A., and Muehlenbachs, K., 2000. Tectonic setting of the Taltson magmatic zone at 1.9-2.0 Ga: a granitoid-based perspective: Canadian Journal of Earth Science, **37**: p. 1597-1609.

Cook, F.A., van der Velden, A.J., and Hall, K.W., 1999. Frozen subduction in Canada's Northwest Territories: Lithoprobe deep lithospheric reflection profiling of the western Canadian Shield: Tectonics, **18**: p. 1-24.

Cook, F.A., and Erdmer, P., 2005. An 1800 km cross section of the lithosphere through the northwestern North American Plate; lessons from 4.0 billion years of Earth's history: Canadian Journal of Earth Sciences, **42**: p. 1295-1311.

Corfu, F., Hanchar, J.M., Hoskin, P.W.O., and Kinny, P., 2003. Atlas of zircon textures: Mineralogical Society of America, **53**: p. 469-500.

Fedo, C.M., Sircombe, K.N., and Rainbird, R.H., 2003. Detrital zircon analysis of the sedimentary record: in Zircon, Reviews in Mineralogy and Geochemistry, **53**: p. 277-303.

Fernández-Viegjo, G., and Clowes, R.M., 2003. Lithospheric structure beneath the Archean Slave Province and Proterozoic Wopmay orogen, northwestern Canada, from a Lithoprobe refraction/wide-angle reflection survey: Geophysical Journal International, **153**: p. 1-19.

Fraser, J.A., Craig, B.G., Davidson, W.L., Fulton, R.J., Heywood, W.W., and Irvine, T.N., 1960. North Central District of Mackenzie, Northwest Territories: Geological Survey of Canada Map 18-1960, scale 8 miles to the inch.

Gandhi, S.S., and van Breeman, O., 2005. SHRIMP U-Pb geochronology of detrital zircons from the Treasure Lake Group – new evidence for Paleoproterozoic collisional tectonics in the southern Hottah terrane, northwestern Canadian Shield: Canadian Journal of Earth Sciences, **42**: p. 833-845

Guan, H., Sun, M., Wilde, S.A., Zhou, X., Zhai, M., 2002. SHRIMP U-Pb Zircon geochronology of the Fuping Complex: implications for formation and assembly of the North China Craton: Precambrian Research, **113**: p. 1-18.

Hartmann, L.A., and Santos, J.O.S. 2004. Predominance of high Th/U, magmatic zircon in Brazilian Shield sandstones: Geological society of America, **32**: p. 73-76.

Hildebrand, R.S., 1981. Early Proterozoic Labine Group of Wopmay Orogen: Remnant of a continental volcanic arc developed during oblique convergence; in Proterozoic Basins of Canada, F.H.A. Campbell, editor: Geological Survey of Canada, Paper 81-10, p. 133-156.

Hildebrand, R.S., 1982a. A continental arc of early Proterozoic age at Great Bear Lake, Northwest Territories: Unpublished Ph.D. thesis dissertation, Memorial University of Newfoundland, St. John's, Newfoundland, p. 237.

Hildebrand, R.S., 1982b. Geology, Echo Bay-MacAlpine Channel area, District of Mackenzie, Northwest Territories: Geological Survey of Canada, Map 1546A, scale 1:50,000.

Hildebrand, R.S., Bowring, S.A., Steer, M.E., and Van Schmus, W.R., 1983. Geology and U-Pb geochronology of parts of the Leith Peninsula and Rivère Grandin map areas, District Mackenzie: in Current Research, Part A, Geological Survey of Canada, Paper 83-1A, p. 329-342.

Hildebrand, R.S., Annesley, I.R., Bardoux, M.V., Davis, W.J., Reichenbach, I.G., and Van Nostrand, T., 1984. Geology of the early Proterozoic rocks in parts of the Leith Peninsula map area, District Mackenzie: in Current Research, Part A, Geological Survey of Canada, Paper 84-1A, p. 217-221.

Hildebrand, R.S., Bowring, S.A., and Housh, T., 1990. The Medial zone of Wopmay orogen, District of Mackenzie, in Current Research, Part C, Geological Survey of Canada Paper 90–1C, p. 167–176.

Hildebrand, R.S., and Roots, C.F. 1985. Geology of the Rivière Grandin map area (Hottah Terrane and western Great Bear Magmatic Zone), District of Mackenzie; in Current Research, Part A, Geological Survey of Canada, paper 85-1A: p. 373-383.

Hildebrand, R.S., Hoffman, P.F., and Bowring, S.A. 1987. Tectono-magmatic evolution of the 1.9 Ga Great Bear magmatic zone, Wopmay Orogen, Northwestern Canada: Journal of Volcanology and Geothermal Research, **32**: p. 99-118.

Hildebrand, R.S., Hoffman, P.F., and Bowring, S.A. 2010. The Calderian orogeny in Wopmay orogen (1.9 Ga), northwestern Canadian Shield: Geological Society of America Bulletin, **122**, p. 794-814.

Hoffman, P.F., 1980. Wopmay orogen: Wilson cycle of early Proterozoic age in the northwest of the Canadian Shield: in Strangway, D.W., ed., The Continental Crust and its Mineral Deposits: Geological Association of Canada Special Paper 20, p. 523–549.

Hoffman, P.F., 1988. United plates of America, the birth of a craton: Earth Planet Annual Reviews of Earth and Planetary Sciences, **16**: p. 543-603.

Hoffman, P.F., and Bowring, S.A., 1984. Short-lived 1.9 Ga continental margin and its destruction, Wopmay orogen, northwest Canada: Geology, **12**, p. 68-72.

Housh, T., Bowring, S.A., and Villeneuve, M., 1989. Lead isotopic study of early Proterozoic Wopmay orogen, NW Canada: Role of continental crust in arc magmatism: The Journal of Geology, **97**: p. 735–747.

Jackson, V.A., Bennett, V., van Breeman, O., Ootes, L., Bleeker, W., and Davis, W.J., 2010. Geochronology of the south-central Paleoproterozoic Wopmay Orogen, northwestern Canadian Shield: GeoCanada 2010, Calgary, AB, May, 2010 1 Poster.

Kidd, D.F., 1936. Rae to Great Bear Lake, Mackenzie District, NWT: Geological Survey of Canada, Memoir 187.

Kretz, R., 1983. Symbols for rock-forming minerals: American Mineralogist, **68**, p. 277-279.

Lord, C.S., 1942. Snare River and Ingray Lake Map-Areas, Northwest Territories: Geological Survey of Canada, Memoir 235.

Ludwig, K.R., 2008. Isoplot/Ex, version 3.6, A geochronological toolkit for Microsoft Excel: Berkely Geochronological Center, Special publication No. 4.

Ludwig, K.R., 2009. SQUID 2.5. The commonwealth of Australia represented by Geoscience Australia, GPO Box 378, Canberra ACT 2601, Australia.

Martin, A.J., DeCelles, P.G., Gehrels, G.E., Patchett, P.J., and Isachsen, C., 2005. Isotopic and structural constraints on the location of the Main Central Thrust in the Annapurna Range, central Nepal Himalaya: Geological Society of America Bulletin: **117**, p. 926–944.

McGlynn, J.C., 1976. Geology of the Calder River map area (86F) and Leith Peninsula (86E) map areas, District Mackenzie; in Report of Activities, Part A, Geological Survey of Canada, Paper 79-1A, p. 339-361.

McGlynn, J.C., 1979. Geology of Precambrian rocks of the Rivière Grandin and in part of the Marian River map areas, District of Mackenzie: in Current Research, Part A, Geological Survey of Canada, Paper 79-1A, p. 127-131.

Ootes, L., Davis, W.J., Bleeker, W., and Jackson, V.A., 2009. Two distinct ages of Neoarchean turbidites in the Western Slave craton: Futher evidence and implications for a possible back-arc model: The Journal of Geology, **117**: p. 15-36.

Reichenbach, I., 1991. The Bell island Bay Group, remnant of an Early Proterozoic ensialic marginal basin in Wopmay orogen, District of Mackenzie: Geological Survey of Canada, Paper 88-28.

Rubatto, D., 2002. Zircon trace element geochemistry: partitioning with garnet and the link between U-Pb ages and metamorphism: Chemical Geology, **184**, p. 123-138.

Sircombe, K.N., 2003. AgeDisplay: an Excel workbook to evaluate and display univariate geocrhonological data using binned frequency histograms and probability density distributions: Computers and Geoscience **30**: p. 22-31.

Spratt, J.E., Jones, A.G., Jackson, V., Collins, L., and Avdeeva, A., 2009. Lithospheric geometry of the Wopmay orogen from a Slave craton to Bear Province magnetotelluric transect: Journal of Geophysical Research, **114**.

Stern, R.N., 1996. A SHRIMP II ion microprobe at the Geological Survey of Canada: Geoscience Canada, **23**: p. 73–76

Stern, R.A. 1997. The SC sensitive high resolution ion microprobe (SHRIMP): analytical techniques of zircon U–Th–Pb age determinations and performance evaluation: In Radiogenic age and isotopic studies: Report 10, Geological Survey of Canada, Current Research, p. 1–31.

Stern, R.A., and Amelin, Y., 2003. Assessment of errors in SIMS zircon U–Pb geochronology using a natural zircon standard and NIST SRM 610 glass: Chemical Geology, **197**: p. 111–116.

Winter, J.D., 2010. Principles of igneous and metamorphic petrology, second addition: Pearson Education, Inc: p. 607-608.

APPENDIX A: ABBREVIATIONS

Abbreviations of Mineral Names

Amphibole:	Am
Biotite:	Bt
K-feldspar	Kfs
Plagioclase:	Pl
Microcline:	Mc
Monazite	Mnz
Muscovite:	Ms
Quartz:	Otz
Sillimanite:	Sil
Tourmaline:	Tur
Zircon:	Zrn

After Kretz (1983)

Abbreviations of Place Names and Dating techniques

Holly Lake Metamorphic Complex:	HLMC
Great Bear Magmatic Zone:	GBMZ
Great Slave Shear Zone:	GSSZ
Wopmay Fault Zone:	WFZ
Thermal Ionization Mass Spectrometry:	TIMS
Sensitive High Resolution Ion Microprobe:	SHRIMP

Abbreviation of Texture Names

Main foliation:	S-main
Internal foliation:	S_i

APPENDIX B: DETRITAL ZIRCON IMAGES

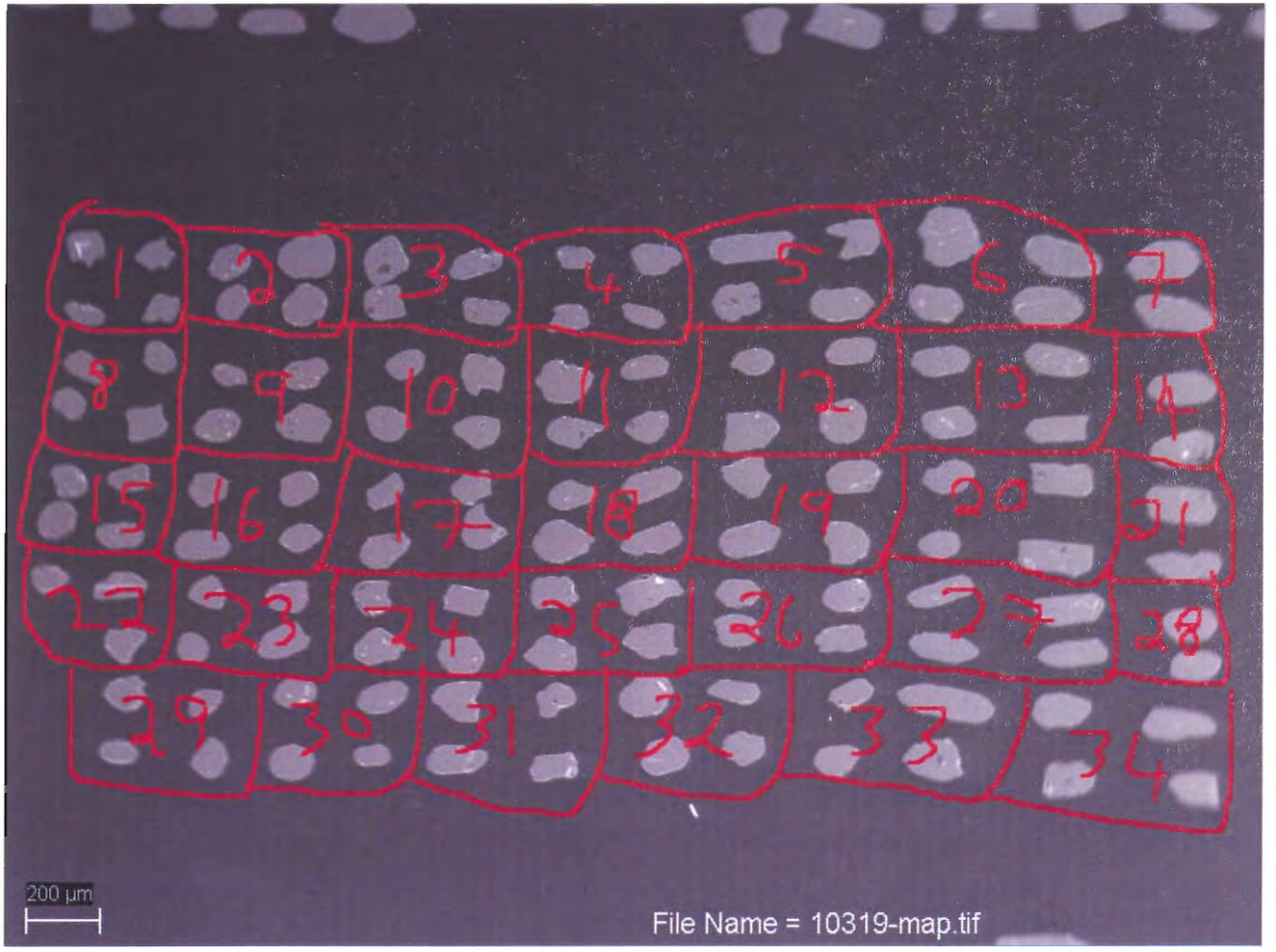

Annotated map of zircons mounted on epoxy disk. Numbers refer to picture sets to follow (10319-01, 10319-02, ext).

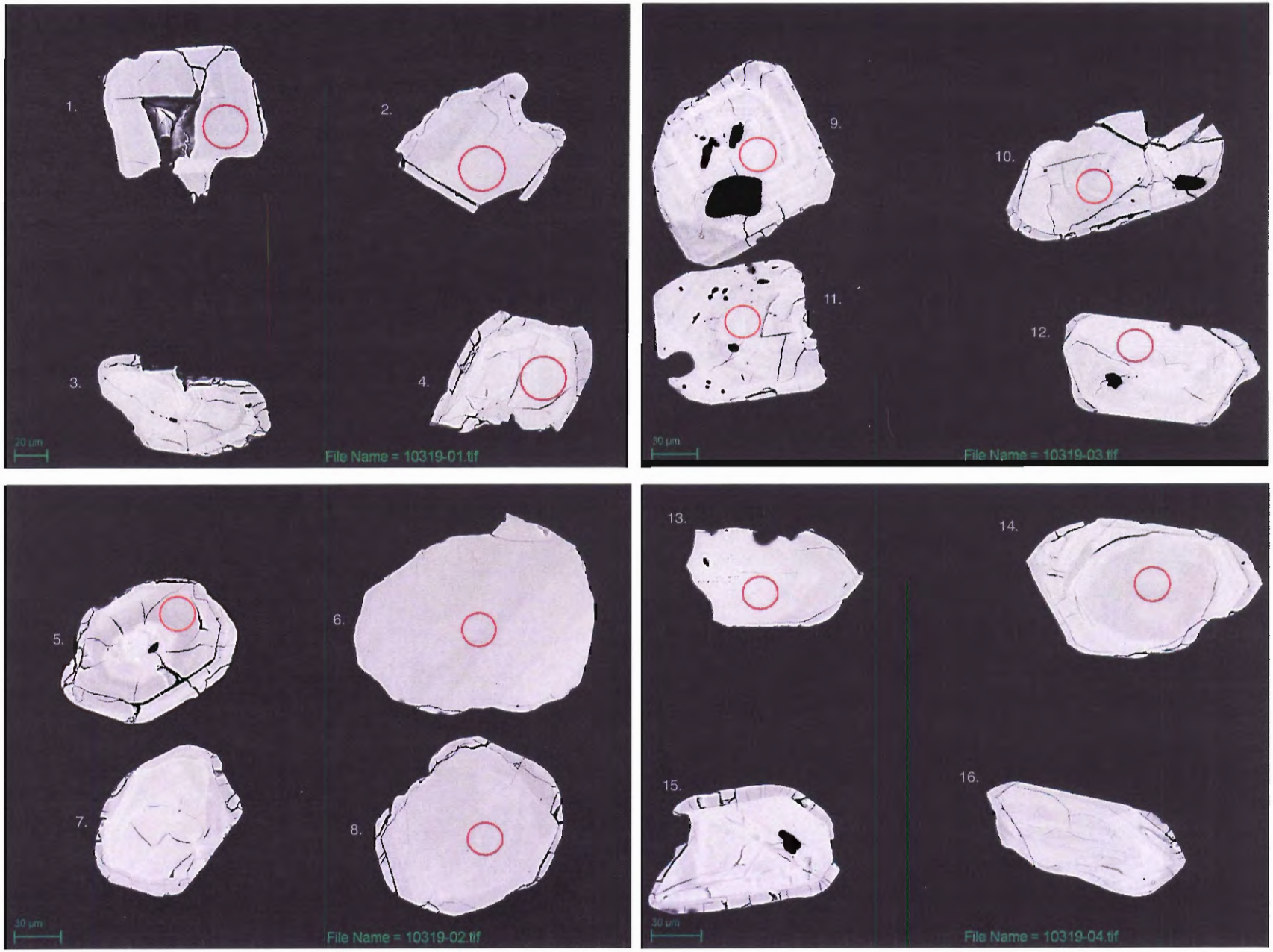

Orange circles refer to analyzed spot location. Beam diameter is 25 µm. Number refers to grain number. See Table 1 in text for isotopic data corresponding to grain number.

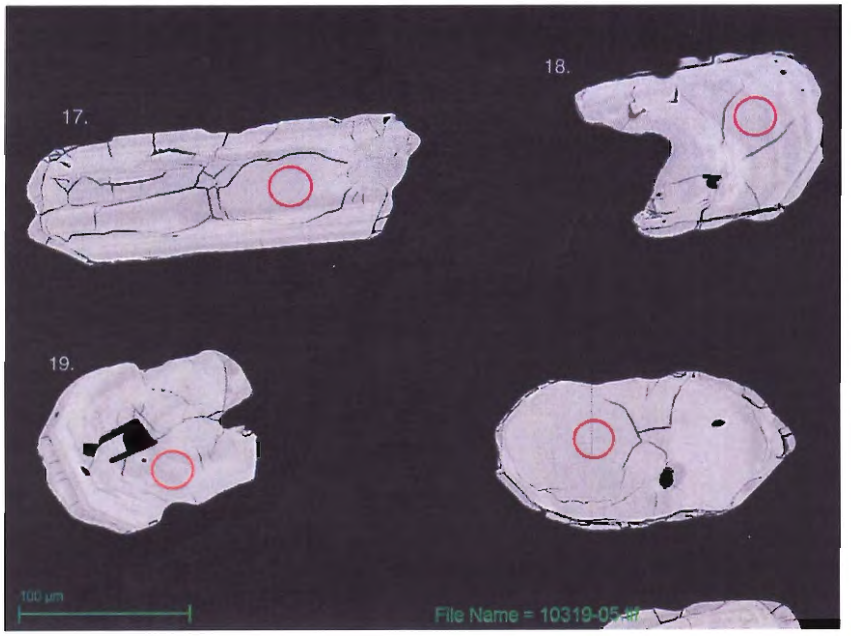
17.
18.
19.
100 µm
File Name = 10319-05.tif

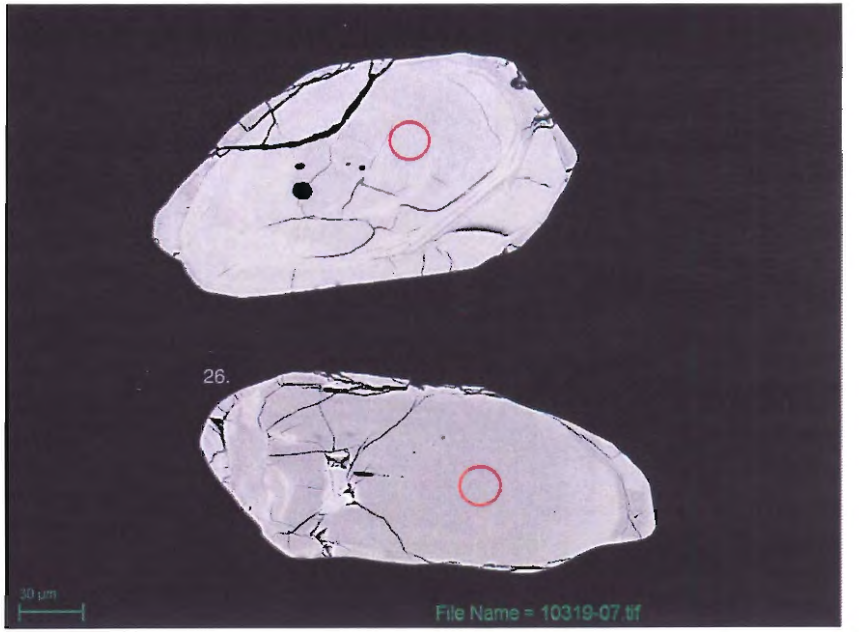
26.
30 µm
File Name = 10319-07.tif

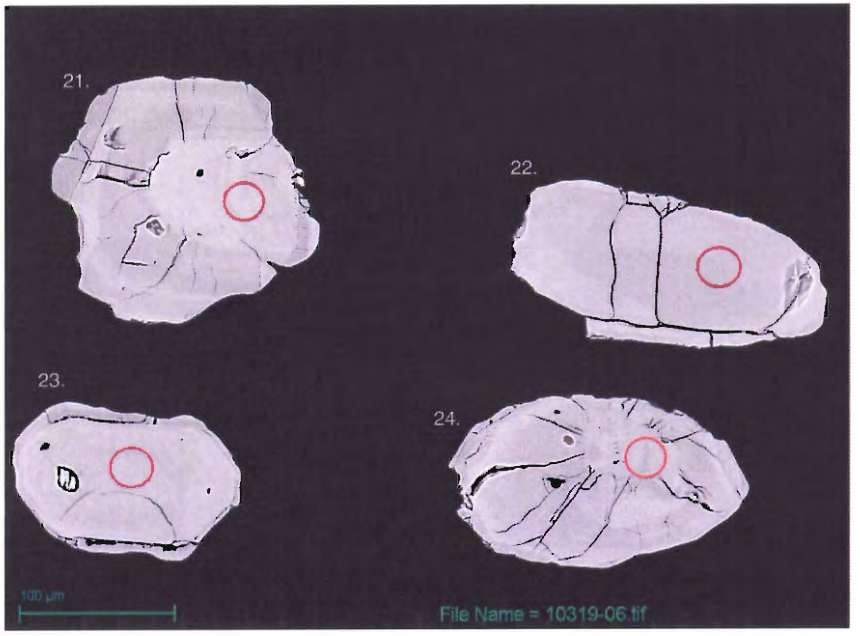
21.
22.
23.
24.
100 µm
File Name = 10319-06.tif

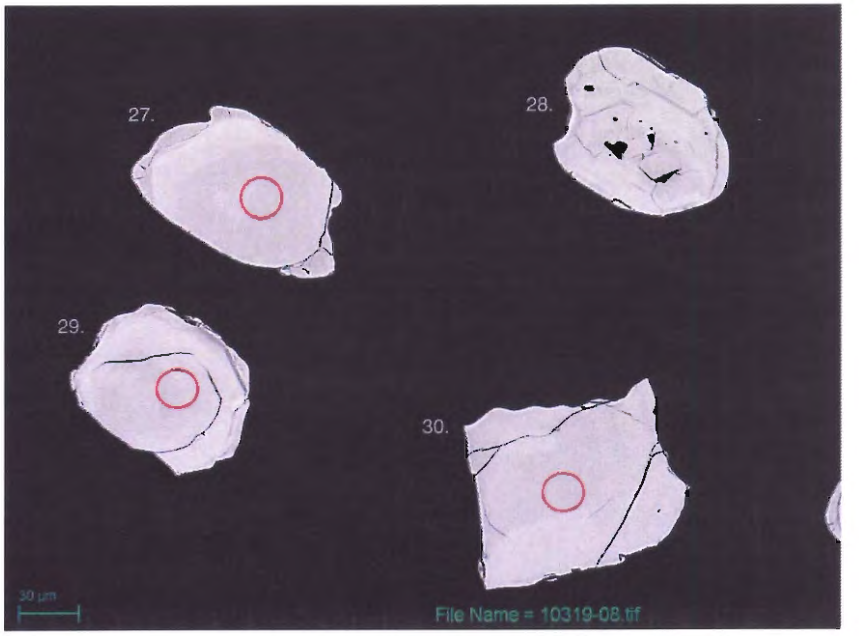
27.
28.
29.
30.
30 µm
File Name = 10319-08.tif

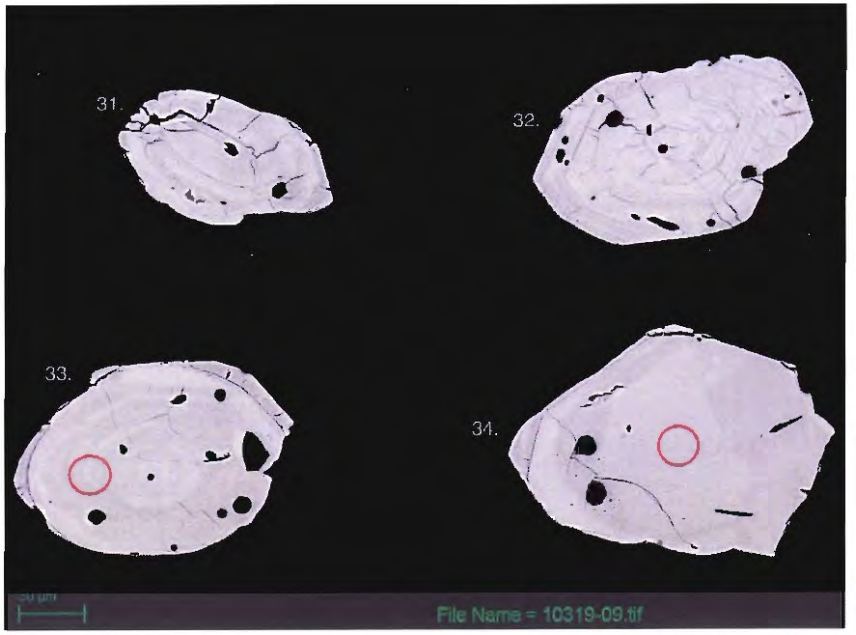
31.
32.
33.
34.
File Name = 10319-09.tif

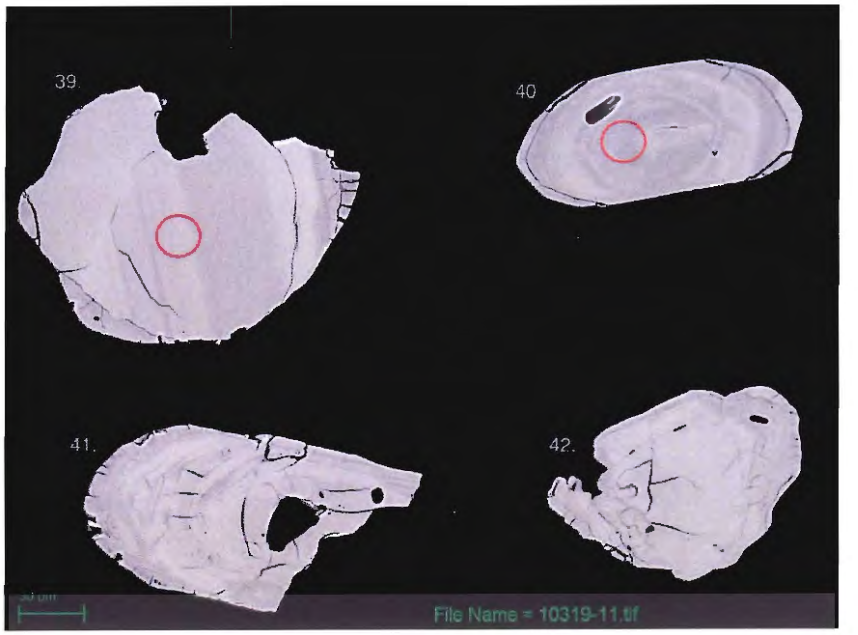
39.
40
41.
42.
File Name = 10319-11.tif

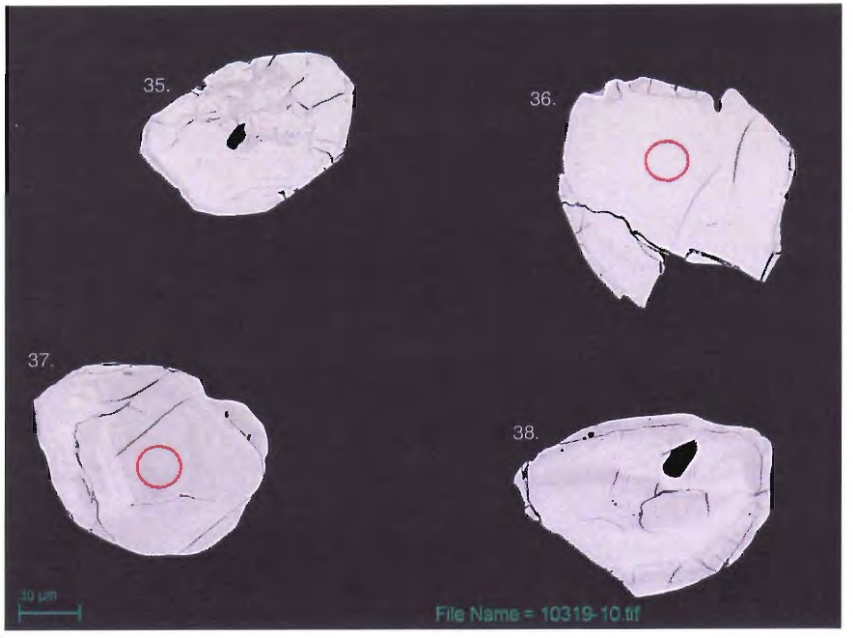
35.
36.
37.
38.
File Name = 10319-10.tif

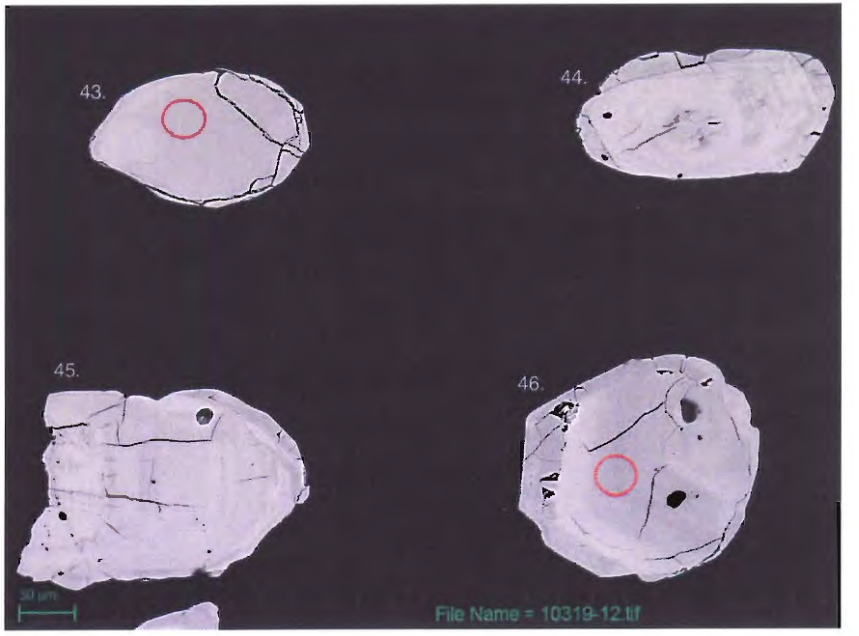
43.
44.
45.
46.
File Name = 10319-12.tif

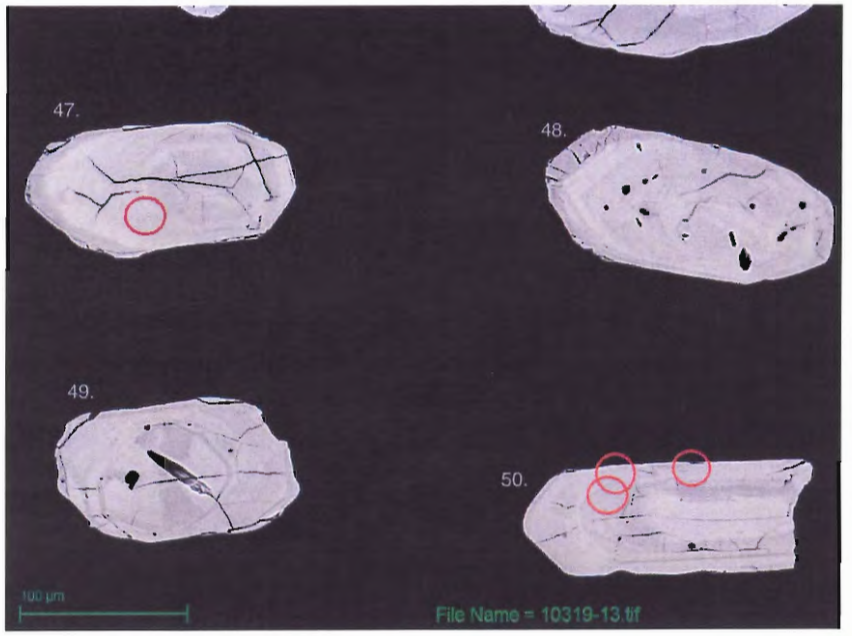
47.
48.
49.
50.
100 µm
File Name = 10319-13.tif

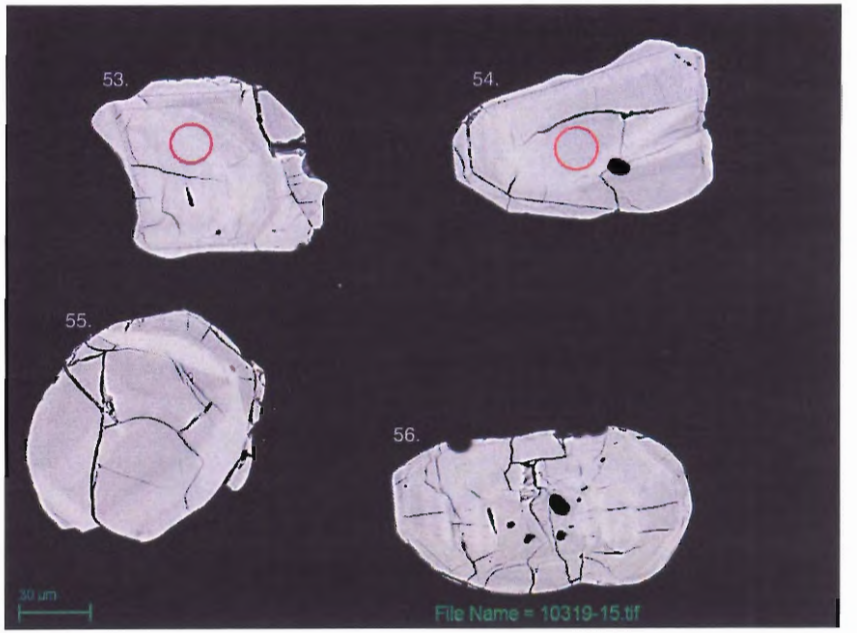
53.
54.
55.
56.
30 µm
File Name = 10319-15.tif

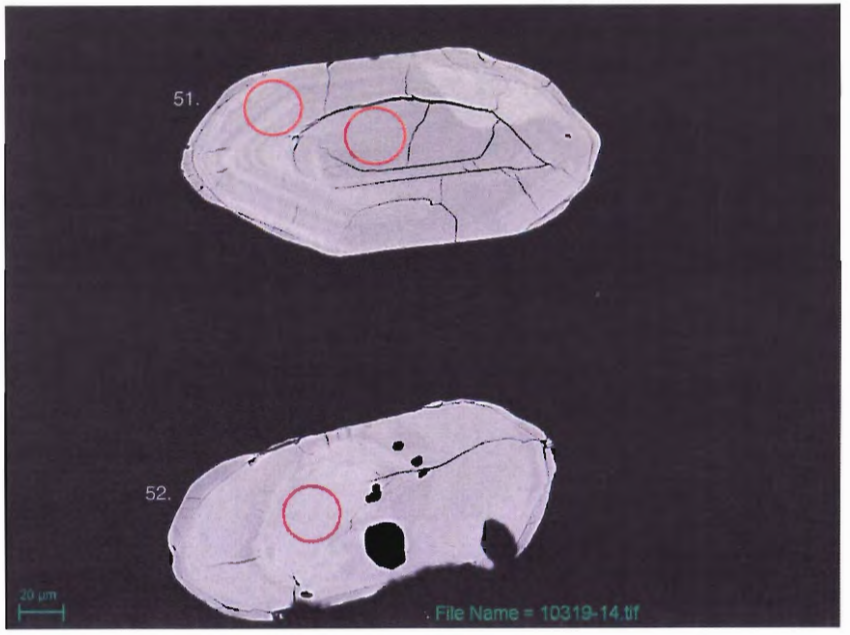
51.
52.
20 µm
File Name = 10319-14.tif

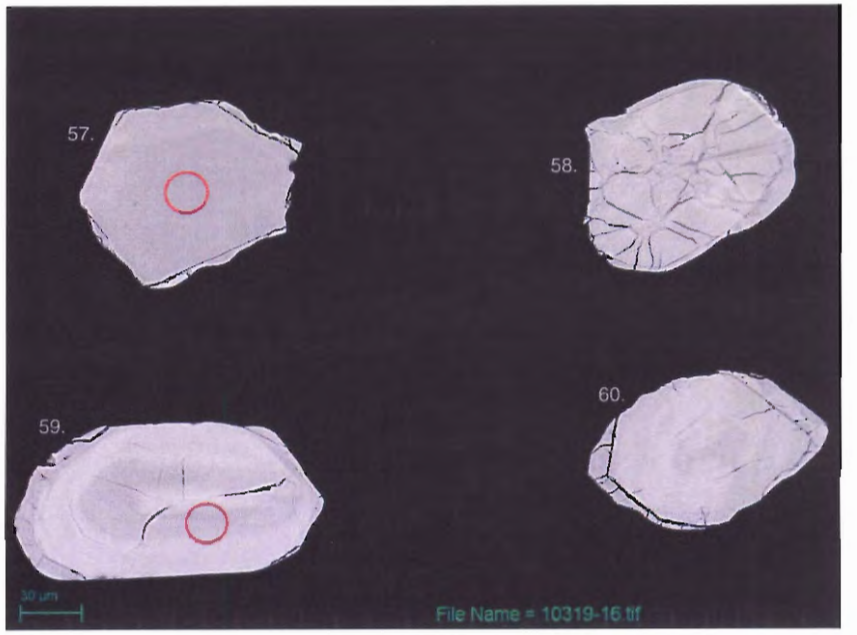
57.
58.
59.
60.
30 µm
File Name = 10319-16.tif

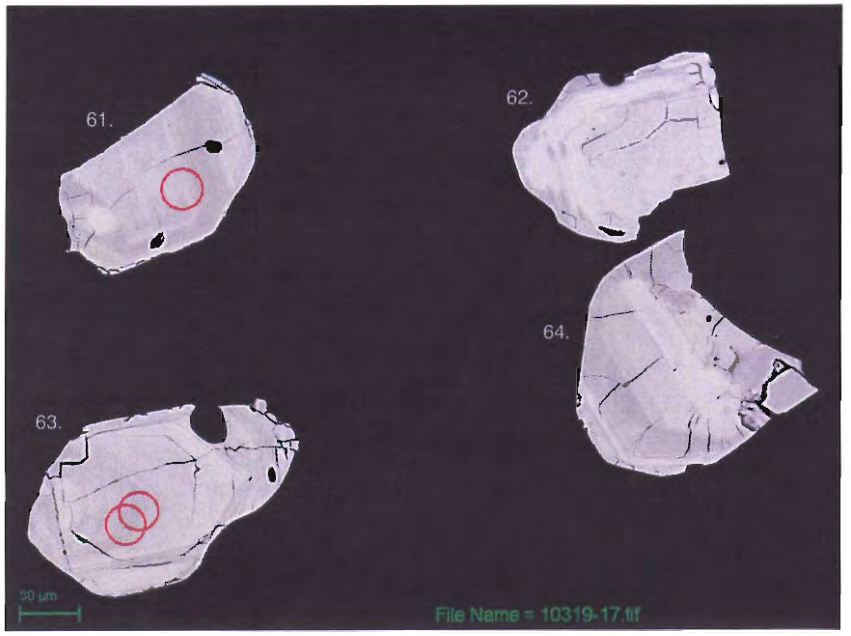
61.
62.
64.
63.
30 µm
File Name = 10319-17.tif

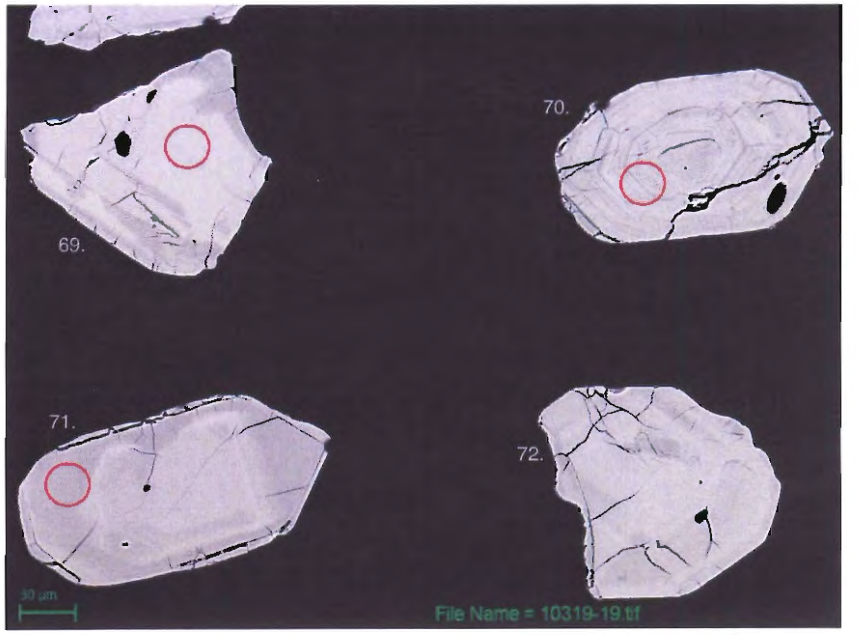
69.
70.
71.
72.
30 µm
File Name = 10319-19.tif

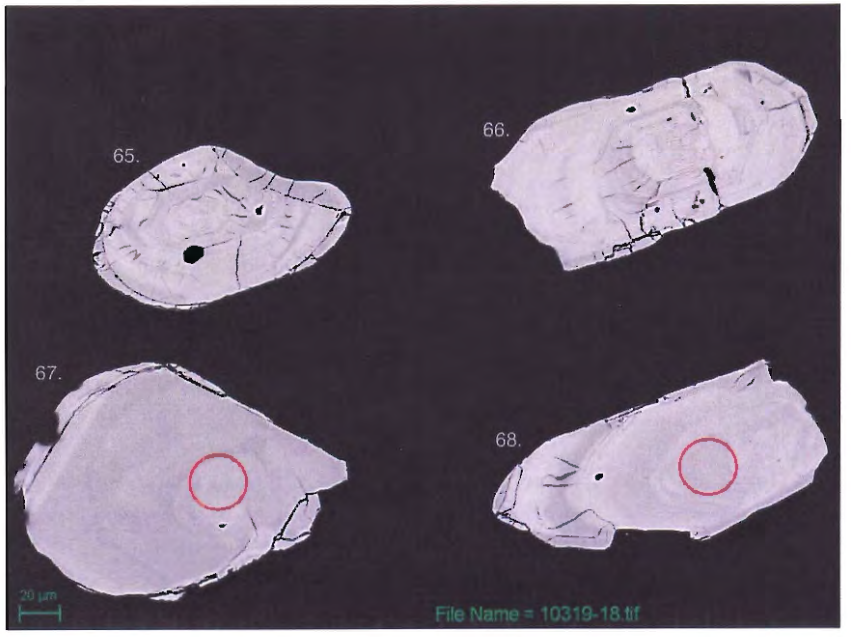
65.
66.
67.
68.
20 µm
File Name = 10319-18.tif

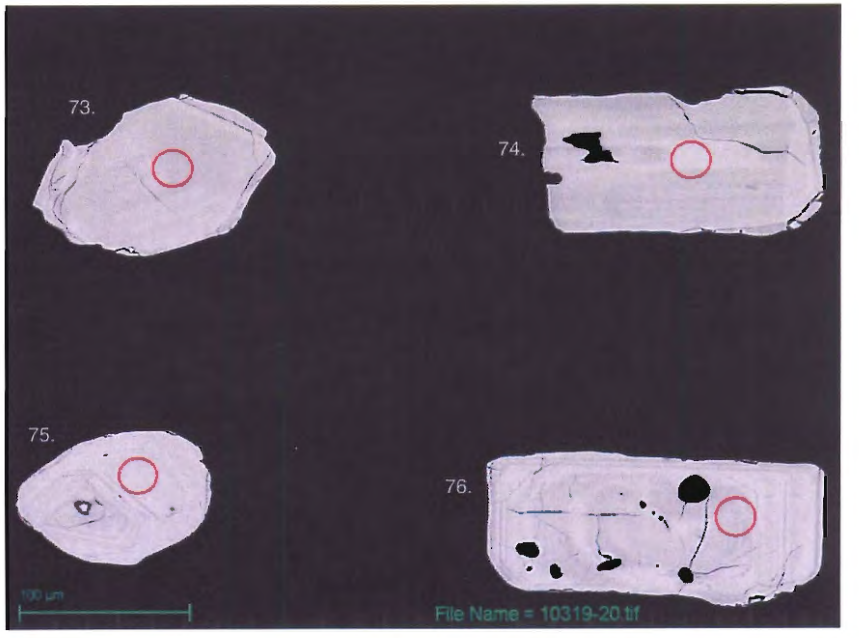
73.
74.
75.
76.
100 µm
File Name = 10319-20.tif

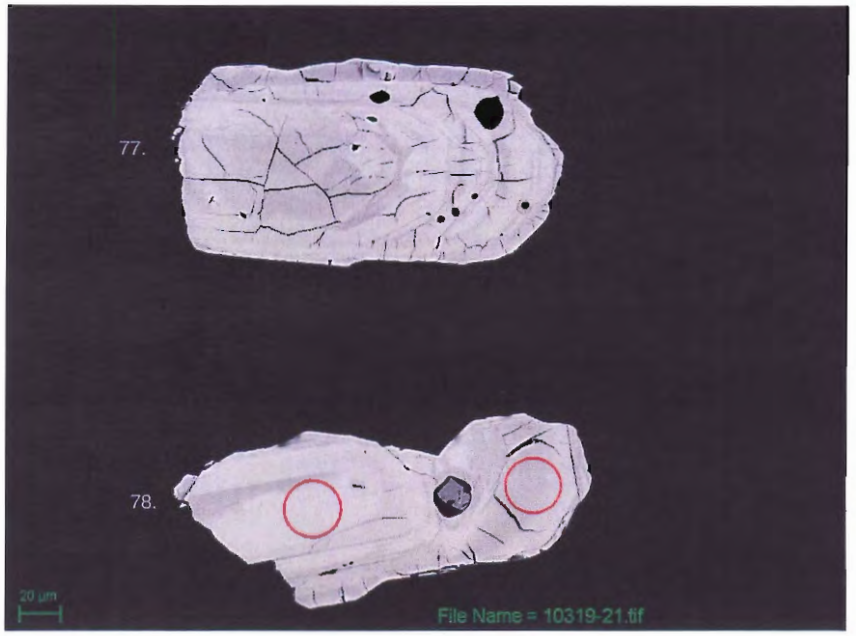
77.
78.
20 µm
File Name = 10319-21.tif

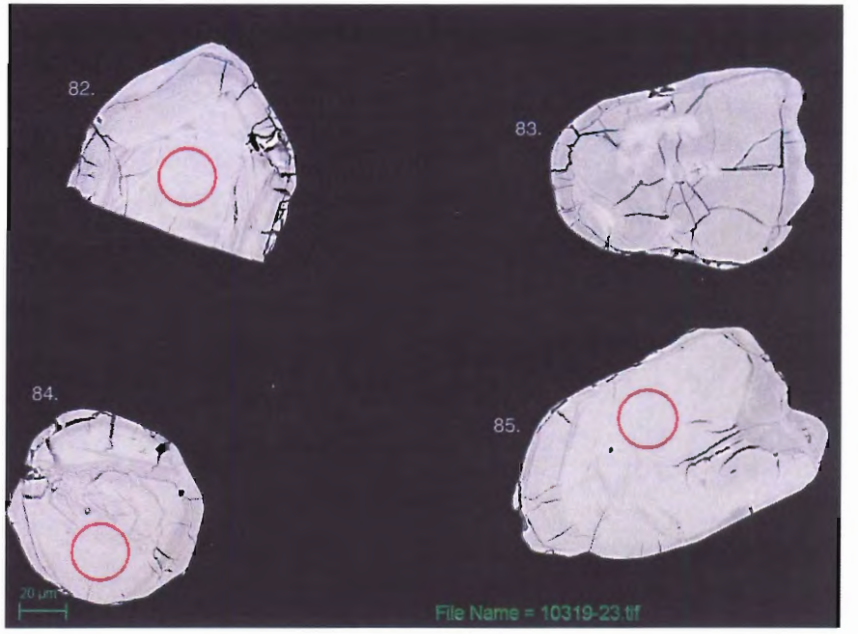
82.
83.
84.
85.
20 µm
File Name = 10319-23.tif

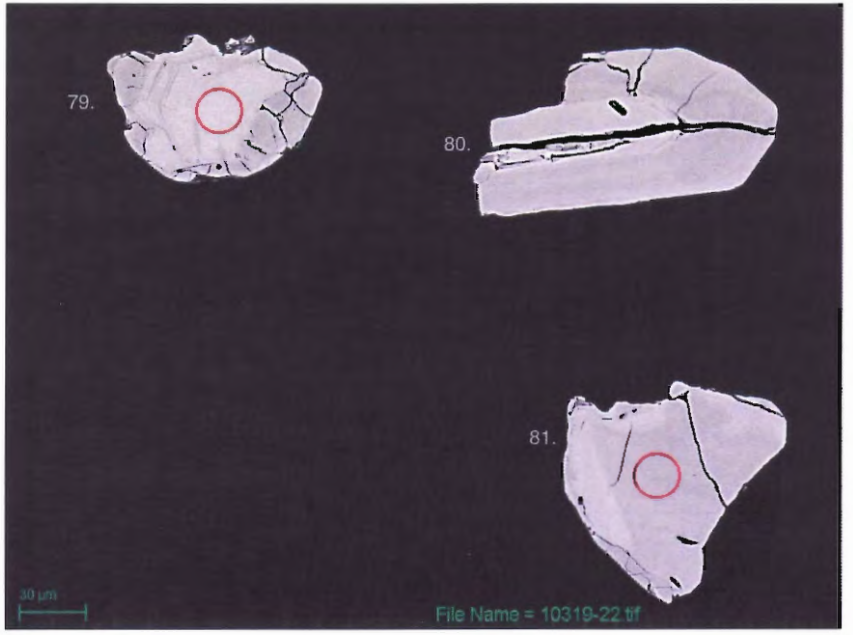
79.
80.
81.
30 µm
File Name = 10319-22.tif

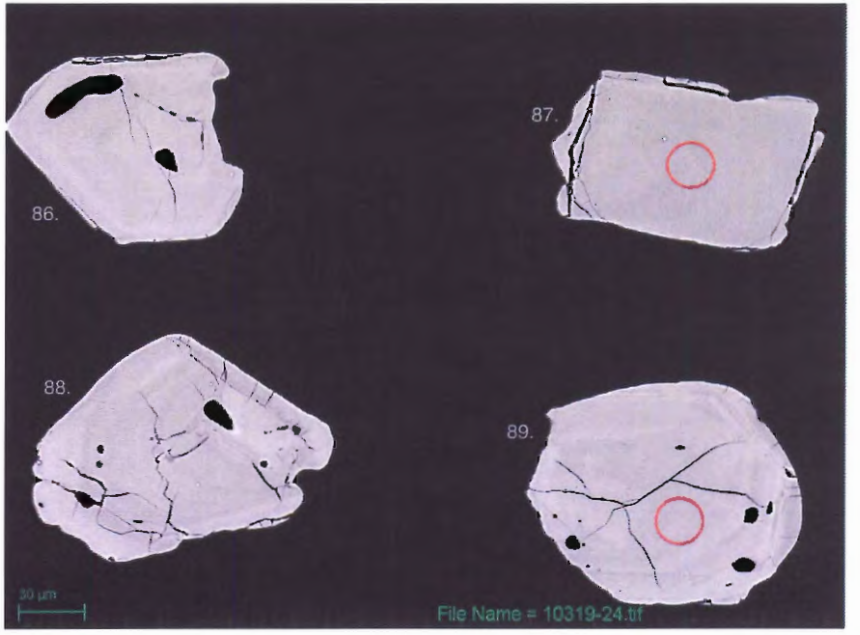
86.
87.
88.
89.
30 µm
File Name = 10319-24.tif

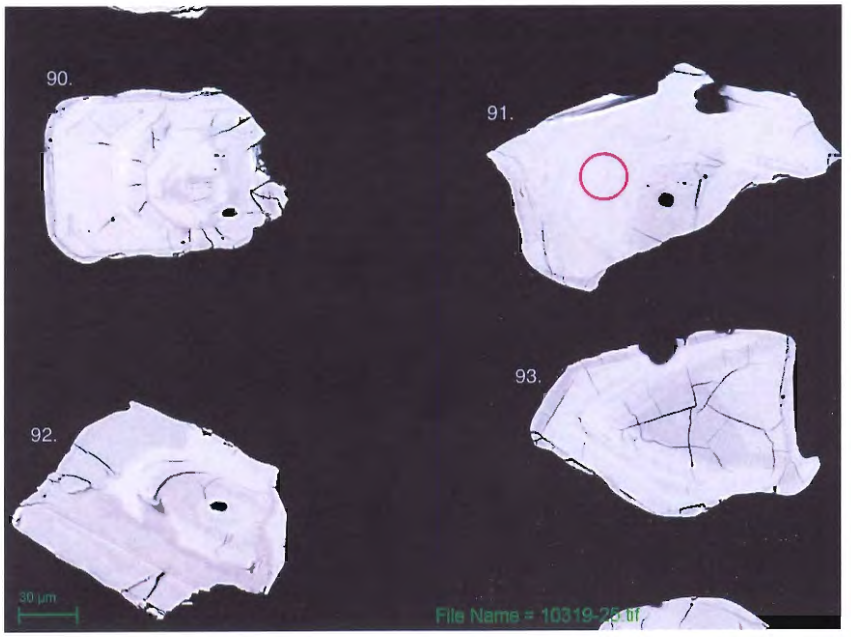
90.
91.
92.
93.
30 µm
File Name = 10319-25.tif

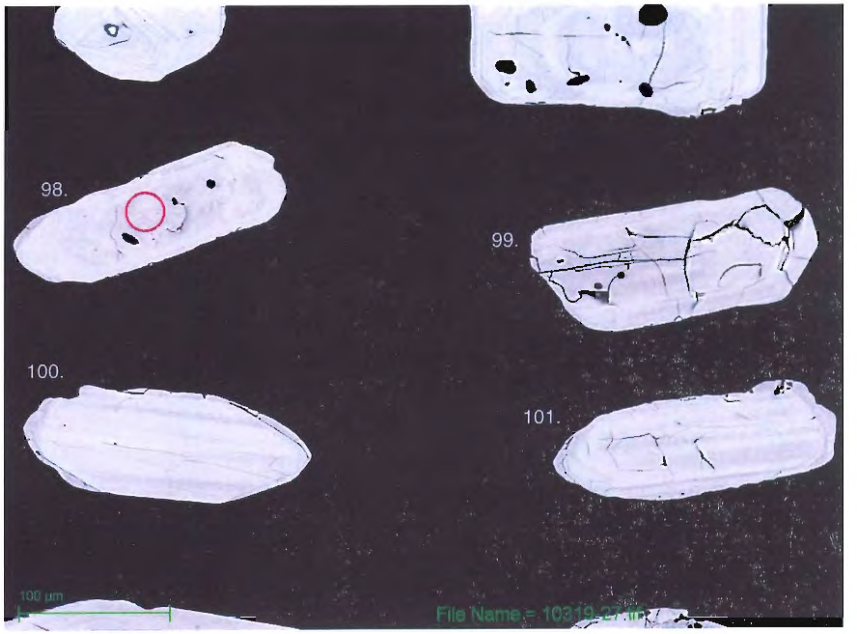
98.
99.
100.
101.
100 µm
File Name = 10319-27.tif

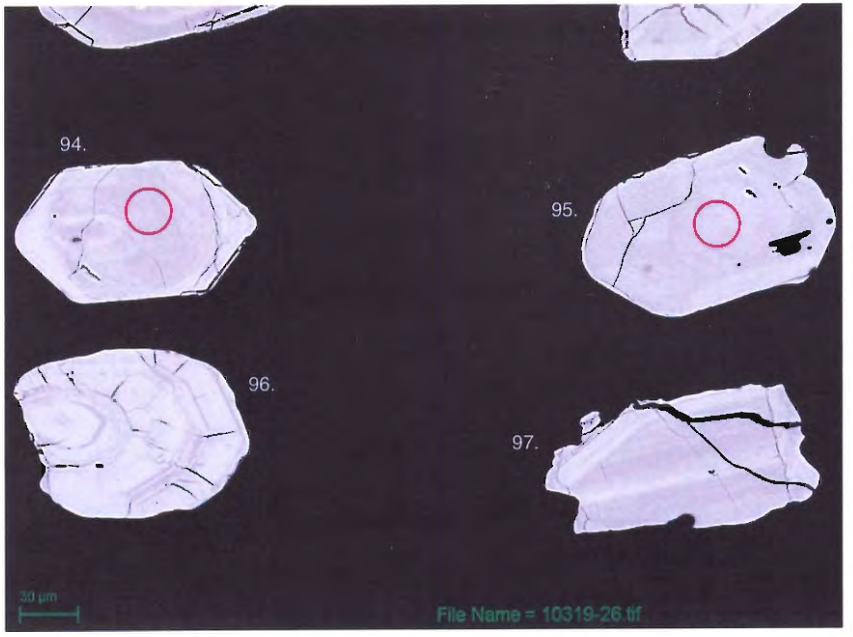
94.
95.
96.
97.
30 µm
File Name = 10319-26.tif

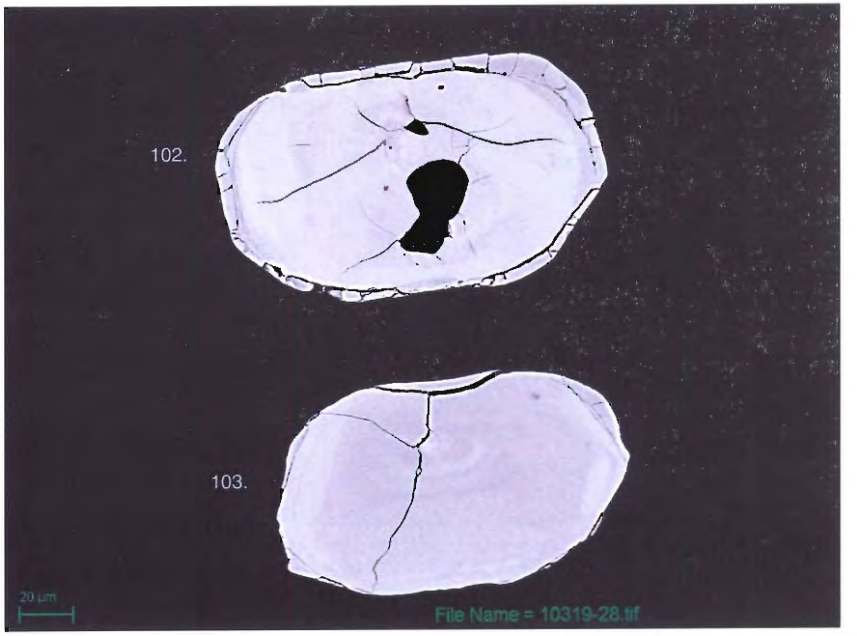
102.
103.
20 µm
File Name = 10319-28.tif

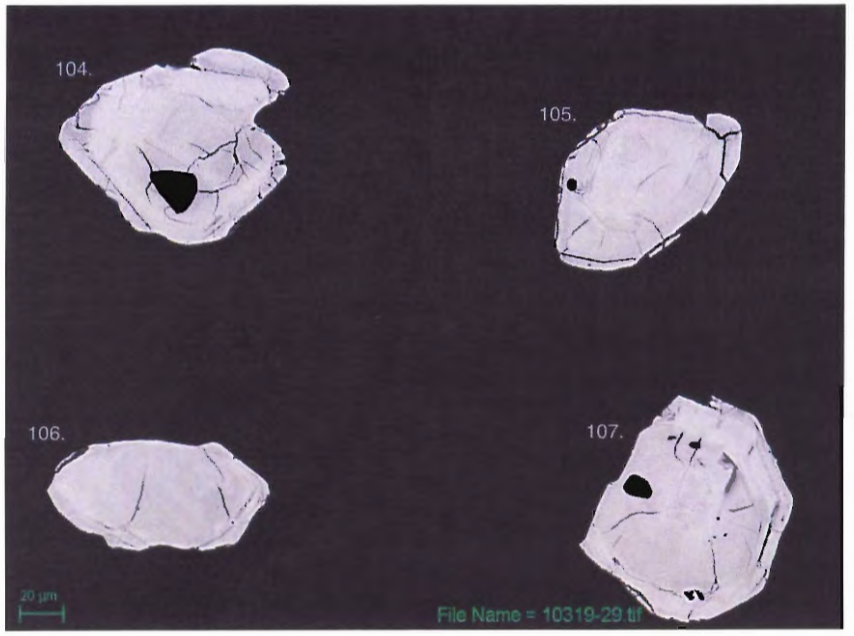
104.
105.
106.
107.
20 µm
File Name = 10319-29.tif

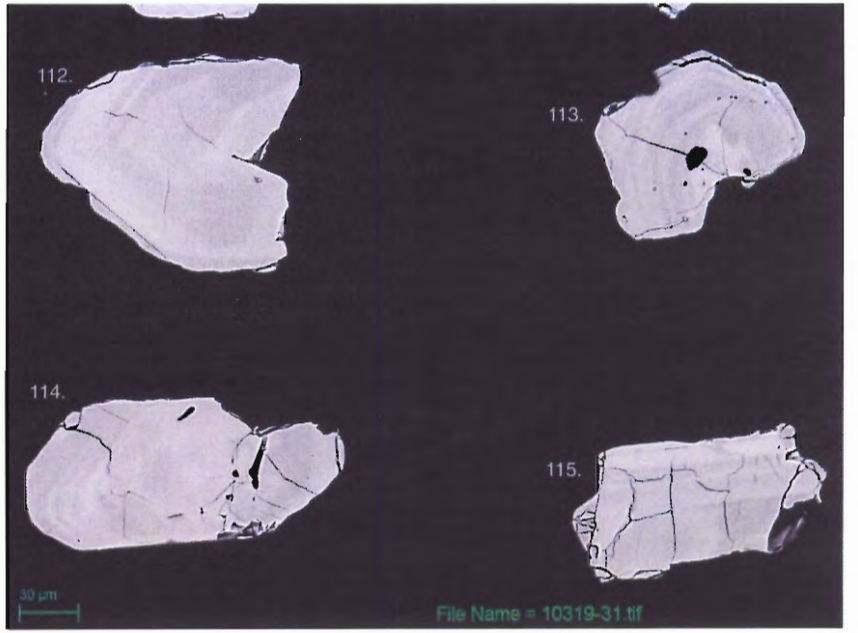
112.
113.
114.
115.
30 µm
File Name = 10319-31.tif


108.
109.
110.
111.
30 µm
File Name = 10319-30.tif

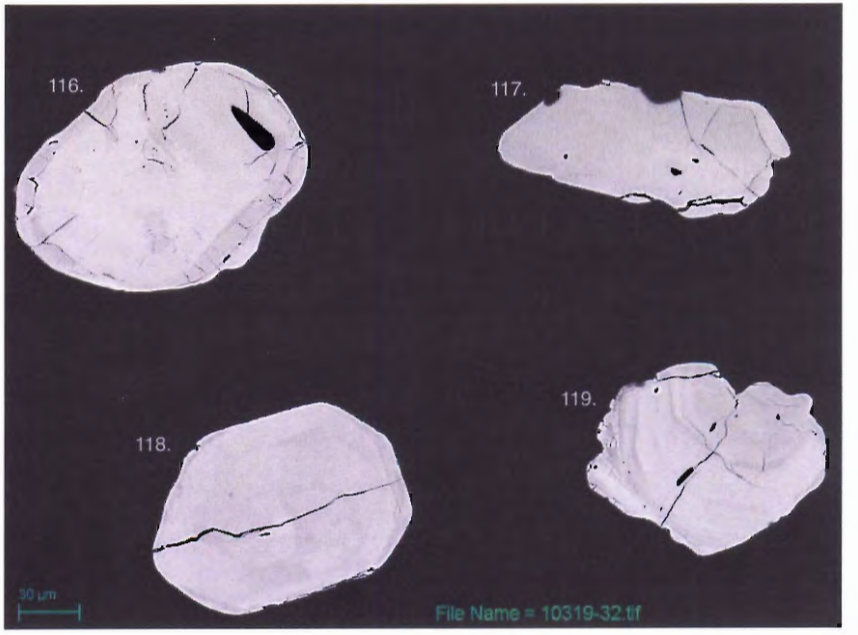
116.
117.
118.
119.
30 µm
File Name = 10319-32.tif

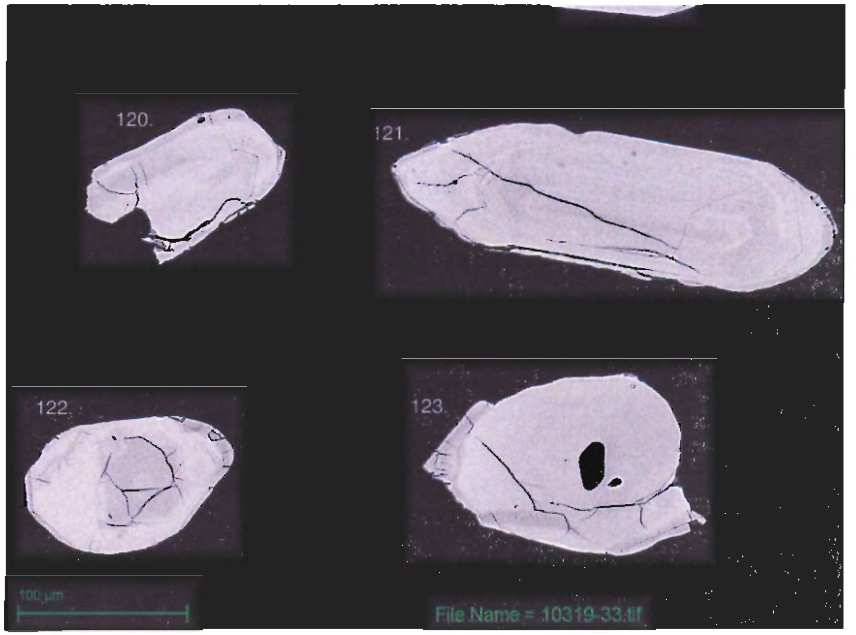
120.
121.
122.
123.
100 µm
File Name = 10319-33.tif

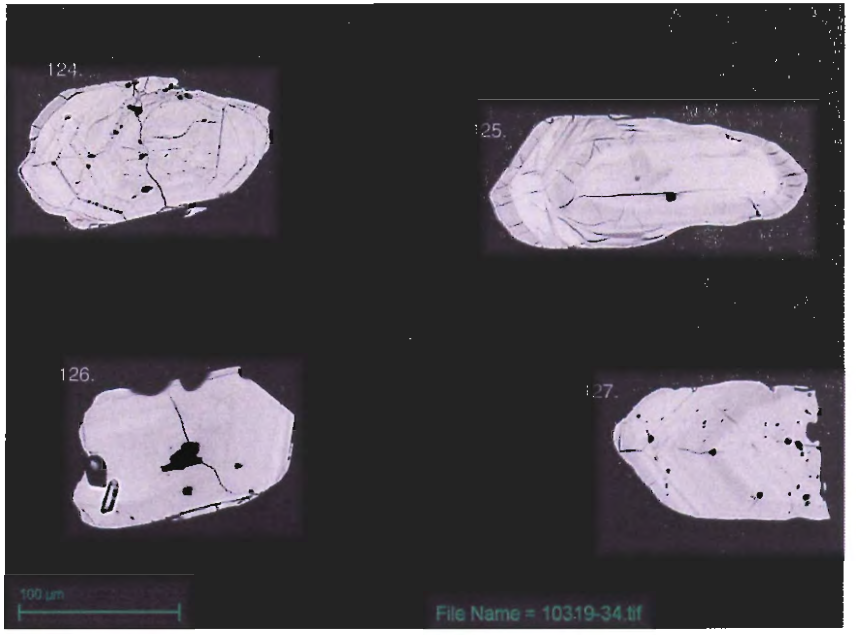
124.
125.
126.
127.
100 µm
File Name = 10319-34.tif

APPENDIX C: U-Pb SHRIMP ISOTOPIC DATA

Errors are 1σ unless otherwise specified

Spot Name	Date/Time	Hours	Bkrd cts /sec	total 195.8 cts /sec	total 204 cts /sec	total 204.1 cts /sec	total 206 cts /sec	total 238 cts /sec	204 /206	% err	207 /206	% err	208 /206	% err	190 /195.8	% err
10319-1.1	2010-12-13, 11:44	2	0.00	11304	0.10	0	697	785	1.2E-4	24	0.124	0.80	0.270	3.0	0.37	0.69
10319-10.1	2010-12-13, 14:48	5	0.00	11144	0.50	0	2016	2352	2.4E-4	18	0.126	0.47	0.108	2.7	0.42	0.67
10319-103.1	2010-12-14, 11:47	26	0.06	12362	0.62	0	1326	1116	4.2E-4	19	0.184	0.51	0.201	2.5	0.36	0.67
10319-11.1	2010-12-13, 15:05	5	0.00	11232	0.38	0	5305	4730	6.8E-5	21	0.162	0.27	0.215	1.2	0.58	0.60
10319-110.1	2010-12-18, 02:09	112	0.13	10916	0.39	0	2829	2512	7.6E-5	64	0.160	0.33	0.242	1.6	0.42	0.67
10319-111.1	2010-12-18, 02:28	112	0.06	9690	0.20	0	2082	1867	8.5E-5	50	0.163	0.38	0.222	1.9	0.41	0.72
10319-112.1	2010-12-18, 02:47	113	0.00	11113	0.44	0	1476	1222	3.1E-4	19	0.174	0.45	0.153	2.8	0.28	0.78
10319-113.1	2010-12-18, 03:43	114	0.15	11067	0.47	0	1468	1273	1.9E-4	61	0.161	0.46	0.298	2.0	0.40	0.68
10319-114.1	2010-12-18, 03:06	113	0.00	10193	0.46	0	2426	2137	1.4E-4	21	0.163	0.36	0.216	1.8	0.64	0.91
10319-116.1	2010-12-18, 04:02	114	0.06	8810	0.26	0	4269	3930	4.0E-5	44	0.157	0.27	0.148	1.7	1.20	0.57
10319-118.1	2010-12-18, 04:21	114	0.10	10863	0.28	0	2341	2682	4.4E-5	37	0.121	0.39	0.306	1.6	0.29	0.78
10319-119.1	2010-12-18, 04:39	115	0.08	10298	0.92	0	3797	3268	2.0E-4	19	0.164	0.28	0.198	1.5	0.88	0.56
10319-121.1	2010-12-14, 14:07	28	0.00	11248	0.19	0	1673	1878	5.3E-5	25	0.125	0.51	0.105	3.1	0.40	0.68
10319-13.1	2010-12-13, 17:45	8	0.00	11102	0.42	0	2815	2718	1.5E-4	20	0.157	0.37	0.080	2.7	0.41	0.83
10319-14.1	2010-12-13, 18:02	8	0.00	11002	0.23	0	1285	1246	1.8E-4	26	0.150	0.55	0.267	2.2	0.37	0.71
10319-17.1	2010-12-13, 18:18	8	0.00	11811	0.16	0	1825	2148	7.8E-5	34	0.122	0.50	0.047	4.3	0.18	0.89
10319-18.1	2010-12-13, 18:51	9	0.10	11919	0.20	0	1596	1695	4.5E-5	40	0.137	0.51	0.198	2.3	0.37	0.68
10319-19.1	2010-12-13, 19:07	9	0.00	11801	0.29	0	3397	3231	9.2E-5	24	0.158	0.34	0.151	1.8	0.47	0.63
10319-2.1	2010-12-13, 12:39	3	0.00	10698	0.10	0	1514	1354	6.0E-5	39	0.159	0.50	0.246	2.1	0.60	0.61
10319-20.1	2010-12-13, 19:24	9	0.00	12420	0.13	0	1743	2063	7.1E-5	37	0.124	0.51	0.117	2.8	0.53	0.59
10319-21.1	2010-12-13, 19:56	10	0.09	12537	0.26	0	3391	3874	4.4E-5	60	0.121	0.37	0.133	1.9	0.32	0.69
10319-22.1	2010-12-13, 20:13	10	0.00	11604	0.06	0	1344	1268	4.0E-5	21	0.161	0.53	0.157	2.8	0.25	0.80
10319-23.1	2010-12-13, 20:29	10	0.00	12571	0.25	0	1711	2018	1.4E-4	26	0.123	0.51	0.162	2.4	0.53	0.58
10319-24.1	2010-12-14, 12:29	26	0.00	9950	3.71	0	13757	15258	2.6E-4	7	0.133	0.18	0.016	2.7	0.29	0.81
10319-25.1	2010-12-13, 11:21	1	0.10	10684	0.10	0	1918	2262	1E-32	100	0.121	0.49	0.088	3.1	0.63	0.60
10319-26.1	2010-12-13, 20:45	11	0.06	11912	0.19	0	439	498	2.3E-4	142	0.130	0.99	0.175	4.7	0.37	0.68
10319-27.1	2010-12-13, 21:18	11	0.00	12281	0.20	0	1885	2070	1.3E-4	25	0.129	0.48	0.141	2.5	0.38	0.66
10319-29.1	2010-12-13, 21:35	11	0.00	11484	0.21	0	2001	2441	1.0E-4	28	0.121	0.48	0.213	2.0	0.32	0.72
10319-30.1	2010-12-13, 21:51	12	0.04	12427	0.12	0	2092	1784	2.1E-5	316	0.171	0.42	0.120	2.6	0.34	0.68
10319-33.1	2010-12-14, 12:49	27	0.06	11484	0.16	0	2073	1892	5.6E-5	122	0.165	0.42	0.115	2.6	0.22	0.84
10319-34.1	2010-12-13, 22:07	12	0.00	11573	0.13	0	1794	1592	5.4E-5	21	0.157	0.46	0.232	3.0	0.61	1.00

Spot Name	206 /238	% err	254 /238	% err	248 /254	% err	206 /254	% err	238 /195.8	% err	195.9 /195.8	% err	206Pb /238U calibr. const	% err	% com 206	208Pb* /206Pb*	% err	ppm U
10319-1.1	0.88	0.82	5.783	0.73	0.84	0.74	0.152	0.69	0.071	0.88	7.78	0.40	0.0112	0.61	0.20	0.266	3.0	67
10319-10.1	0.86	0.48	5.632	0.43	0.36	0.61	0.152	0.41	0.211	0.63	8.38	0.40	0.0115	0.44	0.41	0.100	2.7	202
10319-103.1	1.21	0.66	5.731	0.61	0.66	0.68	0.210	0.54	0.088	0.77	10.27	0.38	0.0156	1.25	0.72	0.187	2.5	84
10319-11.1	1.13	0.33	5.745	0.30	0.71	0.34	0.198	0.27	0.413	0.55	9.76	0.40	0.0147	0.25	0.12	0.213	1.2	391
10319-110.1	1.12	0.57	5.709	0.33	0.80	0.41	0.197	0.56	0.231	0.58	9.06	0.40	0.0147	0.31	0.13	0.239	1.6	219
10319-111.1	1.13	0.46	5.764	0.38	0.71	0.49	0.196	0.40	0.185	0.63	9.69	0.42	0.0145	0.78	0.15	0.219	1.9	173
10319-112.1	1.21	0.55	5.814	0.47	0.47	0.71	0.209	0.48	0.109	0.67	7.56	0.40	0.0153	0.39	0.54	0.142	2.8	103
10319-113.1	1.15	0.55	5.832	0.46	0.92	0.53	0.197	0.47	0.116	0.66	9.23	0.40	0.0143	0.98	0.33	0.292	2.0	107
10319-114.1	1.13	0.43	5.692	0.36	0.66	0.73	0.198	0.37	0.212	0.61	7.86	0.42	0.0149	0.29	0.25	0.211	1.8	202
10319-116.1	1.09	0.32	5.723	0.27	0.48	0.41	0.190	0.28	0.443	0.59	9.86	0.45	0.0143	0.25	0.07	0.147	1.7	421
10319-118.1	0.89	0.40	5.765	0.32	0.97	0.37	0.154	0.36	0.242	0.57	9.91	0.40	0.0114	0.26	0.08	0.304	1.6	229
10319-119.1	1.14	0.34	5.749	0.29	0.63	0.40	0.199	0.30	0.324	0.57	10.29	0.41	0.0148	0.24	0.35	0.191	1.5	309
10319-121.1	0.89	0.53	5.735	0.47	0.32	0.71	0.155	0.45	0.167	0.67	9.25	0.40	0.0115	0.63	0.09	0.103	3.1	158
10319-13.1	1.04	0.43	5.886	0.39	0.23	0.66	0.177	0.36	0.243	0.61	8.42	0.40	0.0127	0.76	0.26	0.075	2.7	227
10319-14.1	1.03	0.64	5.808	0.58	0.85	0.59	0.178	0.53	0.114	0.76	9.62	0.45	0.0128	0.61	0.31	0.262	2.2	107
10319-17.1	0.86	0.50	5.758	0.44	0.16	0.89	0.149	0.42	0.180	0.64	9.37	0.39	0.0111	0.41	0.14	0.044	4.3	171
10319-18.1	0.96	0.56	5.712	0.50	0.61	0.57	0.167	0.46	0.139	0.68	11.90	0.38	0.0125	1.19	0.08	0.197	2.3	132
10319-19.1	1.05	0.40	5.606	0.37	0.50	0.46	0.187	0.33	0.276	0.58	9.89	0.39	0.0146	0.37	0.16	0.148	1.8	266
10319-2.1	1.12	0.61	5.812	0.56	0.81	0.57	0.192	0.50	0.127	0.74	7.50	0.41	0.0141	0.46	0.10	0.244	2.1	118
10319-20.1	0.85	0.51	5.668	0.45	0.37	0.63	0.149	0.44	0.165	0.64	9.95	0.38	0.0113	0.38	0.12	0.114	2.8	156
10319-21.1	0.87	0.37	5.839	0.33	0.43	0.43	0.149	0.32	0.310	0.55	10.59	0.37	0.0108	0.57	0.08	0.132	1.9	290
10319-22.1	1.07	0.63	5.690	0.58	0.52	0.70	0.188	0.52	0.108	0.75	9.36	0.39	0.0142	0.48	0.07	0.155	2.8	103
10319-23.1	0.85	0.52	5.722	0.46	0.50	0.56	0.147	0.44	0.160	0.64	10.20	0.67	0.0111	0.43	0.24	0.157	2.4	152
10319-24.1	0.90	0.19	6.179	0.18	0.02	0.93	0.146	0.17	1.532	0.51	16.36	0.41	0.0098	0.26	0.45	0.007	2.7	1380
10319-25.1	0.86	0.49	5.725	0.43	0.29	0.67	0.150	0.42	0.209	0.65	12.47	0.40	0.0112	0.62	0.00	0.088	3.1	198
10319-26.1	0.89	1.04	5.662	0.91	0.59	1.06	0.157	0.87	0.041	1.05	9.69	0.39	0.0119	0.77	0.39	0.167	4.7	39
10319-27.1	0.91	0.51	5.755	0.45	0.44	0.58	0.159	0.42	0.167	0.64	9.35	0.38	0.0118	0.66	0.22	0.137	2.5	158
10319-29.1	0.82	0.48	5.582	0.42	0.67	0.47	0.148	0.41	0.211	0.62	11.82	0.39	0.0115	0.35	0.17	0.210	2.0	204
10319-30.1	1.17	0.52	5.849	0.48	0.39	0.65	0.200	0.43	0.143	0.66	9.75	0.38	0.0146	0.46	0.04	0.119	2.6	133
10319-33.1	1.09	0.51	5.597	0.47	0.38	0.66	0.195	0.76	0.165	0.66	10.50	0.39	0.0151	0.80	0.10	0.113	2.6	158
10319-34.1	1.13	0.56	5.818	0.51	0.73	0.55	0.194	0.46	0.136	1.06	8.93	0.39	0.0142	0.43	0.09	0.231	3.0	128

Spot Name	ppm Th	ppm Rad 206	232Th /238U	% err	total 206Pb /238U	% err	total 208Pb /232Th	% err	204corr 206Pb /238U Age	1σ err	207corr 206Pb /238U Age	1σ err	208corr 206Pb /238U Age	1σ err	204corr 207Pb /206Pb Age	1σ err
10319-1.1	58	21	0.90	0.54	0.36	1.2	0.108	3.2	**1977**	**20**	**1974**	**24**	**1969**	**10**	**1994**	**15**
10319-10.1	74	64	0.38	0.48	0.37	1.1	0.106	3.0	**2015**	**19**	**2017**	**23**	**2022**	**7**	**2002**	**12**
10319-103.1	57	36	0.70	0.65	0.50	1.6	0.143	3.0	**2602**	**34**	**2585**	**49**	**2610**	**13**	**2640**	**13**
10319-11.1	286	158	0.76	0.18	0.47	1.0	0.134	1.6	**2485**	**21**	**2493**	**29**	**2482**	**11**	**2463**	**5**
10319-110.1	181	88	0.85	0.11	0.47	1.0	0.133	1.9	**2484**	**22**	**2499**	**30**	**2482**	**12**	**2443**	**9**
10319-111.1	127	69	0.76	0.05	0.46	1.3	0.136	2.3	**2457**	**26**	**2451**	**35**	**2449**	**12**	**2472**	**9**
10319-112.1	50	43	0.51	0.24	0.49	1.1	0.148	3.0	**2553**	**23**	**2551**	**32**	**2551**	**12**	**2559**	**11**
10319-113.1	102	42	0.98	0.06	0.46	1.4	0.139	2.4	**2428**	**29**	**2422**	**38**	**2409**	**13**	**2443**	**17**
10319-114.1	137	83	0.70	0.61	0.48	1.0	0.148	2.2	**2511**	**22**	**2530**	**31**	**2493**	**12**	**2464**	**7**
10319-116.1	207	165	0.51	0.18	0.46	1.0	0.134	2.0	**2426**	**21**	**2427**	**28**	**2420**	**10**	**2421**	**5**
10319-118.1	229	71	1.03	0.26	0.36	1.0	0.108	1.9	**1998**	**18**	**2004**	**21**	**1990**	**9**	**1967**	**8**
10319-119.1	200	126	0.67	0.17	0.47	1.0	0.140	1.8	**2498**	**21**	**2510**	**30**	**2493**	**11**	**2466**	**7**
10319-121.1	51	50	0.34	0.28	0.37	1.2	0.116	3.3	**2026**	**21**	**2027**	**24**	**2020**	**7**	**2026**	**10**
10319-13.1	54	79	0.25	0.28	0.41	1.3	0.131	3.0	**2194**	**23**	**2141**	**28**	**2190**	**8**	**2400**	**8**
10319-14.1	94	38	0.90	0.07	0.41	1.2	0.121	2.5	**2212**	**22**	**2184**	**27**	**2206**	**11**	**2321**	**12**
10319-17.1	28	52	0.17	0.49	0.35	1.1	0.100	4.5	**1955**	**18**	**1951**	**21**	**1958**	**6**	**1974**	**10**
10319-18.1	83	45	0.65	0.40	0.40	1.6	0.122	2.8	**2174**	**29**	**2171**	**35**	**2163**	**10**	**2186**	**9**
10319-19.1	136	107	0.53	0.24	0.47	1.1	0.134	2.1	**2470**	**22**	**2488**	**30**	**2469**	**11**	**2418**	**7**
10319-2.1	99	46	0.87	0.40	0.45	1.1	0.128	2.4	**2393**	**22**	**2378**	**29**	**2392**	**12**	**2442**	**9**
10319-20.1	60	48	0.40	0.05	0.36	1.1	0.106	3.0	**1991**	**18**	**1990**	**22**	**1991**	**7**	**1996**	**10**
10319-21.1	129	86	0.46	0.04	0.35	1.1	0.101	2.2	**1921**	**19**	**1913**	**22**	**1921**	**7**	**1966**	**8**
10319-22.1	56	40	0.56	0.54	0.46	1.1	0.128	3.1	**2417**	**22**	**2404**	**30**	**2418**	**11**	**2456**	**9**
10319-23.1	78	46	0.53	0.25	0.35	1.1	0.108	2.7	**1954**	**18**	**1950**	**22**	**1950**	**7**	**1976**	**12**
10319-24.1	26	369	0.02	0.22	0.31	1.0	0.262	2.9	**1746**	**16**	**1697**	**17**	**1745**	**5**	**2086**	**4**
10319-25.1	58	61	0.30	0.05	0.36	1.2	0.104	3.3	**1973**	**20**	**1974**	**24**	**1972**	**7**	**1969**	**9**
10319-26.1	24	13	0.63	0.55	0.38	1.3	0.107	4.9	**2078**	**24**	**2082**	**27**	**2087**	**11**	**2054**	**62**
10319-27.1	72	51	0.47	0.23	0.38	1.2	0.112	2.8	**2055**	**21**	**2055**	**25**	**2054**	**8**	**2056**	**10**
10319-29.1	140	64	0.71	0.39	0.37	1.1	0.111	2.3	**2011**	**18**	**2022**	**22**	**2004**	**8**	**1954**	**10**
10319-30.1	55	53	0.42	0.74	0.47	1.1	0.132	2.9	**2465**	**23**	**2427**	**30**	**2463**	**11**	**2567**	**11**
10319-33.1	62	65	0.40	0.50	0.48	1.3	0.138	3.0	**2534**	**27**	**2548**	**38**	**2533**	**11**	**2500**	**11**
10319-34.1	96	50	0.78	0.42	0.45	1.1	0.135	3.2	**2410**	**22**	**2406**	**29**	**2397**	**13**	**2421**	**8**

														204 Corrected				
Spot Name	204corr 208Pb /232Th Age	1σ err	% Dis- cor- dant	4corr 208* /232	% err	total 238 /206	% err	total 207 /206	% err	4corr 238/ 206*	% err	4corr 207* /206*	% err	4corr 207* /235	% err	4corr 206* /238	% err
10319-1.1	2042	63	+1	0.106	3.3	2.78	1.2	0.124	0.80	2.79	1.2	0.123	0.9	6.1	1.5	0.36	1.2
10319-10.1	1875	61	-1	0.097	3.4	2.71	1.1	0.126	0.47	2.73	1.1	0.123	0.7	6.2	1.3	0.37	1.1
10319-103.1	2512	81	+2	0.132	3.4	2.00	1.6	0.184	0.51	2.01	1.6	0.179	0.8	12.3	1.8	0.50	1.6
10319-11.1	2513	38	-1	0.132	1.6	2.12	1.0	0.162	0.27	2.13	1.0	0.161	0.3	10.4	1.1	0.47	1.0
10319-110.1	2502	48	-2	0.132	2.1	2.12	1.0	0.160	0.33	2.13	1.0	0.159	0.5	10.3	1.2	0.47	1.0
10319-111.1	2542	58	+1	0.134	2.4	2.15	1.3	0.163	0.38	2.16	1.3	0.162	0.5	10.3	1.4	0.46	1.3
10319-112.1	2586	81	+0	0.136	3.3	2.05	1.1	0.174	0.45	2.06	1.1	0.170	0.6	11.4	1.2	0.49	1.1
10319-113.1	2569	69	+1	0.136	2.8	2.18	1.4	0.161	0.46	2.19	1.4	0.159	1.0	10.0	1.8	0.46	1.4
10319-114.1	2719	57	-2	0.144	2.3	2.09	1.0	0.163	0.36	2.10	1.0	0.161	0.4	10.6	1.1	0.48	1.0
10319-116.1	2512	48	-0	0.132	2.0	2.19	1.0	0.157	0.27	2.19	1.0	0.157	0.3	9.9	1.1	0.46	1.0
10319-118.1	2058	37	-2	0.107	1.9	2.75	1.0	0.121	0.39	2.75	1.0	0.121	0.4	6.0	1.1	0.36	1.0
10319-119.1	2558	48	-2	0.135	2.0	2.11	1.0	0.164	0.28	2.11	1.0	0.161	0.4	10.5	1.1	0.47	1.0
10319-121.1	2172	69	-0	0.113	3.3	2.70	1.2	0.125	0.51	2.71	1.2	0.125	0.5	6.4	1.3	0.37	1.2
10319-13.1	2330	73	+10	0.122	3.3	2.46	1.3	0.157	0.37	2.47	1.3	0.155	0.4	8.7	1.3	0.41	1.3
10319-14.1	2263	55	+6	0.118	2.6	2.44	1.2	0.150	0.55	2.44	1.2	0.148	0.7	8.3	1.4	0.41	1.2
10319-17.1	1807	87	+1	0.094	5.0	2.82	1.1	0.122	0.50	2.82	1.1	0.121	0.6	5.9	1.2	0.35	1.1
10319-18.1	2306	61	+1	0.121	2.8	2.49	1.6	0.137	0.51	2.49	1.6	0.137	0.5	7.6	1.6	0.40	1.6
10319-19.1	2488	51	-3	0.131	2.2	2.14	1.1	0.158	0.34	2.14	1.1	0.156	0.4	10.1	1.1	0.47	1.1
10319-2.1	2406	55	+2	0.126	2.4	2.22	1.1	0.159	0.50	2.22	1.1	0.159	0.5	9.8	1.2	0.45	1.1
10319-20.1	1993	60	+0	0.104	3.1	2.76	1.1	0.124	0.51	2.76	1.1	0.123	0.6	6.1	1.2	0.36	1.1
10319-21.1	1917	43	+3	0.099	2.3	2.88	1.1	0.121	0.37	2.88	1.1	0.121	0.5	5.8	1.2	0.35	1.1
10319-22.1	2416	70	+2	0.127	3.1	2.20	1.1	0.161	0.53	2.20	1.1	0.160	0.5	10.0	1.2	0.46	1.1
10319-23.1	2007	54	+1	0.104	2.8	2.82	1.1	0.123	0.51	2.83	1.1	0.121	0.7	5.9	1.3	0.35	1.1
10319-24.1	2032	195	+19	0.106	10.1	3.20	1.0	0.133	0.18	3.22	1.0	0.129	0.3	5.5	1.1	0.31	1.0
10319-25.1	2000	63	-0	0.104	3.3	2.79	1.2	0.121	0.49	2.79	1.2	0.121	0.5	6.0	1.3	0.36	1.2
10319-26.1	1955	161	-1	0.102	8.6	2.62	1.3	0.130	0.99	2.63	1.4	0.127	3.5	6.6	3.8	0.38	1.4
10319-27.1	2078	57	+0	0.108	2.9	2.66	1.2	0.129	0.48	2.66	1.2	0.127	0.6	6.6	1.3	0.38	1.2
10319-29.1	2084	46	-3	0.109	2.3	2.73	1.1	0.121	0.48	2.73	1.1	0.120	0.6	6.0	1.2	0.37	1.1
10319-30.1	2498	84	+5	0.132	3.6	2.15	1.1	0.171	0.42	2.15	1.1	0.171	0.6	11.0	1.3	0.47	1.1
10319-33.1	2560	89	-2	0.135	3.7	2.07	1.3	0.165	0.42	2.08	1.3	0.164	0.7	10.9	1.5	0.48	1.3
10319-34.1	2540	77	+1	0.134	3.2	2.20	1.1	0.157	0.46	2.21	1.1	0.157	0.5	9.8	1.2	0.45	1.1

Spot Name	Yb ppm	Y 1s abs err	Hf ppm	Hf 1s abs err	Mass Fract. Factor	MF_corr. 4corr. 207*/235	MF_corr. 4corr. 207*/235 % err.	MF_corr. 4corr. 206*/238	MF_corr. 4corr. 206*/238 % err.	ERROR Coefficient	MF_corr. 4corr. 7*/6*	MF_corr. 4corr. 7*/6* % err.	MF-corr. 206*/238 Age (Ma)
10319-1.1	189	4	7249	78	1	6.1	1.5	0.36	1.2	0.80	0.123	0.9	1977
10319-10.1	211	4	7812	84	1	6.2	1.3	0.37	1.1	0.85	0.123	0.7	2015
10319-103.1	182	4	9575	102	1	12.3	1.8	0.50	1.6	0.90	0.179	0.8	2602
10319-11.1	294	6	9094	98	1	10.4	1.1	0.47	1.0	0.96	0.161	0.3	2485
10319-110.1	215	4	8446	91	1	10.3	1.2	0.47	1.0	0.90	0.159	0.5	2484
10319-111.1	207	4	9034	98	1	10.3	1.4	0.46	1.3	0.93	0.162	0.5	2457
10319-112.1	141	3	7045	76	1	11.4	1.2	0.49	1.1	0.86	0.170	0.6	2553
10319-113.1	202	4	8605	93	1	10.0	1.8	0.46	1.4	0.81	0.159	1.0	2428
10319-114.1	326	7	7327	79	1	10.6	1.1	0.48	1.0	0.92	0.161	0.4	2511
10319-116.1	608	12	9187	101	1	9.9	1.1	0.46	1.0	0.96	0.157	0.3	2426
10319-118.1	145	3	9236	100	1	6.0	1.1	0.36	1.0	0.92	0.121	0.4	1998
10319-119.1	444	9	9587	104	1	10.5	1.1	0.47	1.0	0.93	0.161	0.4	2498
10319-121.1	203	4	8622	93	1	6.4	1.3	0.37	1.2	0.91	0.125	0.5	2026
10319-13.1	210	4	7849	85	1	8.7	1.3	0.41	1.3	0.94	0.155	0.4	2194
10319-14.1	185	4	8969	99	1	8.3	1.4	0.41	1.2	0.86	0.148	0.7	2212
10319-17.1	93	2	8733	94	1	5.9	1.2	0.35	1.1	0.88	0.121	0.6	1955
10319-18.1	187	4	11093	119	1	7.6	1.6	0.40	1.6	0.94	0.137	0.5	2174
10319-19.1	236	5	9221	99	1	10.1	1.1	0.47	1.1	0.94	0.156	0.4	2470
10319-2.1	302	6	6995	76	1	9.8	1.2	0.45	1.1	0.90	0.159	0.5	2393
10319-20.1	269	5	9271	99	1	6.1	1.2	0.36	1.1	0.88	0.123	0.6	1991
10319-21.1	161	3	9870	105	1	5.8	1.2	0.35	1.1	0.93	0.121	0.5	1921
10319-22.1	125	3	8728	94	1	10.0	1.2	0.46	1.1	0.90	0.160	0.5	2417
10319-23.1	268	5	9510	114	1	5.9	1.3	0.35	1.1	0.86	0.121	0.7	1954
10319-24.1	145	3	15248	165	1	5.5	1.1	0.31	1.0	0.97	0.129	0.3	1746
10319-25.1	321	6	11627	125	1	6.0	1.3	0.36	1.2	0.92	0.121	0.5	1973
10319-26.1	186	4	9028	97	1	6.6	3.8	0.38	1.4	0.36	0.127	3.5	2078
10319-27.1	192	4	8718	93	1	6.6	1.3	0.38	1.2	0.90	0.127	0.6	2055
10319-29.1	164	3	11018	118	1	6.0	1.2	0.37	1.1	0.88	0.120	0.6	2011
10319-30.1	173	3	9090	97	1	11.0	1.3	0.47	1.1	0.86	0.171	0.6	2465
10319-33.1	109	2	9790	105	1	10.9	1.5	0.48	1.3	0.88	0.164	0.7	2534
10319-34.1	307	6	8321	89	1	9.8	1.2	0.45	1.1	0.92	0.157	0.5	2410

Spot Name	MF-corr. 206*/238 Age (Ma) abs. err.	MF_corr. 4corr. 7*/6* Age (Ma)	MF_corr. 4corr. 7*/6* Age (Ma) abs. err.	MF_corr. % Disc.
10319-1.1	20	1994	15	1.0
10319-10.1	19	2002	12	-0.8
10319-103.1	34	2640	13	1.8
10319-11.1	21	2463	5	-1.1
10319-110.1	22	2443	9	-2.0
10319-111.1	26	2472	9	0.8
10319-112.1	23	2559	11	0.3
10319-113.1	29	2443	17	0.8
10319-114.1	22	2464	7	-2.3
10319-116.1	21	2421	5	-0.2
10319-118.1	18	1967	8	-1.9
10319-119.1	21	2466	7	-1.6
10319-121.1	21	2026	10	0.0
10319-13.1	23	2400	8	10.1
10319-14.1	22	2321	12	5.6
10319-17.1	18	1974	10	1.1
10319-18.1	29	2186	9	0.6
10319-19.1	22	2418	7	-2.6
10319-2.1	22	2442	9	2.4
10319-20.1	18	1996	10	0.3
10319-21.1	19	1966	8	2.7
10319-22.1	22	2456	9	1.9
10319-23.1	18	1976	12	1.3
10319-24.1	16	2086	4	18.6
10319-25.1	20	1969	9	-0.2
10319-26.1	24	2054	62	-1.4
10319-27.1	21	2056	10	0.0
10319-29.1	18	1954	10	-3.4
10319-30.1	23	2567	11	4.8
10319-33.1	27	2500	11	-1.7
10319-34.1	22	2421	8	0.6

Spot Name	Date/Time	Hours	Bkrd cts /sec	total 195.8 cts /sec	total 204 cts /sec	total 204.1 cts /sec	total 206 cts /sec	total 238 cts /sec	204 /206	% err	207 /206	% err	208 /206	% err	190 /195.8	% err
10319-36.1	2010-12-13, 22:56	13	0.05	11292	0.10	0	5177	6001	3.4E-6	203	0.120	0.30	0.133	1.5	0.68	0.57
10319-37.1	2010-12-13, 22:40	13	0.00	12172	0.27	0	1384	1552	1.7E-4	30	0.127	0.56	0.173	2.6	0.20	0.85
10319-39.1	2010-12-13, 23:13	13	0.00	12227	0.16	0	1631	1790	6.1E-5	38	0.130	0.51	0.294	2.9	0.53	0.59
10319-40.1	2010-12-13, 23:29	13	0.00	11724	0.16	0	1421	1618	5.5E-5	37	0.124	0.56	0.099	3.4	0.25	0.79
10319-43.1	2010-12-13, 23:45	14	0.00	11620	0.15	0	1510	1335	6.1E-5	25	0.166	0.50	0.126	2.9	0.35	0.70
10319-46.1	2010-12-14, 00:02	14	0.05	12237	0.22	0	929	814	1.4E-4	39	0.162	0.64	0.197	3.0	0.29	0.73
10319-49.1	2010-12-14, 00:34	14	0.10	13519	1.58	0	1962	1822	8.6E-4	10	0.175	0.71	0.342	1.6	0.40	0.62
10319-5.1	2010-12-13, 14:10	4	0.00	10426	0.19	0	1100	958	1.8E-4	37	0.160	0.59	0.375	2.0	0.29	0.79
10319-50.1	2010-12-14, 01:07	15	0.14	9970	1.03	0	2308	3659	3.7E-4	16	0.123	0.44	0.143	2.2	0.46	0.69
10319-50.1.2	2010-12-14, 14:57	29	0.05	10526	1.07	0	2466	2905	3.9E-4	13	0.124	0.43	0.186	1.9	0.56	0.63
10319-50.2	2010-12-14, 01:40	16	0.00	10811	5.66	0	3844	4234	1.5E-3	5	0.138	0.61	0.316	1.2	0.96	0.54
10319-50.3	2010-12-17, 16:27	102	0.13	7571	0.53	0	1872	2314	1.8E-4	44	0.123	0.44	0.159	2.4	0.41	0.82
10319-51.1	2010-12-14, 02:13	16	0.05	11486	0.66	0	2433	2871	2.2E-4	18	0.124	0.43	0.056	3.5	0.36	0.70
10319-51.2	2010-12-14, 13:08	27	0.00	11500	0.18	0	705	798	2.6E-4	29	0.127	0.79	0.110	4.6	0.22	0.83
10319-52.1	2010-12-14, 01:56	16	0.06	11854	2.21	0	2611	3249	8.5E-4	9	0.133	0.40	0.245	1.6	0.33	0.71
10319-53.1	2010-12-14, 07:41	22	0.06	10767	3.16	0	4889	5103	5.9E-4	7	0.129	0.30	0.170	1.4	0.86	0.55
10319-54.1	2010-12-14, 07:24	21	0.00	11426	0.34	0	1426	1823	2.1E-4	22	0.126	0.56	0.419	1.7	1.13	0.50
10319-57.1	2010-12-14, 06:35	20	0.10	11748	0.19	0	589	536	1.7E-4	45	0.162	1.33	0.228	3.5	0.25	0.79
10319-59.1	2010-12-14, 06:51	21	0.06	11732	0.14	0	4315	4794	2.5E-5	103	0.121	0.32	0.131	1.7	1.26	0.48
10319-6.1	2010-12-13, 12:55	3	0.05	10977	0.22	0	849	720	1.8E-4	42	0.172	0.65	0.146	3.6	0.23	0.84
10319-61.1	2010-12-14, 06:18	20	0.00	11809	0.44	0	1120	970	3.2E-4	22	0.176	0.57	0.190	2.8	0.29	0.74
10319-63.1	2010-12-14, 06:02	20	0.00	12178	0.27	0	1312	1623	1.6E-4	22	0.120	0.59	0.135	3.0	0.24	0.79
10319-63.1.2	2010-12-14, 15:16	29	0.06	10274	0.16	0	1102	1440	1.1E-4	69	0.120	0.64	0.136	3.3	0.24	0.85
10319-63.1.3	2010-12-18, 00:35	110	0.06	10692	0.34	0	1080	1427	2.3E-4	32	0.122	0.57	0.145	3.3	0.23	0.85
10319-67.1	2010-12-14, 05:46	20	0.08	11695	0.19	0	817	903	1.3E-4	64	0.131	0.73	0.135	3.9	0.46	0.63
10319-68.1	2010-12-14, 05:29	19	0.00	11981	0.21	0	1904	2166	1.0E-4	27	0.122	0.49	0.092	3.1	0.35	0.69
10319-69.1	2010-12-14, 04:40	19	0.00	11855	0.25	0	5499	6311	3.5E-5	39	0.121	0.29	0.262	1.1	0.54	0.60
10319-7.1	2010-12-13, 12:20	2	0.00	11918	0.12	0	3038	2937	2.7E-5	30	0.145	0.36	0.073	2.7	1.01	0.50
10319-70.1	2010-12-14, 04:24	18	0.05	11046	3.54	0	5217	5579	6.8E-4	7	0.134	0.29	0.236	1.2	0.70	0.58
10319-71.1	2010-12-14, 04:56	19	0.08	11670	0.21	0	1386	1308	7.9E-5	58	0.163	0.52	0.241	2.2	0.35	0.70
10319-73.1	2010-12-14, 03:35	17	0.13	12022	0.20	0	874	861	6.5E-5	146	0.150	0.67	0.184	3.2	0.27	0.76
10319-74.1	2010-12-14, 03:18	17	0.09	11657	0.16	0	3505	4050	2.6E-5	110	0.123	0.36	0.208	1.5	2.05	0.44

Spot Name	206 /238	% err	254 /238	% err	248 /254	% err	206 /254	% err	238 /195.8	% err	195.9 /195.8	% err	206Pb /238U calibr. const	% err	% com 206	208Pb* /206Pb*	% err	ppm U
10319-36.1	0.87	0.30	5.812	0.27	0.43	0.36	0.149	0.26	0.531	0.53	8.85	0.40	0.0109	0.22	0.01	0.133	1.5	499
10319-37.1	0.90	0.59	5.692	0.52	0.54	0.62	0.158	0.49	0.125	0.69	10.82	0.38	0.0119	0.77	0.29	0.167	2.6	119
10319-39.1	0.91	0.54	5.673	0.49	0.96	0.48	0.161	0.46	0.146	0.66	9.51	0.38	0.0121	0.94	0.11	0.292	2.9	140
10319-40.1	0.89	1.39	5.764	0.51	0.30	0.77	0.153	0.55	0.136	0.69	9.79	0.39	0.0114	0.48	0.10	0.097	3.4	127
10319-43.1	1.12	0.61	5.735	0.56	0.41	0.75	0.196	0.50	0.116	0.73	9.19	0.39	0.0146	0.47	0.11	0.124	2.9	110
10319-46.1	1.14	0.77	5.832	0.71	0.64	0.79	0.196	0.63	0.066	0.86	9.11	0.38	0.0139	0.75	0.25	0.192	3.0	61
10319-49.1	1.07	0.52	5.559	0.48	0.99	0.47	0.192	0.66	0.134	0.64	6.33	0.37	0.0149	0.89	1.50	0.315	1.6	129
10319-5.1	1.16	0.72	6.064	0.65	1.22	0.58	0.191	0.58	0.091	0.83	6.56	0.42	0.0131	0.55	0.31	0.370	2.0	83
10319-50.1	0.63	1.17	4.363	1.13	0.39	0.53	0.143	0.38	0.363	1.77	10.60	0.42	0.0159	1.34	0.64	0.130	2.2	410
10319-50.1.2	0.85	0.43	5.584	0.39	0.56	0.46	0.151	0.37	0.277	0.61	10.40	0.41	0.0117	0.32	0.67	0.172	1.9	268
10319-50.2	0.91	0.55	5.984	0.32	0.81	0.33	0.152	0.30	0.389	0.57	10.49	0.40	0.0106	0.26	2.54	0.269	1.2	358
10319-50.3	0.81	0.44	5.530	0.35	0.52	0.51	0.146	0.40	0.306	0.66	12.25	0.47	0.0115	0.28	0.30	0.153	2.4	297
10319-51.1	0.86	0.44	5.620	0.39	0.17	0.77	0.152	0.37	0.246	0.60	10.42	0.39	0.0117	0.32	0.39	0.048	3.5	235
10319-51.2	0.89	0.82	5.859	0.72	0.32	1.06	0.152	0.68	0.069	0.87	8.63	0.39	0.0110	1.01	0.45	0.101	4.6	64
10319-52.1	0.80	0.41	5.668	0.36	0.69	0.82	0.141	0.35	0.276	1.03	10.49	0.62	0.0107	0.57	1.48	0.217	1.6	263
10319-53.1	0.96	0.49	6.185	0.29	0.46	0.60	0.156	0.27	0.471	0.56	12.09	0.40	0.0104	0.24	1.03	0.149	1.4	425
10319-54.1	0.78	0.56	5.659	0.48	1.30	0.43	0.138	0.47	0.160	0.67	8.59	0.40	0.0105	0.63	0.37	0.412	1.7	153
10319-57.1	1.10	0.96	5.615	0.88	0.75	0.94	0.195	0.79	0.045	1.02	9.78	0.39	0.0150	1.27	0.30	0.223	3.5	44
10319-59.1	0.91	0.34	5.776	0.30	0.41	0.40	0.157	0.28	0.406	0.54	11.80	0.38	0.0115	0.28	0.04	0.130	1.7	383
10319-6.1	1.20	0.83	5.747	0.76	0.48	0.95	0.208	0.67	0.064	0.92	9.05	0.40	0.0155	0.64	0.31	0.140	3.6	60
10319-61.1	1.16	0.71	5.705	0.65	0.62	0.74	0.204	0.58	0.081	0.81	10.21	0.39	0.0153	0.93	0.55	0.179	2.8	77
10319-63.1	0.81	0.58	5.529	0.51	0.44	0.67	0.147	0.50	0.134	0.68	10.43	0.38	0.0115	0.70	0.27	0.130	3.0	131
10319-63.1.2	0.77	0.63	5.421	0.54	0.45	0.71	0.142	0.54	0.140	0.73	10.66	0.41	0.0115	0.98	0.19	0.132	3.3	138
10319-63.1.3	0.75	0.57	5.327	0.44	0.45	0.70	0.141	0.52	0.135	0.65	10.09	0.41	0.0117	0.58	0.40	0.137	3.3	134
10319-67.1	0.91	0.77	5.733	0.68	0.41	0.91	0.158	0.64	0.077	1.25	9.08	0.39	0.0119	0.65	0.22	0.131	3.9	73
10319-68.1	0.88	0.50	5.789	0.44	0.28	0.69	0.152	0.42	0.179	0.63	9.89	0.38	0.0113	0.45	0.18	0.088	3.1	169
10319-69.1	0.87	0.30	5.761	0.27	0.84	0.28	0.151	0.25	0.537	0.52	10.59	0.38	0.0112	0.70	0.06	0.261	1.1	507
10319-7.1	1.04	0.42	5.769	0.38	0.24	0.63	0.180	0.35	0.246	0.59	13.54	0.38	0.0133	0.32	0.05	0.072	2.7	230
10319-70.1	0.94	0.31	6.026	0.28	0.67	0.31	0.156	0.26	0.498	0.54	11.22	0.40	0.0108	0.23	1.17	0.213	1.2	456
10319-71.1	1.07	0.62	5.573	0.57	0.76	0.60	0.191	0.51	0.111	0.74	6.98	0.39	0.0147	0.54	0.14	0.239	2.2	108
10319-73.1	1.02	0.77	5.679	0.70	0.57	0.82	0.180	0.64	0.071	0.85	10.20	0.38	0.0134	0.72	0.11	0.182	3.2	67
10319-74.1	0.86	0.37	5.675	0.33	0.66	0.37	0.152	0.50	0.350	0.56	7.87	0.39	0.0114	0.33	0.05	0.207	1.5	334

Spot Name	ppm Th	ppm Rad 206	232Th /238U	% err	total 206Pb /238U	% err	total 208Pb /232Th	% err	204corr 206Pb /238U Age	1σ err	207corr 206Pb /238U Age	1σ err	208corr 206Pb /238U Age	1σ err	204corr 207Pb /206Pb Age	1σ err
10319-36.1	220	149	0.46	0.03	0.35	1.0	0.102	1.9	**1929**	**17**	**1925**	**20**	**1927**	**6**	**1952**	**6**
10319-37.1	67	39	0.58	0.06	0.38	1.3	0.114	2.9	**2079**	**22**	**2088**	**27**	**2076**	**9**	**2033**	**14**
10319-39.1	139	47	1.03	0.18	0.39	1.4	0.112	3.2	**2116**	**25**	**2124**	**30**	**2115**	**12**	**2082**	**10**
10319-40.1	39	40	0.32	0.28	0.37	1.1	0.112	3.6	**2010**	**19**	**2010**	**23**	**2006**	**7**	**2007**	**11**
10319-43.1	46	44	0.43	0.41	0.47	1.1	0.136	3.2	**2475**	**23**	**2463**	**31**	**2472**	**11**	**2507**	**9**
10319-46.1	40	23	0.68	0.64	0.45	1.3	0.129	3.3	**2371**	**25**	**2345**	**32**	**2369**	**12**	**2453**	**13**
10319-49.1	131	52	1.05	0.05	0.48	1.3	0.156	2.1	**2488**	**28**	**2483**	**38**	**2462**	**14**	**2501**	**17**
10319-5.1	106	30	1.32	0.08	0.42	1.1	0.119	2.3	**2252**	**22**	**2203**	**27**	**2255**	**13**	**2429**	**13**
10319-50.1	160	179	0.40	0.38	0.51	1.7	0.181	2.8	**2646**	**36**	**2951**	**74**	**2625**	**12**	**1930**	**15**
10319-50.1.2	155	86	0.60	0.41	0.38	1.0	0.117	2.2	**2044**	**18**	**2062**	**22**	**2042**	**8**	**1945**	**13**
10319-50.2	303	102	0.87	0.04	0.34	1.0	0.123	1.6	**1845**	**17**	**1831**	**19**	**1831**	**8**	**1936**	**21**
10319-50.3	158	93	0.55	0.56	0.37	1.0	0.106	2.7	**2009**	**18**	**2018**	**21**	**2013**	**8**	**1959**	**17**
10319-51.1	40	75	0.18	0.41	0.37	1.1	0.119	3.7	**2042**	**18**	**2054**	**22**	**2044**	**7**	**1978**	**11**
10319-51.2	21	19	0.34	0.33	0.35	1.4	0.113	4.8	**1937**	**24**	**1925**	**28**	**1934**	**8**	**2007**	**20**
10319-52.1	188	76	0.74	0.67	0.34	1.2	0.113	2.1	**1868**	**19**	**1851**	**21**	**1865**	**8**	**1977**	**17**
10319-53.1	206	120	0.50	0.53	0.33	1.0	0.113	1.8	**1833**	**16**	**1812**	**19**	**1829**	**6**	**1970**	**10**
10319-54.1	205	44	1.39	0.05	0.34	1.2	0.101	2.1	**1860**	**19**	**1839**	**22**	**1849**	**10**	**1997**	**13**
10319-57.1	34	18	0.80	0.54	0.48	1.6	0.137	3.9	**2516**	**34**	**2540**	**49**	**2515**	**15**	**2454**	**25**
10319-59.1	164	121	0.44	0.13	0.37	1.0	0.109	2.0	**2021**	**18**	**2029**	**22**	**2017**	**7**	**1973**	**8**
10319-6.1	30	26	0.51	0.68	0.49	1.2	0.142	3.9	**2585**	**25**	**2598**	**37**	**2586**	**13**	**2556**	**14**
10319-61.1	49	32	0.66	0.32	0.49	1.4	0.141	3.1	**2555**	**29**	**2547**	**41**	**2559**	**13**	**2574**	**13**
10319-63.1	59	41	0.47	0.23	0.37	1.2	0.106	3.3	**2022**	**21**	**2040**	**26**	**2026**	**8**	**1924**	**13**
10319-63.1.2	63	43	0.47	0.53	0.37	1.4	0.105	3.6	**2016**	**24**	**2032**	**29**	**2019**	**8**	**1929**	**19**
10319-63.1.3	62	43	0.47	0.40	0.37	1.2	0.114	3.5	**2044**	**20**	**2065**	**25**	**2043**	**8**	**1933**	**19**
10319-67.1	31	24	0.43	0.59	0.38	1.2	0.119	4.1	**2080**	**21**	**2077**	**26**	**2074**	**9**	**2094**	**20**
10319-68.1	49	52	0.30	0.87	0.36	1.1	0.112	3.4	**1989**	**19**	**1993**	**22**	**1987**	**7**	**1969**	**10**
10319-69.1	442	156	0.90	0.08	0.36	1.2	0.104	1.6	**1971**	**21**	**1971**	**24**	**1967**	**8**	**1968**	**6**
10319-7.1	58	84	0.26	0.21	0.42	1.0	0.120	2.9	**2282**	**20**	**2280**	**26**	**2283**	**9**	**2288**	**6**
10319-70.1	318	134	0.72	0.24	0.35	1.0	0.113	1.6	**1898**	**17**	**1877**	**19**	**1893**	**7**	**2022**	**10**
10319-71.1	84	44	0.81	0.30	0.47	1.1	0.141	2.5	**2490**	**24**	**2496**	**33**	**2475**	**13**	**2474**	**11**
10319-73.1	39	25	0.60	0.45	0.43	1.2	0.131	3.5	**2303**	**24**	**2293**	**31**	**2291**	**11**	**2336**	**18**
10319-74.1	228	105	0.71	0.18	0.37	1.1	0.108	1.8	**2007**	**18**	**2009**	**22**	**2002**	**8**	**1995**	**8**

Spot Name	204corr 208Pb /232Th Age	1σ err	% Dis- cor- dant	4corr 208* /232	% err	total 238 /206	% err	total 207 /206	% err	4corr 238/ 206*	% err	4corr 207* /206*	% err	4corr 207* /235	% err	4corr 206* /238	% err
10319-36.1	1963	35	+1	0.102	1.9	2.87	1.0	0.120	0.30	2.87	1.0	0.120	0.3	5.8	1.1	0.35	1.0
10319-37.1	2112	62	-3	0.110	3.1	2.62	1.3	0.127	0.56	2.63	1.3	0.125	0.8	6.6	1.5	0.38	1.3
10319-39.1	2123	66	-2	0.111	3.3	2.57	1.4	0.130	0.51	2.57	1.4	0.129	0.6	6.9	1.5	0.39	1.4
10319-40.1	2112	74	-0	0.110	3.7	2.73	1.1	0.124	0.56	2.73	1.1	0.123	0.6	6.2	1.3	0.37	1.1
10319-43.1	2534	76	+2	0.134	3.2	2.13	1.1	0.166	0.50	2.14	1.1	0.165	0.5	10.6	1.2	0.47	1.1
10319-46.1	2392	79	+4	0.126	3.5	2.24	1.3	0.162	0.64	2.25	1.3	0.160	0.8	9.8	1.5	0.44	1.3
10319-49.1	2675	58	+1	0.142	2.3	2.09	1.3	0.175	0.71	2.12	1.3	0.164	1.0	10.7	1.7	0.47	1.3
10319-5.1	2238	51	+9	0.117	2.4	2.38	1.1	0.160	0.59	2.39	1.1	0.158	0.8	9.1	1.4	0.42	1.1
10319-50.1	3064	93	-45	0.164	3.3	1.96	1.7	0.123	0.44	1.97	1.7	0.118	0.8	8.3	1.9	0.51	1.7
10319-50.1.2	2070	49	-6	0.108	2.5	2.66	1.0	0.124	0.43	2.68	1.1	0.119	0.7	6.1	1.3	0.37	1.1
10319-50.2	1960	36	+5	0.102	1.9	2.94	1.0	0.138	0.61	3.02	1.0	0.119	1.1	5.4	1.6	0.33	1.0
10319-50.3	1956	61	-3	0.102	3.3	2.73	1.0	0.123	0.44	2.73	1.0	0.120	1.0	6.1	1.4	0.37	1.0
10319-51.1	1946	90	-4	0.101	4.9	2.67	1.1	0.124	0.43	2.68	1.1	0.121	0.6	6.2	1.2	0.37	1.1
10319-51.2	1992	105	+4	0.104	5.5	2.84	1.4	0.127	0.79	2.85	1.4	0.123	1.2	6.0	1.8	0.35	1.4
10319-52.1	1902	44	+6	0.099	2.4	2.93	1.2	0.133	0.40	2.98	1.2	0.121	0.9	5.6	1.5	0.34	1.2
10319-53.1	1892	39	+8	0.098	2.1	3.01	1.0	0.129	0.30	3.04	1.0	0.121	0.6	5.5	1.2	0.33	1.0
10319-54.1	1917	38	+8	0.100	2.1	2.98	1.2	0.126	0.56	2.99	1.2	0.123	0.8	5.7	1.4	0.33	1.2
10319-57.1	2524	98	-3	0.133	4.1	2.09	1.6	0.162	1.33	2.09	1.6	0.160	1.5	10.5	2.2	0.48	1.6
10319-59.1	2084	42	-3	0.109	2.1	2.72	1.0	0.121	0.32	2.72	1.0	0.121	0.4	6.1	1.1	0.37	1.0
10319-6.1	2575	106	-1	0.136	4.4	2.02	1.2	0.172	0.65	2.03	1.2	0.170	0.9	11.6	1.5	0.49	1.2
10319-61.1	2511	81	+1	0.132	3.4	2.04	1.4	0.176	0.57	2.06	1.4	0.172	0.8	11.5	1.6	0.49	1.4
10319-63.1	1961	64	-6	0.102	3.4	2.71	1.2	0.120	0.59	2.71	1.2	0.118	0.7	6.0	1.4	0.37	1.2
10319-63.1.2	1967	79	-5	0.102	4.2	2.72	1.4	0.120	0.64	2.72	1.4	0.118	1.1	6.0	1.8	0.37	1.4
10319-63.1.3	2063	80	-7	0.107	4.1	2.67	1.2	0.122	0.57	2.68	1.2	0.118	1.0	6.1	1.6	0.37	1.2
10319-67.1	2195	98	+1	0.115	4.7	2.62	1.2	0.131	0.73	2.63	1.2	0.130	1.1	6.8	1.6	0.38	1.2
10319-68.1	2054	69	-1	0.107	3.5	2.76	1.1	0.122	0.49	2.77	1.1	0.121	0.6	6.0	1.2	0.36	1.1
10319-69.1	1997	31	-0	0.104	1.6	2.80	1.2	0.121	0.29	2.80	1.2	0.121	0.3	6.0	1.3	0.36	1.2
10319-7.1	2259	63	+0	0.118	2.9	2.35	1.0	0.145	0.36	2.35	1.0	0.145	0.4	8.5	1.1	0.42	1.0
10319-70.1	1951	33	+7	0.101	1.8	2.89	1.0	0.134	0.29	2.92	1.0	0.125	0.6	5.9	1.2	0.34	1.0
10319-71.1	2638	65	-1	0.139	2.6	2.12	1.1	0.163	0.52	2.12	1.1	0.162	0.6	10.5	1.3	0.47	1.1
10319-73.1	2452	92	+2	0.129	4.0	2.33	1.2	0.150	0.67	2.33	1.2	0.149	1.1	8.8	1.6	0.43	1.2
10319-74.1	2063	38	-1	0.107	1.9	2.74	1.1	0.123	0.36	2.74	1.1	0.123	0.5	6.2	1.2	0.37	1.1

Spot Name	Yb ppm	Y 1s abs err	Hf ppm	Hf 1s abs err	Mass Fract. Factor	MF_corr. 4corr. 207*/235	MF_corr. 4corr. 207*/235 % err.	MF_corr. 4corr. 206*/238	MF_corr. 4corr. 206*/238 % err.	ERROR Coefficient	MF_corr. 4corr. 7*/6*	MF_corr. 4corr. 7*/6* % err.	MF-corr. 206*/238 Age (Ma)
10319-36.1	342	7	8246	89	1	5.8	1.1	0.35	1.0	0.96	0.120	0.3	1929
10319-37.1	100	2	10089	108	1	6.6	1.5	0.38	1.3	0.85	0.125	0.8	2079
10319-39.1	267	5	8860	95	1	6.9	1.5	0.39	1.4	0.92	0.129	0.6	2116
10319-40.1	125	3	9124	98	1	6.2	1.3	0.37	1.1	0.88	0.123	0.6	2010
10319-43.1	180	4	8561	92	1	10.6	1.2	0.47	1.1	0.91	0.165	0.5	2475
10319-46.1	148	3	8489	91	1	9.8	1.5	0.44	1.3	0.85	0.160	0.8	2371
10319-49.1	203	4	5905	63	1	10.7	1.7	0.47	1.3	0.79	0.164	1.0	2488
10319-5.1	145	3	6112	66	1	9.1	1.4	0.42	1.1	0.82	0.158	0.8	2252
10319-50.1	230	5	9883	107	1	8.3	1.9	0.51	1.7	0.90	0.118	0.8	2646
10319-50.1.2	285	6	9693	105	1	6.1	1.3	0.37	1.1	0.82	0.119	0.7	2044
10319-50.2	485	9	9778	105	1	5.4	1.6	0.33	1.0	0.67	0.119	1.1	1845
10319-50.3	205	4	11423	126	1	6.1	1.4	0.37	1.0	0.73	0.120	1.0	2009
10319-51.1	183	4	9708	104	1	6.2	1.2	0.37	1.1	0.86	0.121	0.6	2042
10319-51.2	113	2	8043	86	1	6.0	1.8	0.35	1.4	0.78	0.123	1.2	1937
10319-52.1	165	3	9774	115	1	5.6	1.5	0.34	1.2	0.78	0.121	0.9	1868
10319-53.1	437	8	11269	121	1	5.5	1.2	0.33	1.0	0.87	0.121	0.6	1833
10319-54.1	573	11	8004	86	1	5.7	1.4	0.33	1.2	0.84	0.123	0.8	1860
10319-57.1	125	3	9119	98	1	10.5	2.2	0.48	1.6	0.74	0.160	1.5	2516
10319-59.1	636	12	11002	118	1	6.1	1.1	0.37	1.0	0.92	0.121	0.4	2021
10319-6.1	116	2	8436	91	1	11.6	1.5	0.49	1.2	0.81	0.170	0.9	2585
10319-61.1	148	3	9515	102	1	11.5	1.6	0.49	1.4	0.87	0.172	0.8	2555
10319-63.1	122	2	9722	104	1	6.0	1.4	0.37	1.2	0.86	0.118	0.7	2022
10319-63.1.2	122	2	9937	107	1	6.0	1.8	0.37	1.4	0.80	0.118	1.1	2016
10319-63.1.3	117	2	9405	102	1	6.1	1.6	0.37	1.2	0.75	0.118	1.0	2044
10319-67.1	235	5	8465	91	1	6.8	1.6	0.38	1.2	0.73	0.130	1.1	2080
10319-68.1	177	3	9216	99	1	6.0	1.2	0.36	1.1	0.88	0.121	0.6	1989
10319-69.1	276	5	9869	106	1	6.0	1.3	0.36	1.2	0.97	0.121	0.3	1971
10319-7.1	512	10	12616	135	1	8.5	1.1	0.42	1.0	0.94	0.145	0.4	2282
10319-70.1	352	7	10456	112	1	5.9	1.2	0.34	1.0	0.87	0.125	0.6	1898
10319-71.1	176	3	6502	70	1	10.5	1.3	0.47	1.1	0.87	0.162	0.6	2490
10319-73.1	136	3	9503	102	1	8.8	1.6	0.43	1.2	0.76	0.149	1.1	2303
10319-74.1	1038	20	7332	79	1	6.2	1.2	0.37	1.1	0.91	0.123	0.5	2007

Spot Name	MF-corr. 206*/238 Age (Ma) abs. err.	MF_corr. 4corr. 7*/6* Age (Ma)	MF_corr. 4corr. 7*/6* Age (Ma) abs. err.	MF_corr. % Disc.
10319-36.1	17	1952	6	1.4
10319-37.1	22	2033	14	-2.6
10319-39.1	25	2082	10	-1.9
10319-40.1	19	2007	11	-0.2
10319-43.1	23	2507	9	1.5
10319-46.1	25	2453	13	4.0
10319-49.1	28	2501	17	0.6
10319-5.1	22	2429	13	8.6
10319-50.1	36	1930	15	-45.3
10319-50.1.2	18	1945	13	-5.9
10319-50.2	17	1936	21	5.4
10319-50.3	18	1959	17	-3.0
10319-51.1	18	1978	11	-3.8
10319-51.2	24	2007	20	4.0
10319-52.1	19	1977	17	6.4
10319-53.1	16	1970	10	8.0
10319-54.1	19	1997	13	7.9
10319-57.1	34	2454	25	-3.0
10319-59.1	18	1973	8	-2.8
10319-6.1	25	2556	14	-1.4
10319-61.1	29	2574	13	0.9
10319-63.1	21	1924	13	-6.0
10319-63.1.2	24	1929	19	-5.3
10319-63.1.3	20	1933	19	-6.7
10319-67.1	21	2094	20	0.8
10319-68.1	19	1969	10	-1.2
10319-69.1	21	1968	6	-0.1
10319-7.1	20	2288	6	0.3
10319-70.1	17	2022	10	7.1
10319-71.1	24	2474	11	-0.8
10319-73.1	24	2336	18	1.7
10319-74.1	18	1995	8	-0.7

Spot Name	Date/Time	Hours	Bkrd cts /sec	total 195.8 cts /sec	total 204 cts /sec	total 204.1 cts /sec	total 206 cts /sec	total 238 cts /sec	204 /206	% err	207 /206	% err	208 /206	% err	190 /195.8	% err
10319-75.1	2010-12-14, 04:07	18	0.05	11897	0.14	0	3942	4046	2.3E-5	83	0.135	0.33	0.086	3.7	0.48	0.62
10319-76.1	2010-12-14, 03:02	17	0.05	11518	0.62	0	3761	4477	1.4E-4	19	0.123	0.35	0.095	2.1	0.44	0.65
10319-78.1	2010-12-14, 02:46	17	0.10	11611	4.90	0	6973	8635	6.8E-4	6	0.129	0.25	0.190	1.1	0.93	0.52
10319-78.2	2010-12-14, 13:45	28	0.00	11356	0.24	0	1886	2312	1.4E-4	24	0.120	0.49	0.101	2.9	0.26	0.79
10319-78.3	2010-12-18, 01:13	111	0.00	9686	0.91	0	5982	7665	1.5E-4	13	0.122	0.25	0.166	1.3	0.95	0.56
10319-79.1	2010-12-14, 08:14	22	0.10	11255	1.27	0	5275	5674	2.0E-4	13	0.128	0.55	0.217	1.2	0.80	0.55
10319-8.1	2010-12-13, 13:11	3	0.10	12047	0.15	0	1719	1569	1.9E-5	216	0.154	0.48	0.099	3.1	0.29	0.73
10319-81.1	2010-12-14, 08:30	22	0.00	11647	0.18	0	1833	1667	7.1E-5	30	0.172	0.45	0.138	2.6	0.29	0.75
10319-82.1	2010-12-14, 09:19	23	0.00	11550	0.21	0	6937	6165	1.4E-5	24	0.160	0.24	0.148	1.3	0.41	0.66
10319-84.1	2010-12-14, 08:46	23	0.12	11388	0.75	0	7568	5762	8.0E-5	21	0.171	0.22	0.186	1.1	0.59	0.59
10319-85.1	2010-12-14, 09:36	23	0.10	11458	0.15	0	4718	5138	1.0E-5	175	0.125	0.31	0.120	1.7	0.49	0.63
10319-85.2	2010-12-18, 01:32	111	0.06	6801	5.20	0	4912	5818	1.0E-3	5	0.127	0.27	0.131	1.6	1.03	1.42
10319-87.1	2010-12-14, 10:08	24	0.00	11952	0.17	0	849	871	1.7E-4	25	0.142	0.69	0.143	3.7	0.26	0.77
10319-89.1	2010-12-14, 10:25	24	0.14	12189	1.30	0	1599	1579	6.9E-4	14	0.156	0.49	0.226	2.1	0.38	0.66
10319-9.1	2010-12-13, 14:29	4	0.00	11688	0.57	0	4319	3695	1.2E-4	19	0.164	0.30	0.137	1.7	0.52	0.61
10319-91.1	2010-12-14, 10:41	25	0.10	11954	0.16	0	4339	4070	2.0E-5	213	0.152	0.30	0.115	1.8	0.41	0.65
10319-94.1	2010-12-14, 11:14	25	0.15	12507	0.33	0	1318	1192	6.8E-5	73	0.159	0.54	0.223	2.4	0.45	0.62
10319-95.1	2010-12-14, 11:30	25	0.00	12338	0.72	0	1708	1669	3.7E-4	18	0.159	0.47	0.131	2.7	0.33	0.69
10319-98.1	2010-12-14, 13:27	27	0.08	11137	0.20	0	2578	2210	4.9E-5	91	0.171	0.38	0.193	1.8	0.46	0.64

Spot Name	206 /238	% err	254 /238	% err	248 /254	% err	206 /254	% err	238 /195.8	% err	195.9 /195.8	% err	206Pb /238U calibr. const	% err	% com 206	208Pb* /206Pb*	% err	ppm U
10319-75.1	0.98	0.36	5.800	0.33	0.27	0.51	0.168	0.30	0.341	0.55	10.95	0.38	0.0123	0.27	0.04	0.085	3.7	321
10319-76.1	0.84	0.35	5.734	0.31	0.30	0.48	0.147	0.30	0.386	0.55	12.02	0.39	0.0110	0.26	0.24	0.090	2.1	364
10319-78.1	0.81	0.74	5.788	0.23	0.51	0.29	0.140	0.66	0.759	0.51	11.24	0.39	0.0103	0.54	1.17	0.167	1.1	719
10319-78.2	0.82	0.49	5.600	0.43	0.34	0.95	0.146	0.42	0.203	0.63	11.44	0.39	0.0113	0.65	0.25	0.096	2.9	195
10319-78.3	0.80	0.25	5.706	0.20	0.52	0.29	0.140	0.23	0.772	0.53	11.55	0.42	0.0105	0.16	0.27	0.160	1.3	738
10319-79.1	0.93	0.31	5.952	0.28	0.66	0.31	0.157	0.26	0.500	0.53	12.16	0.39	0.0110	0.23	0.35	0.210	1.2	459
10319-8.1	1.09	0.56	5.729	0.52	0.31	0.78	0.190	0.46	0.132	0.69	7.76	0.38	0.0142	1.04	0.03	0.098	3.1	125
10319-81.1	1.10	0.55	5.672	0.50	0.43	0.66	0.194	0.45	0.142	0.69	9.30	0.39	0.0147	0.42	0.12	0.135	2.6	135
10319-82.1	1.12	0.29	5.791	0.27	0.50	0.34	0.194	0.24	0.534	0.52	10.90	0.39	0.0143	0.22	0.02	0.147	1.3	500
10319-84.1	1.30	0.29	6.026	0.28	0.58	0.32	0.216	0.24	0.506	0.53	10.71	0.39	0.0149	0.23	0.14	0.183	1.1	465
10319-85.1	0.92	0.32	5.858	0.29	0.38	0.40	0.157	0.27	0.446	0.54	11.60	0.39	0.0114	0.24	0.02	0.120	1.7	414
10319-85.2	0.86	0.28	6.019	0.23	0.25	0.44	0.141	0.29	0.825	0.63	12.55	0.51	0.0098	0.65	1.79	0.094	1.6	754
10319-87.1	0.97	0.77	5.563	0.69	0.45	0.90	0.175	0.64	0.073	0.84	10.03	0.38	0.0136	1.66	0.30	0.137	3.7	70
10319-89.1	1.02	0.57	5.625	0.52	0.66	0.58	0.181	0.47	0.129	0.69	10.39	0.38	0.0139	0.43	1.19	0.203	2.1	123
10319-9.1	1.18	0.37	5.827	0.34	0.43	0.44	0.203	0.30	0.310	0.57	10.66	0.39	0.0147	0.28	0.21	0.132	1.7	291
10319-91.1	1.07	0.35	5.728	0.33	0.38	0.45	0.186	0.30	0.341	0.55	11.61	0.38	0.0139	0.42	0.03	0.114	1.8	324
10319-94.1	1.11	0.64	5.722	0.59	0.69	0.65	0.194	0.53	0.095	0.75	8.66	0.38	0.0145	1.00	0.12	0.221	2.4	90
10319-95.1	1.02	0.55	5.587	0.50	0.40	0.69	0.183	0.46	0.134	0.68	9.46	0.38	0.0141	0.52	0.65	0.118	2.7	128
10319-98.1	1.17	0.47	5.753	0.44	0.61	0.50	0.203	0.39	0.197	0.64	9.48	0.40	0.0151	0.54	0.09	0.191	1.8	186

Spot Name	ppm Th	ppm Rad 206	232Th /238U	% err	total 206Pb /238U	% err	total 208Pb /232Th	% err	204corr 206Pb /238U Age	1σ err	207corr 206Pb /238U Age	1σ err	208corr 206Pb /238U Age	1σ err	204corr 207Pb /206Pb Age	1σ err
10319-75.1	91	109	0.29	0.20	0.39	1.0	0.116	3.9	**2145**	**19**	**2140**	**23**	**2143**	**8**	**2164**	**7**
10319-76.1	111	110	0.32	0.42	0.35	1.0	0.106	2.4	**1939**	**17**	**1934**	**20**	**1939**	**6**	**1971**	**8**
10319-78.1	380	202	0.55	0.03	0.33	1.1	0.115	1.6	**1822**	**18**	**1801**	**20**	**1814**	**6**	**1960**	**9**
10319-78.2	68	60	0.36	0.76	0.36	1.2	0.101	3.3	**1988**	**20**	**1998**	**24**	**1994**	**7**	**1932**	**11**
10319-78.3	397	212	0.55	0.03	0.34	1.0	0.100	1.7	**1861**	**16**	**1847**	**19**	**1861**	**6**	**1957**	**6**
10319-79.1	315	139	0.71	0.16	0.35	1.0	0.108	1.6	**1945**	**17**	**1930**	**20**	**1939**	**7**	**2034**	**11**
10319-8.1	40	49	0.33	0.28	0.45	1.4	0.136	3.4	**2413**	**29**	**2420**	**39**	**2407**	**10**	**2389**	**10**
10319-81.1	60	55	0.46	0.37	0.47	1.1	0.142	2.8	**2486**	**22**	**2455**	**30**	**2477**	**11**	**2565**	**8**
10319-82.1	257	196	0.53	0.15	0.46	1.0	0.127	1.6	**2423**	**21**	**2412**	**28**	**2424**	**10**	**2455**	**4**
10319-84.1	282	191	0.63	0.39	0.48	1.0	0.142	1.5	**2516**	**21**	**2500**	**29**	**2506**	**11**	**2555**	**4**
10319-85.1	162	129	0.40	0.33	0.36	1.0	0.108	2.0	**2000**	**18**	**1995**	**21**	**1997**	**7**	**2028**	**6**
10319-85.2	195	199	0.27	0.17	0.31	1.2	0.153	2.0	**1727**	**18**	**1711**	**20**	**1715**	**5**	**1851**	**14**
10319-87.1	32	26	0.48	0.47	0.44	1.9	0.131	4.2	**2326**	**38**	**2355**	**50**	**2323**	**11**	**2226**	**14**
10319-89.1	84	46	0.71	0.44	0.44	1.1	0.142	2.4	**2344**	**22**	**2355**	**28**	**2339**	**11**	**2308**	**17**
10319-9.1	130	118	0.46	0.04	0.47	1.0	0.139	2.0	**2489**	**21**	**2491**	**30**	**2485**	**11**	**2484**	**6**
10319-91.1	127	124	0.40	0.19	0.45	1.1	0.127	2.1	**2375**	**22**	**2377**	**28**	**2374**	**10**	**2367**	**8**
10319-94.1	64	36	0.73	0.41	0.46	1.4	0.141	2.8	**2452**	**29**	**2457**	**39**	**2435**	**12**	**2441**	**11**
10319-95.1	52	49	0.42	0.33	0.45	1.1	0.140	2.9	**2386**	**23**	**2383**	**30**	**2385**	**10**	**2394**	**13**
10319-98.1	117	77	0.65	0.34	0.48	1.1	0.143	2.2	**2536**	**24**	**2525**	**33**	**2524**	**12**	**2562**	**8**

Spot Name	204corr 208Pb /232Th Age	1σ err	% Dis- cor- dant	4corr 208* /232	% err	total 238 /206	% err	total 207 /206	% err	4corr 238/ 206*	% err	4corr 207* /206*	% err	4corr 207* /235	% err	4corr 206* /238	% err
10319-75.1	**2204**	**83**	+1	0.115	4.0	2.53	1.0	0.135	0.33	2.53	1.0	0.135	0.4	7.3	1.1	0.39	1.0
10319-76.1	**1933**	**49**	+2	0.100	2.7	2.84	1.0	0.123	0.35	2.85	1.0	0.121	0.5	5.9	1.1	0.35	1.0
10319-78.1	**1922**	**33**	+8	0.100	1.8	3.03	1.1	0.129	0.25	3.06	1.1	0.120	0.5	5.4	1.3	0.33	1.1
10319-78.2	**1854**	**62**	-3	0.096	3.5	2.76	1.2	0.120	0.49	2.77	1.2	0.118	0.6	5.9	1.4	0.36	1.2
10319-78.3	**1868**	**31**	+6	0.097	1.7	2.98	1.0	0.122	0.25	2.99	1.0	0.120	0.3	5.5	1.1	0.33	1.0
10319-79.1	**2006**	**32**	+5	0.104	1.7	2.83	1.0	0.128	0.55	2.84	1.0	0.125	0.6	6.1	1.2	0.35	1.0
10319-8.1	**2558**	**90**	-1	0.135	3.8	2.20	1.4	0.154	0.48	2.20	1.4	0.154	0.6	9.6	1.6	0.45	1.4
10319-81.1	**2634**	**71**	+4	0.139	2.9	2.12	1.1	0.172	0.45	2.13	1.1	0.171	0.5	11.1	1.2	0.47	1.1
10319-82.1	**2411**	**37**	+2	0.127	1.6	2.19	1.0	0.160	0.24	2.19	1.0	0.160	0.2	10.1	1.1	0.46	1.0
10319-84.1	**2645**	**39**	+2	0.140	1.6	2.09	1.0	0.171	0.22	2.09	1.0	0.170	0.3	11.2	1.1	0.48	1.0
10319-85.1	**2069**	**41**	+2	0.108	2.1	2.75	1.0	0.125	0.31	2.75	1.0	0.125	0.4	6.3	1.1	0.36	1.0
10319-85.2	**2079**	**60**	+8	0.108	3.1	3.20	1.2	0.127	0.27	3.25	1.2	0.113	0.8	4.8	1.4	0.31	1.2
10319-87.1	**2383**	**98**	-5	0.125	4.4	2.29	1.9	0.142	0.69	2.30	1.9	0.140	0.8	8.4	2.1	0.43	1.9
10319-89.1	**2397**	**68**	-2	0.126	3.0	2.25	1.1	0.156	0.49	2.28	1.1	0.147	1.0	8.9	1.5	0.44	1.1
10319-9.1	**2555**	**50**	-0	0.135	2.1	2.12	1.0	0.164	0.30	2.12	1.0	0.163	0.3	10.6	1.1	0.47	1.0
10319-91.1	**2394**	**57**	-0	0.126	2.5	2.24	1.1	0.152	0.30	2.25	1.1	0.152	0.5	9.3	1.2	0.45	1.1
10319-94.1	**2639**	**72**	-1	0.139	2.9	2.16	1.4	0.159	0.54	2.16	1.4	0.159	0.7	10.1	1.6	0.46	1.4
10319-95.1	**2391**	**82**	+0	0.126	3.6	2.22	1.1	0.159	0.47	2.23	1.1	0.154	0.8	9.5	1.4	0.45	1.1
10319-98.1	**2682**	**59**	+1	0.142	2.3	2.07	1.1	0.171	0.38	2.08	1.1	0.170	0.5	11.3	1.2	0.48	1.1

Spot Name	Yb ppm	Y 1s abs err	Hf ppm	Hf 1s abs err	Mass Fract. Factor	MF_corr. 4corr. 207*/235	MF_corr. 4corr. 207*/235 % err.	MF_corr. 4corr. 206*/238	MF_corr. 4corr. 206*/238 % err.	ERROR Coefficient	MF_corr. 4corr. 7*/6*	MF_corr. 4corr. 7*/6* % err.	MF-corr. 206*/238 Age (Ma)
10319-75.1	241	5	10205	109	1	7.3	1.1	0.39	1.0	0.94	0.135	0.4	2145
10319-76.1	221	4	11202	120	1	5.9	1.1	0.35	1.0	0.91	0.121	0.5	1939
10319-78.1	471	9	10478	112	1	5.4	1.3	0.33	1.1	0.91	0.120	0.5	1822
10319-78.2	130	3	10667	115	1	5.9	1.4	0.36	1.2	0.88	0.118	0.6	1988
10319-78.3	478	9	10763	117	1	5.5	1.1	0.33	1.0	0.95	0.120	0.3	1861
10319-79.1	407	8	11331	122	1	6.1	1.2	0.35	1.0	0.85	0.125	0.6	1945
10319-8.1	148	3	7235	78	1	9.6	1.6	0.45	1.4	0.93	0.154	0.6	2413
10319-81.1	148	3	8671	93	1	11.1	1.2	0.47	1.1	0.92	0.171	0.5	2486
10319-82.1	209	4	10161	109	1	10.1	1.1	0.46	1.0	0.97	0.160	0.2	2423
10319-84.1	299	6	9987	107	1	11.2	1.1	0.48	1.0	0.97	0.170	0.3	2516
10319-85.1	246	5	10812	116	1	6.3	1.1	0.36	1.0	0.94	0.125	0.4	2000
10319-85.2	520	12	11697	131	1	4.8	1.4	0.31	1.2	0.85	0.113	0.8	1727
10319-87.1	134	3	9349	100	1	8.4	2.1	0.43	1.9	0.92	0.140	0.8	2326
10319-89.1	194	4	9686	104	1	8.9	1.5	0.44	1.1	0.74	0.147	1.0	2344
10319-9.1	262	5	9939	107	1	10.6	1.1	0.47	1.0	0.95	0.163	0.3	2489
10319-91.1	206	4	10821	116	1	9.3	1.2	0.45	1.1	0.92	0.152	0.5	2375
10319-94.1	227	4	8070	86	1	10.1	1.6	0.46	1.4	0.90	0.159	0.7	2452
10319-95.1	168	3	8820	94	1	9.5	1.4	0.45	1.1	0.83	0.154	0.8	2386
10319-98.1	234	5	8838	95	1	11.3	1.2	0.48	1.1	0.92	0.170	0.5	2536

Spot Name	MF-corr. 206*/238 Age (Ma) abs. err.	MF_corr. 4corr. 7*/6* Age (Ma)	MF_corr. 4corr. 7*/6* Age (Ma) abs. err.	MF_corr. % Disc.
10319-75.1	19	2164	7	1.1
10319-76.1	17	1971	8	1.9
10319-78.1	18	1960	9	8.1
10319-78.2	20	1932	11	-3.3
10319-78.3	16	1957	6	5.6
10319-79.1	17	2034	11	5.0
10319-8.1	29	2389	10	-1.2
10319-81.1	22	2565	8	3.7
10319-82.1	21	2455	4	1.6
10319-84.1	21	2555	4	1.9
10319-85.1	18	2028	6	1.6
10319-85.2	18	1851	14	7.6
10319-87.1	38	2226	14	-5.4
10319-89.1	22	2308	17	-1.9
10319-9.1	21	2484	6	-0.2
10319-91.1	22	2367	8	-0.4
10319-94.1	29	2441	11	-0.6
10319-95.1	23	2394	13	0.4
10319-98.1	24	2562	8	1.3